



AEDC-TR-59-12
ASTIA DOCUMENT NO.:
AD-216698

MAR 13 1979

DEC 11 1984

PROPERTY OF U.S. AIR FORCE
NO. 40000000 JV
ARX
PROPERTY OF U.S. AIR FORCE



WALL-INTERFERENCE EFFECTS ON AXISYMMETRIC BODIES IN TRANSONIC WIND TUNNELS WITH PERFORATED WALL TEST SECTIONS



By

Bruce B. Estabrooks

PWT, ARO, Inc.



June 1959



Distribution/Classification

Distribution Code: 01 - APPROVED FOR PUBLIC
RELEASE

Distribution Statement: Approved for public release;
distribution is unlimited.

Citation Classification: Unclassified

Report Classification: Unclassified

Collection: Technical Reports

ARNOLD ENGINEERING DEVELOPMENT CENTER

AIR RESEARCH AND DEVELOPMENT COMMAND



ERRATA AEDC-TR-59-12, June 1959

Please note the following corrections:

1. p. 28 Data presented here belong on page 36.
2. p. 36 Data presented here belong on page 28.
(Note: The curves appearing on pp. 28 and 36 were inadvertently transposed in printing. The figure titles are correct as presented.)
3. p. 68 $\underline{M_{\infty} = 1.20}$ should read $\underline{M_{\infty} = 1.05}$.

**WALL-INTERFERENCE EFFECTS ON AXISYMMETRIC BODIES
IN TRANSONIC WIND TUNNELS
WITH PERFORATED WALL TEST SECTIONS**

By

**Bruce B. Estabrooks
PWT, ARO, Inc.**

June 1959

ARO Project No. 210612

Contract No. AF 40(600)-700 S/A 13(59-1)

CONTENTS

	<u>Page</u>
ABSTRACT	6
NOMENCLATURE	6
INTRODUCTION	7
APPARATUS AND TEST PROCEDURE	
1-Foot Transonic Tunnel	7
16-Foot Transonic Circuit	8
Test Articles	9
Instrumentation	10
RESULTS AND DISCUSSION	
Interference-Free Investigation	11
20° Cone-Cylinder Model	11
Parabolic Nose-Cylinder Model	12
Effect of Wall Geometry	12
Effect of Model Shape	13
2-Percent Blockage, Conical Nose Model	13
2-Percent Blockage, Parabolic Nose Model	14
Effect of Model Blockage	15
Effect of Wall Open-Area Ratio	15
Effect of Wall-Interference on Model Forces	16
CONCLUDING REMARKS	17
REFERENCES	18

ILLUSTRATIONS

Figure

1. Reynolds Number Variation in 1-Foot and 16-Foot Transonic Tunnels	21
2. Details of 1-Foot Transonic Tunnel Wall Configurations	22
3. Details of 16-Foot Transonic Circuit Wall Configurations	23
4. Basic Dimensions of Models Tested in 1-Foot Transonic Tunnel	24
5. Basic Dimensions of Models Tested in 16-Foot Transonic Circuit	25
6. Installation of Model and Support in 1-Foot Transonic Tunnel	26
7. Installation of Model and Support in 16-Foot Transonic Circuit	27

<u>Figure</u>	<u>Page</u>
8. Body Pressure Distributions on the 0.008-Percent Blockage, 20° Cone-Cylinder Model in the 16T	
a. M = 0.700, 0.800, and 0.900	28
b. M = 0.950 and 0.975	29
c. M = 1.000, 1.025, and 1.050	30
d. M = 1.100, 1.150, and 1.200	31
e. M = 1.300 and 1.400	32
9. Comparison of Body Pressure Distributions on the 0.008-Percent Blockage, 20° Cone-Cylinder Model at Tunnel Stagnation Pressures of 700 and 2000 psfa and Mach Number 1.00	33
10. Comparison of Body Pressure Distributions on Several Small Blockage, 20° Cone-Cylinder Models at Mach Number 1.00.	34
11. Comparison of Experimental and Theoretical Pressure Distributions on 20° Conical Bodies at Mach Number 1.00	35
12. Body Pressure Distributions on the 0.008-Percent Blockage, Parabolic Nose-Cylinder Model in the 16T	
a. M = 0.700, 0.800, 0.900, and 0.950	36
b. M = 0.975, 1.000, and 1.025	37
c. M = 1.050, 1.100, and 1.150	38
d. M = 1.200, 1.300, and 1.400	39
13. Body Pressure Distributions on the 2-Percent Blockage, 20° Cone-Cylinder Model in the 1T - Effect of Wall Geometry	
a. M = 0.95	40
b. M = 1.00	41
c. M = 1.05	42
d. M = 1.10	43
e. M = 1.20	44
f. M = 1.40	45
14. Body Pressure Distributions on the 2-Percent Blockage, 20° Cone-Cylinder Model in the 1T - Effect of Open-Area Ratio with 60° Inclined-Hole Walls	
a. M = 0.95	46
b. M = 1.00	47
c. M = 1.05	48
d. M = 1.10	49
e. M = 1.20	50
f. M = 1.40	51

<u>Figure</u>	<u>Page</u>
15. Body Pressure Distributions on the 2-Percent Blockage, Parabolic Nose-Cylinder Model in the 1T — Effect of Open-Area Ratio with 60° Inclined-Hole Walls	
a. M = 0.95	52
b. M = 1.00	53
c. M = 1.05	54
d. M = 1.10	55
e. M = 1.20	56
f. M = 1.40	57
16. Body Pressure Distributions on 20° Cone-Cylinder Models in the 1T and 16T — Effect of Model Blockage Ratio with 60° Inclined-Hole, 6-Percent Open-Area Ratio Walls	
a. M = 0.95	58
b. M = 1.00	60
c. M = 1.05	62
d. M = 1.10	64
e. M = 1.20	66
17. Body Pressure Distributions on the 2-Percent Blockage, 20° Cone-Cylinder Model in the 1T — Effect of Reducing the Open-Area Ratio of the 60° Inclined-Hole Wall to 1.5 Percent	
a. M = 0.95, 1.00, and 1.05	68
b. M = 1.10 and 1.20	69
18. Summary of the Most Favorable Body Pressure Distributions Obtained on the 2-Percent Blockage, 20° Cone-Cylinder Model in the 1T with 60° Inclined-Hole Walls	
a. M = 0.95, 1.00, and 1.05	70
b. M = 1.10, 1.20, and 1.40	71
19. Effect of Boundary Interference on the Forebody Pressure Drag of the 0.5- and 2-Percent Blockage, Cone-Cylinder Models Tested with the 60° Inclined-Hole, 6-Percent Open-Area Ratio Walls	72
20. Effect of Boundary Interference on the Forebody Pressure Drag of the 2-Percent Blockage, Parabolic Nose-Cylinder Model Tested with the 60° Inclined-Hole, 6-Percent Open-Area Ratio Walls	72

ABSTRACT

Feasibility of alleviating the wall-interference effects on models was investigated in the PWT 1-Foot Transonic Tunnel. Interference effects were evaluated by comparing the body pressure distributions obtained from tests in the 1-foot tunnel with interference-free data obtained from tests of identical models in the PWT 16-Foot Transonic Circuit.

Satisfactory pressure distributions were obtained on a 2-percent blockage, 20° cone-cylinder model by varying the wall open-area ratio of 60° inclined-hole, test section walls from 1.5 to 6.0 percent with increase in Mach number from 0.95 to 1.10. The reduction of blockage ratio of the 20° cone-cylinder model from 4.0 to 0.5 percent when testing with the 60° inclined-hole, 6-percent open-area test section walls did not materially influence the boundary interference effects.

NOMENCLATURE

d	Body diameter
l	Length of conical nose
M_{∞}	Free-stream Mach number
P_t	Free-stream total pressure
Δp	Local pressure minus free-stream pressure
q	Free-stream dynamic pressure
T_t	Free-stream total temperature
x	Axial distance downstream of model nose
y	Distance measured perpendicular to model axis
θ_w	Angular position of test section walls (+ represents diverged position)

INTRODUCTION

The attainment of satisfactory, interference-free results from wind tunnel tests at transonic speeds has been the objective of a number of experimental and theoretical investigations. Previous studies conducted at the Arnold Engineering Development Center (Refs. 1 - 4) have shown that wind tunnels with perforated wall test sections are capable of providing interference-free test conditions at Mach number 1.20. These studies concluded that perforated walls with the axes of the holes inclined 60° into the airstream and with an open-area ratio of 6 percent produced reasonably good test results for models having blockage ratios as large as 2 percent. However, wall-interference effects in the Mach number range from 0.95 to 1.10 were not satisfactorily eliminated with this wall configuration.

The present study was conducted in the 1-Foot Transonic Tunnel (1T) to experimentally investigate the feasibility of alleviating the wall-interference effects in this Mach number range. Wall-interference effects on the pressure distributions of several non-lifting bodies of revolution were obtained as a function of Mach number, wall porosity, and wall angle. In addition, to establish a basis for comparison, interference-free data were obtained from tests of 0.008-percent blockage models in the 16-Foot Transonic Circuit (16T).

APPARATUS AND TEST PROCEDURE

1-FOOT TRANSONIC TUNNEL

The 1-Foot Transonic Tunnel (1T) is an open-circuit, continuous-flow facility capable of operating at Mach numbers throughout the transonic range. The test section is 12 in. square by 37.5 in. long. Test section Mach numbers up to $M = 1.20$ are controlled by tunnel pressure ratio and plenum suction. Supersonic test section Mach numbers are established by setting the corresponding nozzle contour and maintaining sufficient test section pressure ratio and plenum suction to maintain the tunnel normal shock downstream of the test section. A detailed description of the facility is presented in Ref. 5.

Manuscript released by author May 1959.

The tunnel stagnation pressure was maintained at approximately 2900 psfa. The tunnel stagnation temperature was varied from 120 to 170° F, depending on ambient conditions, to eliminate moisture condensation effects. The Reynolds number per foot was approximately 5.25×10^6 (Fig. 1a) for the range of Mach numbers (0.95 to 1.40) investigated.

Test section wall configurations are readily changed by removing the walls, which are mounted to structural frames secured to the nozzle exit and diffuser entrance. The upper and lower wall frames, hinged by a flexure joint at the nozzle exit, are supported by screw actuators at the downstream end for wall-angle adjustment.

A series of perforated-wall configurations (Fig. 2) was used during the test program in the 1T. Three of the wall liners had normal perforations of 1/16-in. diam in metal plates of 1/16-in. thickness. The ratios of the open-area to the total area of the plates were 12, 22, and 33 percent. Three other perforated plate configurations were tested which had the axes of the perforations inclined into the airstream at an angle of 60 deg. This general type of wall configuration is termed a differential-resistance wall. The hole diameter of these walls was 1/8 in., and the plate thickness was 1/8 in. The open area ratios were 6, 3, and 1-1/2 percent. The 3 and the 1-1/2 percent liners were obtained by filling alternate diagonal rows of the 6-percent liners with commercial water putty (Fig. 2).

From the nozzle exit to approximately ten inches downstream, thin aluminum taper strips were mounted to the underside of all of the different perforated liners to improve the development of supersonic flow. The test-section-empty calibrations of the three vertical-hole, perforated-wall test sections (referred to hereafter as normal) are presented in Ref. 6. These data indicate that the Mach number distribution in the region occupied by the models generally does not vary more than ± 0.005 . Test section calibration data for the 6-percent open, differential-resistance wall are presented in Ref. 5, which indicates that the Mach number distribution in the test region varies a maximum of ± 0.002 for Mach numbers less than 1.20 and less than ± 0.005 for Mach numbers above 1.20.

16-FOOT TRANSONIC CIRCUIT

The 16-Foot Transonic Circuit (16T) of the Propulsion Wind Tunnel Facility is a continuous-flow, closed-return, variable-density tunnel capable of operating at Mach numbers from 0.50 to 1.60. The test section is 16 ft square and 40 ft long. The tunnel stagnation pressures may be varied from about 100 to 4000 psf at tunnel stagnation temperatures from about 60 to 160° F.

Two perforated plate configurations were used as the test section walls for the test program in the 16T. One of the test section wall liners had normal perforations of 1.00-in. diam in metal plates of 3/8-in. thickness (Fig. 3). The ratio of open area to total area for these wall liners was 20 percent. Test section calibration data (Ref. 7) indicate that the Mach number distribution in the test region varies a maximum of ± 0.005 of stream Mach number. In order to obtain relatively interference-free data, several of the models previously tested in the 1T were tested in the 16T using these 20-percent open wall liners. The tests were conducted at Mach numbers from 0.70 to 1.40 at a tunnel stagnation pressure of 1500 psfa. The stagnation temperature was maintained at 120° F.

The second perforated test section wall liner used during this test program was of the differential-resistance type. The axes of the 0.750-in. -diam holes were inclined into the airstream at an angle of 60°. The plate thickness was 0.750 in. and had an open-area ratio of 6 percent (Fig. 3). Test section calibration data presented in Ref. 8, show that the Mach number distribution in the test region varies a maximum of ± 0.003 and ± 0.010 at subsonic and supersonic Mach numbers, respectively. The tests with this wall liner were conducted at a stagnation pressure of 1200 psfa at Mach numbers from 0.95 to 1.10 and 1000 psfa at Mach number 1.20. The variation of Reynolds number per foot with Mach number is shown in Fig. 1b.

TEST ARTICLES

The data were primarily obtained from models that were geometrically similar, each having a conical nose with a total included angle of 20° followed by constant-diameter cylindrical bodies. Three models tested in the 1T with conical noses had body diameters of 1.000, 1.915, and 2.708 in., corresponding to 0.50, 2.00, and 4.00 percent blockage ratios (ratio of model cross-sectional area to nozzle-exit area). The 1.915-in. -diam cylindrical body was also tested with a parabolic shaped nose. The contour of the parabolic shaped nose is described by the following equation:

$$r = r_{\max} \left[\frac{2x}{\ell} - \left(\frac{x}{\ell} \right)^2 \right]$$

where: r = radius at body station, x , in.

x = distance from nose apex, in.

ℓ = distance from nose apex to maximum diameter station, in.

r_{\max} = maximum radius, 0.957 in.

Dimensional details of these models are shown in Fig. 4. The models were mounted on a cylindrical sting cantilevered from a vertical-pitch strut as shown in Fig. 6. The models were oriented along the tunnel centerline at zero angle of attack with the model bases positioned slightly upstream of the test section exit.

The 1.915-in. -diam body was also tested in the 16T with both the conical and parabolic noses. The blockage ratio of this body in the 16T was 0.008 percent. Also, a 20° conical nose model having a diameter of 21.60 in., corresponding to a blockage ratio of 1.000 percent, was tested in the 16T. The dimensional details of these models are shown in Fig. 5. The models in the 16T were mounted along the tunnel centerline on a cylindrical extension cantilevered from the sting support strut as shown in Fig. 7.

Each of the models was instrumented with one row of static pressure orifices spaced along one meridian of the model.

INSTRUMENTATION

The body static pressures for the test conducted in the 1T were measured by a mercury multi-manometer board and photographically recorded. The basic tunnel operating conditions were measured on individual instruments and manually recorded. The accuracy of the reading of all these pressures is considered to be within ± 0.05 in. of the mercury column. Based upon comparisons of body-pressure distributions at identical test conditions, the experimental repeatability of the ratio of static-to-total pressure was found to be within ± 0.002 . The accuracy of determining the free-stream Mach number is within ± 0.003 .

All data obtained during the tests in the 16T were obtained with the on-line data reduction system. Consolidated Electro-dynamic Corporation Precision Pressure Balance Systems and Ideal Micro-manometers were used for the pressure inputs, which were transmitted to the ERA 1102 computer from Coleman Binary Digitizers. The results were tabulated on electric typewriters and plotted on Librascope X-Y Plotters. Reference 5 has a more complete description of the instrumentation system.

RESULTS AND DISCUSSION

INTERFERENCE-FREE INVESTIGATION

The determination of essentially interference-free pressure distributions along a 20° cone-cylinder model and along a parabolic nose-cylinder model were obtained from tests in the 16T. The test section wall liners had normal perforations and an open-area ratio of 20 percent. The models had a maximum diameter of 1.915 in. and blockage ratio of 0.008 percent. The results obtained for the Mach number range from 0.70 to 1.40 are presented in the form of pressure ratio (ratio of local static pressure to stream total pressure) distributions along the model.

20° Cone-Cylinder Model

The pressure distributions along the 20° cone-cylinder model for the Mach number range from 0.70 to 1.40 are presented in Figs. 8a-e. The pressure distributions over the entire Mach number range show the expected flow expansion at the juncture of the cone and cylinder, followed by the recompression to approximately stream conditions along the cylindrical afterbody. The data appear to be relatively free of wall-interference effects throughout the Mach number range. Comparisons of the experimental results with theoretical distributions obtained by the method outlined in Ref. 3 indicate excellent agreement at Mach numbers from 1.20 to 1.40 (Figs. 8d and e).

Model pressure distributions obtained at tunnel stagnation pressures of 700 and 2000 psfa for a Mach number of 1.00 are compared in Fig. 9. The 700 and 2000 psfa pressures correspond to Reynolds number per foot values of 1.36×10^6 and 3.87×10^6 , respectively. These data indicate that this variation of Reynolds number at Mach number 1.00 had no significant influence on the model pressure distributions. Therefore, the data presented herein, which have been obtained at Reynolds number per foot values from about 2×10^6 to 4×10^6 in the Mach number range from 0.70 to 1.40, may also be considered to be independent of Reynolds number for comparison purposes.

A comparison of body pressure distributions obtained from tests of similar 20° cone-cylinder models in three large wind tunnels at a Mach number of 1.00 is shown in Fig. 10. The models were relatively small compared with the tunnel cross-sectional areas. The blockage ratios of the models were 0.008 percent (PWT-16T), 0.024 percent (WADC 10 Ft), and 0.187 percent (Boeing 8 x 12 Ft). Comparison of these results indicates that the PWT test data exhibited the least adverse wall-interference effects and represented essentially interference-free

pressure distributions. However, even these models with blockage ratios as small as 0.008 percent experienced a certain degree of interference at this Mach number.

The pressure coefficient distributions over the conical nose section of these models at Mach number 1.00 are compared with the theoretical solution of Yoshihara (Ref. 9) and with the experimental results obtained on a 0.005-percent blockage model in Fig. 11. The theoretical and the 0.005-percent blockage model distributions were obtained from Ref. 10 and have been adjusted by use of the transonic similarity parameters for bodies of revolution (Ref. 11) from a cone half-angle of $6^{\circ} 59'$ to the present cone half-angle of 10° . The shapes of the experimental curves were similar, although some displacement of the curves over a portion of the nose existed. The theoretical curve, however, exhibits a considerable deviation in shape from the experimental data.

Parabolic Nose-Cylinder Model

The pressure distributions along the parabolic nose-cylinder model are presented in Figs. 12a-d. This model does not have the abrupt change in body contour at the juncture of the nose and afterbody as does the cone-cylinder model. The smoothly contoured, parabolic nose distributed the expansion flow field over a greater portion of the body and eliminated the abrupt accelerations present with the cone-cylinder model. Otherwise the data exhibit the same systematic trends of pressure distributions throughout the Mach number range as noted for the cone-cylinder investigation. The slight perturbation in the pressure distributions in the vicinity of body stations $x/d = 1.5$ and 5.2 may be attributed to a discontinuity along the model surface at these stations.

EFFECT OF WALL GEOMETRY

Wall-interference effects on the pressure distributions along a non-lifting body of revolution tested in conjunction with various perforated wall test sections were obtained in the 1T. The body pressure distributions in the Mach number range from 0.95 to 1.40 with a 2-percent blockage, 20° cone-cylinder model are presented in Figs. 13a-f. The test section wall configurations included three walls having normal perforations with open-area ratios of 12, 22, and 33 percent and one wall having 60° inclined perforations with an open area of 6 percent. The interference-free data obtained with the same model in the 16T (0.008-percent blockage) are also presented.

The body pressure distributions indicate that these variations of wall geometry had little effect on alleviating the wall-boundary interference

in the Mach number range from 0.95 to 1.05 (Fig. 13a-c). References 1-4 explain in detail the flow phenomena related to these interference problems. In brief, these wall-interference effects are predominantly those caused by the supersonic flow expansions emanating from the nose-cylinder juncture which impinge on the wall and are reflected back to the model as compression waves. This type of interference is associated with a wall having too low resistance to inflow of air into the expansion wave region, thereby creating a flow disturbance at the wall that initiates the compression wave system.

With increase in Mach number to 1.10 (Fig. 13d), an additional disturbance due to the reflection of the attached nose shock wave back to the model as expansion waves was evident with the 22- and 33-percent open-area, normal-hole walls and the 6-percent open, 60° inclined-hole wall. This type of disturbance is caused by too low resistance to outflow. As noted in Ref. 4, the resistance to outflow of the 6-percent open, 60° inclined-hole wall was similar to that of the 22-percent open, normal-hole wall.

The beneficial influence of restricting the wall inflow characteristics by slanting the holes 60° may be noted at Mach numbers from 1.10 to 1.40. The wall-reflected compression wave strength was considerably reduced with this wall at Mach number 1.10 and nearly eliminated at Mach numbers 1.20 and 1.40 (Figs 13e and f). The normal-hole wall configurations experienced severe interference effects throughout this supersonic Mach number range.

EFFECT OF MODEL SHAPE

2-Percent Blockage, Conical Nose Model

Previous investigations (Refs. 1 to 4) conducted at Mach number 1.20 concluded that a 60° inclined-hole, 6-percent open-ratio test section wall produced satisfactory cancellation of both expansion and compression waves. However, as discussed in the preceding section, this wall configuration does not satisfactorily eliminate interference effects in the Mach number range from 0.95 to 1.10. Therefore, further investigation with a 2-percent blockage, 20° cone-cylinder model was conducted to determine the effect of decreasing the wall open-area ratio to 3 percent. Comparisons of the data are shown in Figs. 14a-f.

At Mach numbers 0.95 to 1.00 (Figs. 14a and b), the wall boundary conditions were not significantly affected by reducing the wall open-area ratio from 6 to 3 percent. Attempts to alleviate the wall interference by varying the wall angular position were not successful. The variation of the angular position of the test section walls influences the effective open

area of the walls. The effective porosity of the wall is increased with an increase in boundary-layer thickness. The results of Ref. 4 have shown that there is an appreciable increase in the boundary-layer thickness as the walls are moved from a converged to a diverged wall position.

At Mach numbers 1.05 and 1.10 (Figs. 14c and d), the reduction of wall open area to 3 percent contributed to a considerable alleviation of the disturbances present with the 6-percent open wall. The reduction of open area at Mach number 1.05 sufficiently restricted the inflow so as to nearly eliminate the wall reflected compression waves. At Mach number 1.10, the 3-percent open wall alleviated the wall reflection of both expansion and compressions.

At Mach numbers 1.20 and 1.40 (Figs. 14e and f) the results indicate that the 6-percent open wall more closely fulfilled the wall boundary requirements. The 3-percent open wall exhibited characteristics of a too closed wall as the model-induced shock and expansion systems were reflected as compression and expansion waves, respectively. The model-induced expansion systems were absorbed satisfactorily at both Mach numbers with the 6-percent open wall; however, a slight disturbance due to the reflection of the nose shock wave as an expansion wave is noticeable at Mach number 1.20.

2-Percent Blockage, Parabolic Nose Model

The abrupt change in body shape at the nose-cylinder juncture of the 20° cone-cylinder model creates a concentrated expansion field which, together with the bow wave compression system, presents a difficult problem for obtaining interference-free flow conditions. Tests were therefore conducted with the 3- and 6-percent open-area ratio walls with a smoothly contoured, 2-percent blockage, parabolic nose-cylinder model which extends the flow field of the expansion field emanating from the nose-body juncture over a greater portion of the wall. Comparisons of these data with interference-free results obtained utilizing the same identical model in the 16T are presented in Figs. 15a-f. The slight perturbations noticeable for all of the pressure distributions in the vicinity of body station $x/d = 1.5$ may be attributed to a small error in model fabrication. Model measurements obtained after the tests indicate that the radius values of the nose contour in this region were somewhat less than specified.

Although the smooth contour of the parabolic nose model tended to distribute the model-induced disturbance fields to a greater extent than realized with the cone-cylinder model, the problem of alleviation of the wall-boundary reflected disturbances was not reduced. Comparison of the body pressure distributions on the two models (Figs. 14 and 15)

indicate that the wall-interference effects noticeable with the cone-cylinder model were also prevalent with the parabolic nose model. In fact, in the Mach number range from 1.10 to 1.40 these test section walls more closely satisfied the requirements for the cone-cylinder model as shown by the more notable pressure distribution perturbations present with the parabolic nose model.

EFFECT OF MODEL BLOCKAGE

A comparison of the body pressure distributions obtained from tests on 20° cone-cylinder models having blockage ratios of 0.50, 2.0, and 4.0 percent in the 1T and a blockage ratio of 1.0 percent in the 16T are presented in Figs. 16a-e. The interference-free results obtained in the 16T are also presented. The models were tested at zero angle of attack through a Mach number range from 0.95 to 1.20. The 60° inclined-hole, 6-percent, open-area ratio, test section walls oriented at zero degree were utilized.

The data in Figs. 16a-e indicate that the boundary interference effects were not significantly minimized by reducing the model blockage from 4.0 to 0.5 percent when testing in the Mach number range from 0.95 to 1.20. With few exceptions, the wall-interference effects realized with the various sized models exhibited similar characteristics as previously discussed concerning the 2-percent blockage model. As expected, reducing model blockage shifted the location of the boundary-reflected disturbance downstream and increased the portion of the model affected by the disturbance.

Comparisons of the body distribution obtained on the 0.5, 2.0, and 4.0 percent blockage models in the 1T with the distributions measured on the 1.0-percent blockage model in the 16T indicate that the trends characteristic of the 1T data are compatible with the 16T results. This compatibility is indicative that the flow disturbances affecting the various blockage models in the 1T would also be applicable to similar blockage models in the 16T.

EFFECT OF WALL OPEN-AREA RATIO

The preceding sections have shown that some alleviation of the wall-interference effects was realized when the open-area ratio of the 60° inclined-hole walls was reduced from 6 to 3 percent. However, this reduction of open area was not sufficient to satisfy the wall requirements at Mach numbers in the immediate vicinity of 1.00. Therefore, tests were conducted with the 2-percent blockage, 20° cone-cylinder model with a wall open-area ratio of 1.5 percent in the Mach number range from 0.95 to 1.20. Pressure distributions obtained on the body are presented in Figs. 17a and b.

At Mach numbers 0.95 and 1.00 reasonably good results were obtained when the walls were diverged 40 minutes. This is indicative that the 1.5 open wall was too closed and that an effective wall open area of somewhat greater than 1.5 percent is required for satisfactory absorption of model-induced disturbances. At Mach numbers 1.05 and above, the 1.5-percent open wall at all wall angles has a too closed characteristic to produce disturbance-free data. This is shown by the model-induced compressions and expansions being reflected by the wall as compressions and expansions, respectively.

The optimum wall porosity and angular position of the 60° inclined-hole walls for producing essentially interference-free results with the 2-percent blockage, 20° cone-cylinder model are shown in Fig. 18 for the Mach number range from 0.95 to 1.40. The effective wall open-area ratio requirements varied from approximately 1.5 percent at Mach number 0.95 to about 6.0 percent at Mach number 1.40. The data show for a unique model that proper adjustment of wall boundary conditions, such as realized by varying the wall porosity and/or angle, will provide test results essentially free of wall-interference effects.

EFFECT OF WALL-INTERFERENCE ON MODEL FORCES

Investigations of the attenuation of model-induced disturbances by the utilization of various types of perforated test section walls have been discussed in the foregoing sections. The boundary requirements for satisfactory cancellation of model-induced disturbances were not realized with any particular wall at all Mach numbers. The 60° inclined-hole wall with 6-percent open-area ratio (at present employed in the 16T and 1T) provided boundary conditions capable of producing relatively interference-free data at Mach numbers greater than 1.10. However, in the Mach number range from 0.95 to 1.10 the magnitude of the wall-reflected disturbances (due primarily to model-induced expansion waves) on the body pressure distributions were significant.

The perturbations to the body pressure distributions caused by the boundary-reflected disturbances are indicative of the problem of obtaining accurate aerodynamic data in the Mach number range from 0.95 to 1.10. The impingement of the wall-reflected compression wave on model surfaces would provide erroneous flow fields over certain portions of the model. Appreciable errors in measurement of lift and pitching moment could occur if a portion of the model, such as a control surface, were subject to the disturbance. In addition, the impingement of the disturbance compression field on a convergent afterbody or other surfaces capable of producing an adverse pressure gradient flow field could prematurely induce flow separation along the surface which would adversely affect the measured aerodynamic force data. The flow

conditions existing at the base of models could also be adversely affected by the wall-reflected disturbances.

The effect of boundary interference on the forebody pressure drag of the 0.5- and 2.0-percent blockage cone-cylinder models tested in conjunction with the 60° inclined-hole, 6-percent open, test section walls is shown in Fig. 19. The pressure drag results obtained from the 0.5-percent blockage model did not exhibit any great departure from the interference-free results throughout most of the Mach number range. However, the adverse influence of the boundary-reflected disturbances on the drag data of the 2-percent blockage model is noticeable in the Mach number range from 1.00 to 1.10. These differences in drag can be attributed solely to disturbances impinging on the model nose since these models employed cylindrical afterbodies.

The pressure drag data of the 2-percent blockage, parabolic nose model obtained with the 60° inclined-hole, 6-percent open, test section walls are compared with interference-free results in Fig. 20. The adverse influence of wall interference is also noticeable on these data in the Mach number range from 1.00 to 1.05, although the effect on drag was not as severe as noted with the conical nose model. Estimations and/or corrections for the wall-interference effect on the model drag, as well as the other aerodynamic coefficients, would be difficult or impossible to predict because of the complicated nature of the three-dimensional flow present with any particular model and Mach number.

CONCLUDING REMARKS

An experimental investigation of the wall-interference effects on several non-lifting bodies of revolution has been conducted in the Mach number range from 0.95 to 1.40 in conjunction with various perforated test section walls. The data obtained during this investigation are summarized as follows:

1. The 60° inclined-hole, 6-percent open-area ratio; test section walls, which have previously been shown to provide satisfactory boundary conditions for interference-free testing of models at Mach number 1.20, did not provide interference-free results at Mach numbers between 0.95 and 1.10. Boundary interference due to non-cancellation of model-induced compression and expansion flow fields exists in this Mach number range.
2. Wall open-area ratio requirements for minimum boundary interference vary with Mach number. Satisfactory pressure distributions were obtained on the 2-percent blockage, 20° cone-cylinder model by varying the wall open-area ratio of

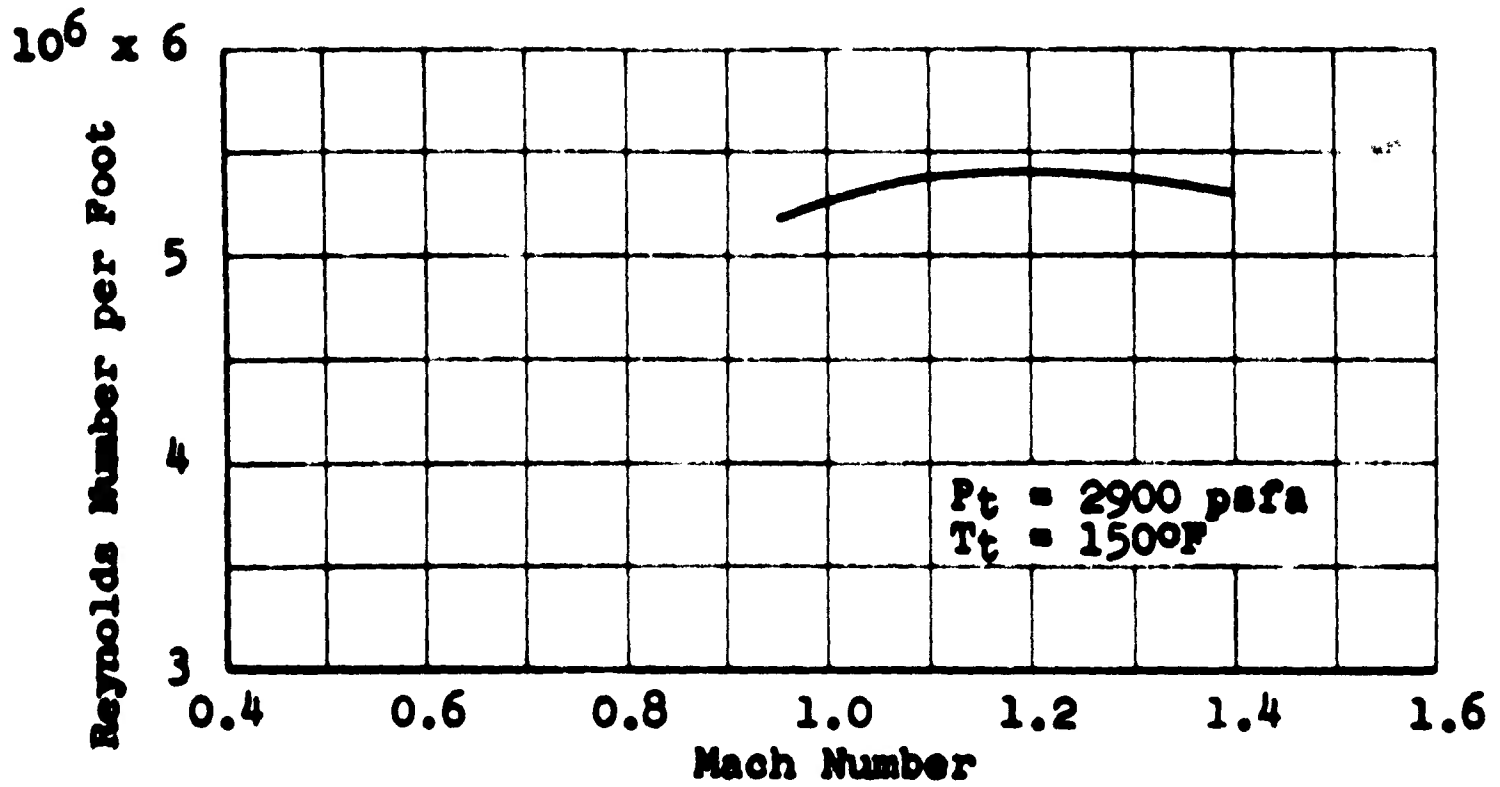
the 60° inclined-hole walls from 1.5 to 6.0 percent while increasing the Mach number from 0.95 to 1.10.

3. The change of model nose shape from a 20° cone to a parabolic nose in order to obtain a smooth body contour which would distribute the model-induced disturbance fields to a greater degree did not reduce the interference effects due to the wall-reflected disturbances.
4. The reduction of the blockage ratio of the 20° cone-cylinder models from 4.0 to 0.5 percent when testing with the 60° inclined-hole, 6-percent open-area walls did not materially influence the boundary interference effects. As expected, the reduction of model blockage shifted the location of the disturbances downstream and increased the portion of the model affected by the disturbance.
5. The 60° inclined-hole, 6-percent open-area ratio walls produced representative forebody pressure drag results throughout the Mach number range from 0.90 to 1.50 for the 0.5-percent blockage, cone-cylinder model. The forebody pressure drag of the 2-percent blockage models was relatively interference free except for the Mach number ranges of 1.00 to 1.10 and 1.00 to 1.05 for the cone-cylinder and the parabolic cylinder models, respectively.

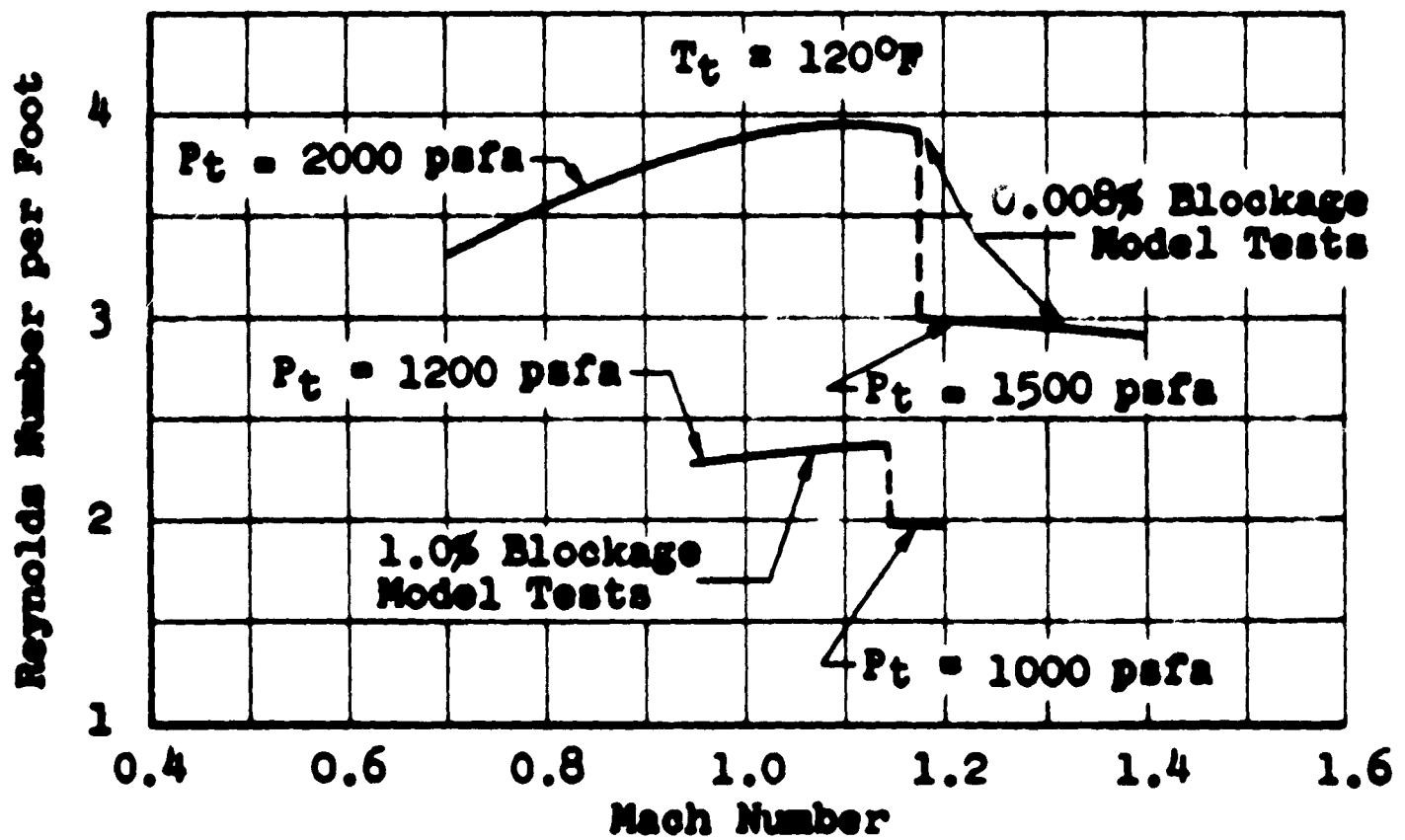
REFERENCES

1. Goethert, B. H. "Physical Aspects of Three-Dimensional Wave Reflections in Transonic Wind Tunnels at Mach Number 1.20 (Perforated, Slotted, and Combined Slotted-Perforated Walls)." AEDC-TR-55-45, March 1956. (AD-84159)
2. Gray, J. Don and Gardenier, Hugh E. "Experimental and Theoretical Studies on Three-Dimensional Wave Reflection in Transonic Test Sections - Part I: Wind Tunnel Tests on Wall Interference of Axisymmetric Bodies at Transonic Mach Numbers." AEDC-TN-55-42, March 1956. (AD-82559)
3. DuBose, H. C. "Experimental and Theoretical Studies on Three-Dimensional Wave Reflection in Transonic Test Sections - Part II: Theoretical Investigation of the Supersonic Flow Field about a Two-Dimensional Body and Several Three-Dimensional Bodies at Zero Angle of Attack." AEDC-TN-55-43, March 1956. (AD-83539)
4. Chew, W. L. "Experimental and Theoretical Studies on Three-Dimensional Wave Reflection in Transonic Test Sections - Part III: Characteristics of Perforated Test Section Walls with Differential Resistance to Cross-Flow." AEDC-TN-55-44, March 1956. (AD-84158)

5. Test Facilities Handbook. "Propulsion Wind Tunnel Facility, Vol. 3." Arnold Engineering Development Center. January 1959.
6. Chew, W. L. "Wind Tunnel Investigations of Transonic Test Sections - Phase II: Comparison of Results of Tests on Five Perforated Wall Test Sections in Conjunction with a Sonic Nozzle." AEDC-TR-54-52, March 1955.
7. Dick, R. S. "Calibration of the PWT 16-Foot Transonic Circuit - With an Aerodynamic Test Cart Having 20-Percent-Open Perforated Walls and Without Plenum Auxiliary Suction." AEDC-TN-58-24, June 1958. (AD-157139)
8. Dick, R. S. "Calibration of the 16-Foot Transonic Circuit of the Propulsion Wind Tunnel with an Aerodynamic Test Cart Having 6-Percent-Open Inclined-Hole Walls." AEDC-TN-58-90, November 1958. (AD-204846)
9. Yoshihara, H. "On the Flow Over a Cone-Cylinder Body at Mach Number One." WADC TR 52-295, November 1952.
10. Page, W. A. "Experimental Study of the Equivalence of Transonic Flow about Slender Cone-Cylinders of Circular and Elliptic Cross Section." NACA TN 4233, April 1958.
11. Oswatitsch, Klaus and Berndt, Sune B. "Aerodynamic Similarity at Axisymmetric Transonic Flow Around Slender Bodies." KTH-AERO TN 15, Roy. Inst. Tech., Division of Aeronautics, Stockholm, Sweden, 1950.

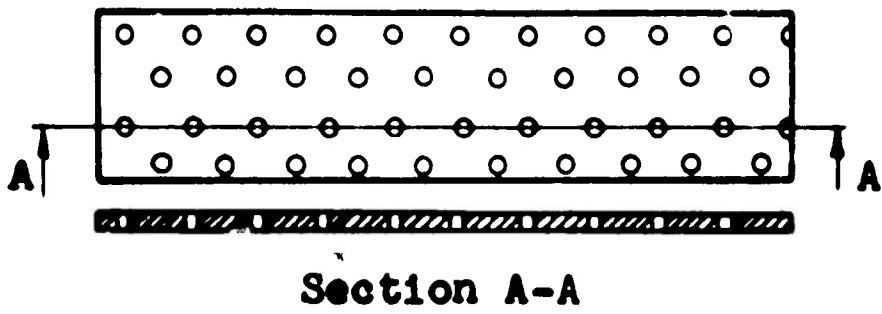


a. Reynolds Number Variation in 1-Foot Transonic Tunnel

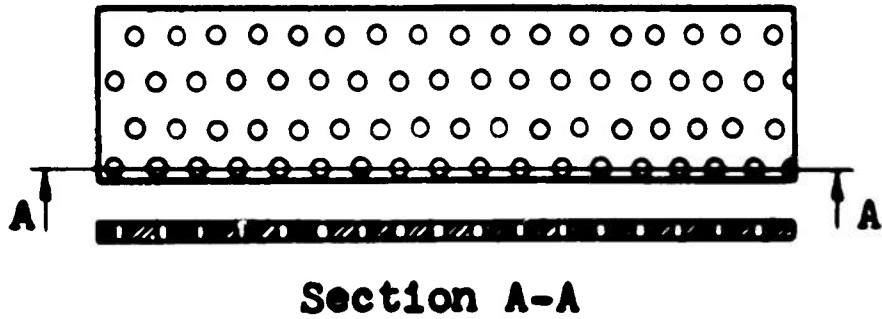


b. Reynolds Number Variation in 16-Foot Transonic Tunnel

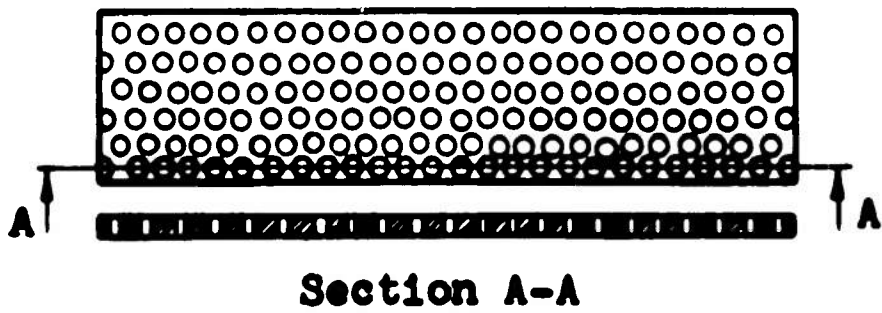
Fig. 1 Reynolds Number Variation in 1-Foot and 16-Foot Transonic Tunnels



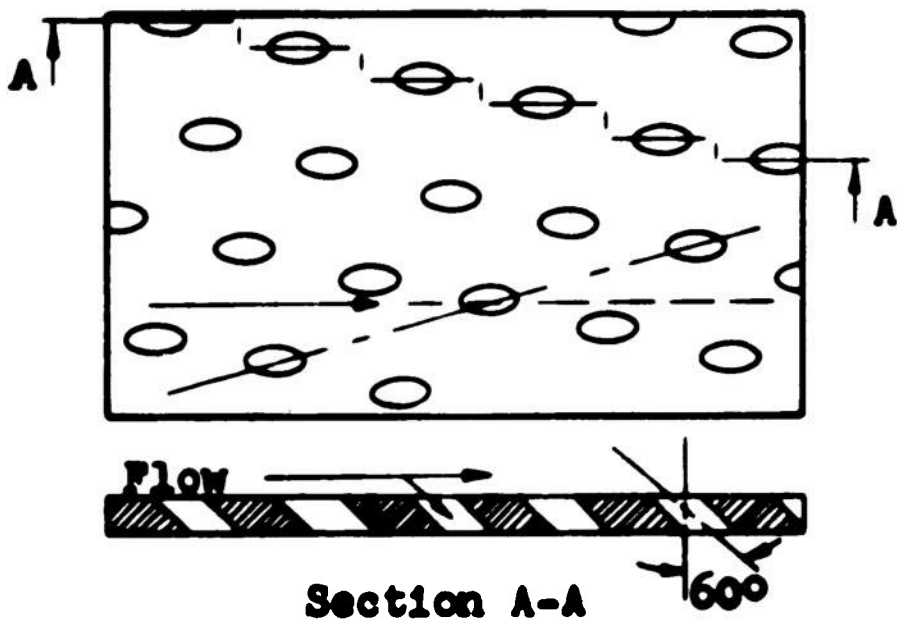
12%-Open, Perforated Wall
Hole Diameter 1/16 In.
Plate Thickness 1/16 In.



22%-Open, Perforated Wall
Hole Diameter 1/16 In.
Plate Thickness 1/16 In.

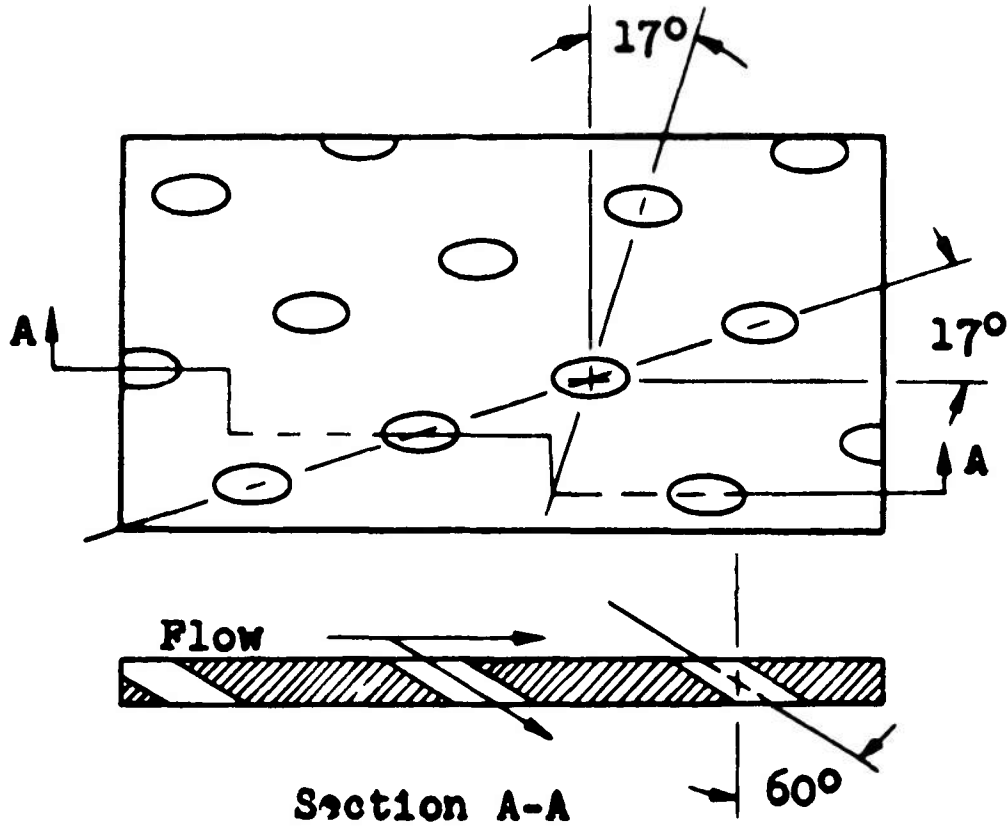


33%-Open, Perforated Wall
Hole Diameter 1/16 In.
Plate Thickness 1/16 In.

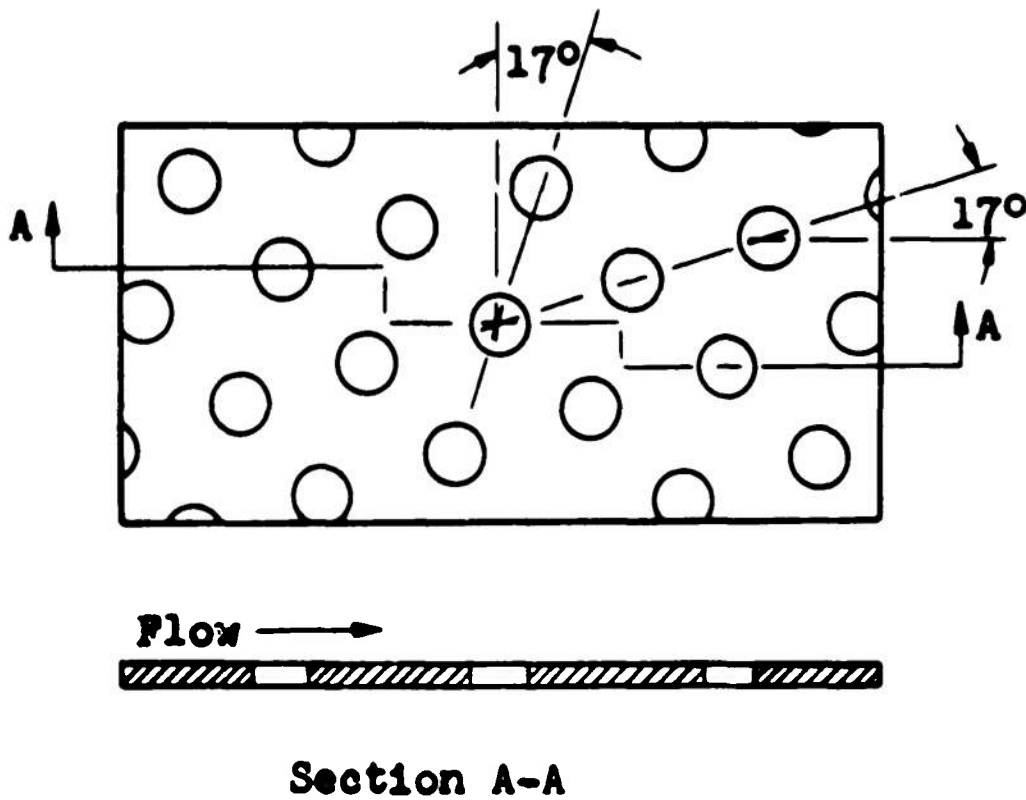


6%-Open, Inclined Hole Wall
Hole Diameter 1/8 In.
Plate Thickness 1/8 In.
Hole Angle 60°

Fig. 2 Details of 1-Foot Transonic Tunnel Wall Configurations



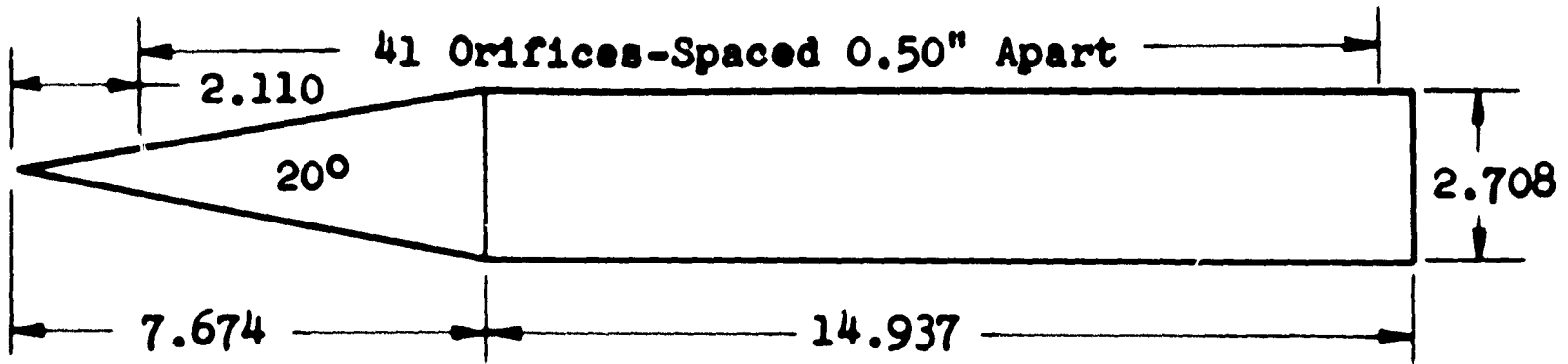
6% Open, Inclined Hole Wall
 Hole Diameter = 0.75 In.
 Plate Thickness = 0.75 In.
 Hole Angle = 60°



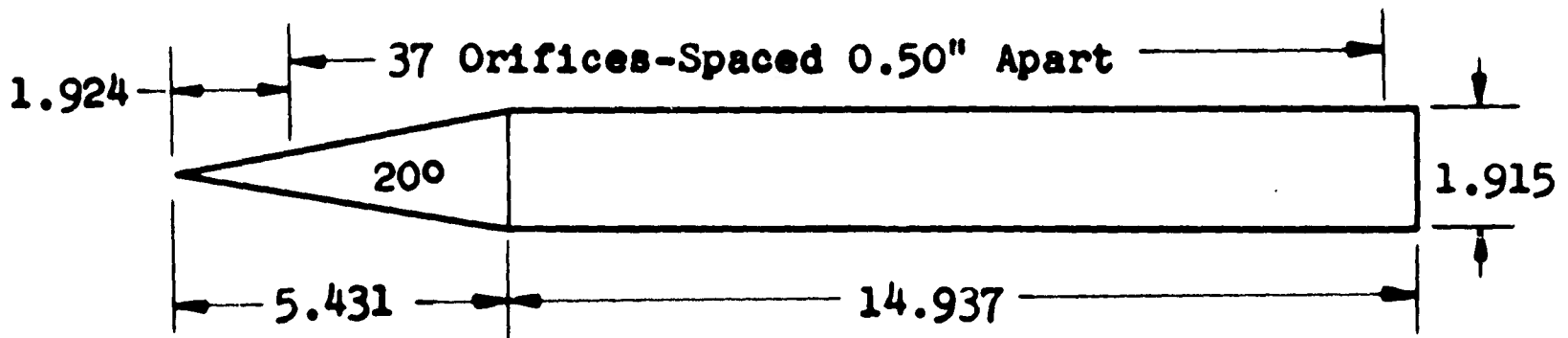
20% Open, Normal Hole Wall
 Hole Diameter = 1.00 In.
 Plate Thickness = 0.375 In.

Fig. 3 Details of 16-Foot Transonic Circuit Wall Configurations

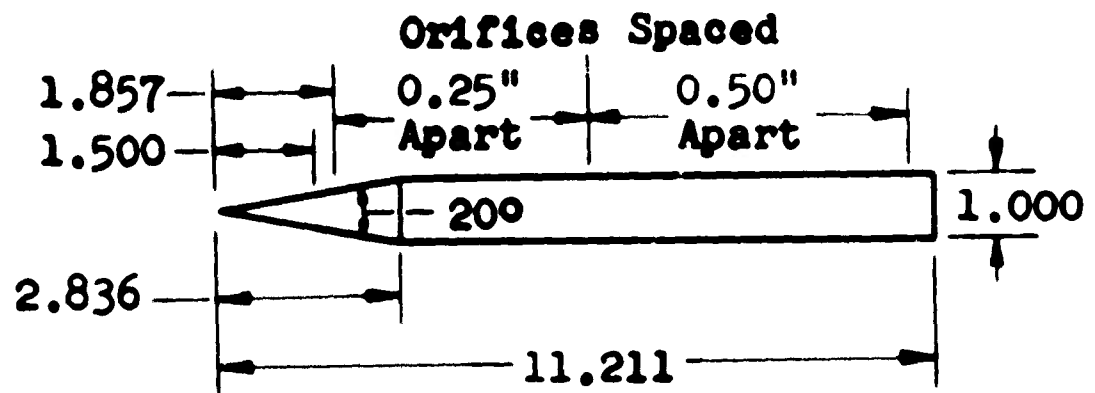
All Dimensions in Inches



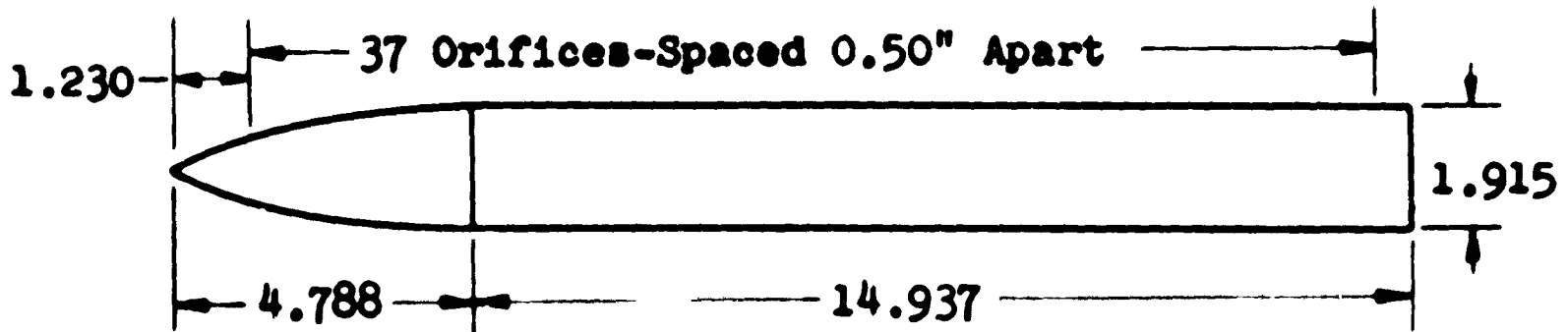
4% Blockage Cone-Cylinder Model



2% Blockage Cone-Cylinder Model



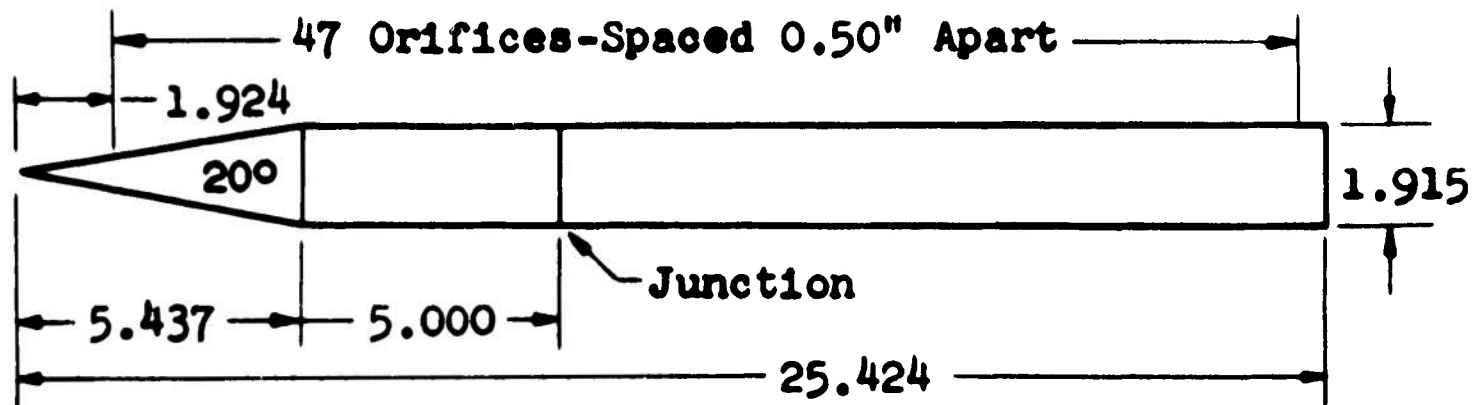
0.50% Blockage Cone-Cylinder Model



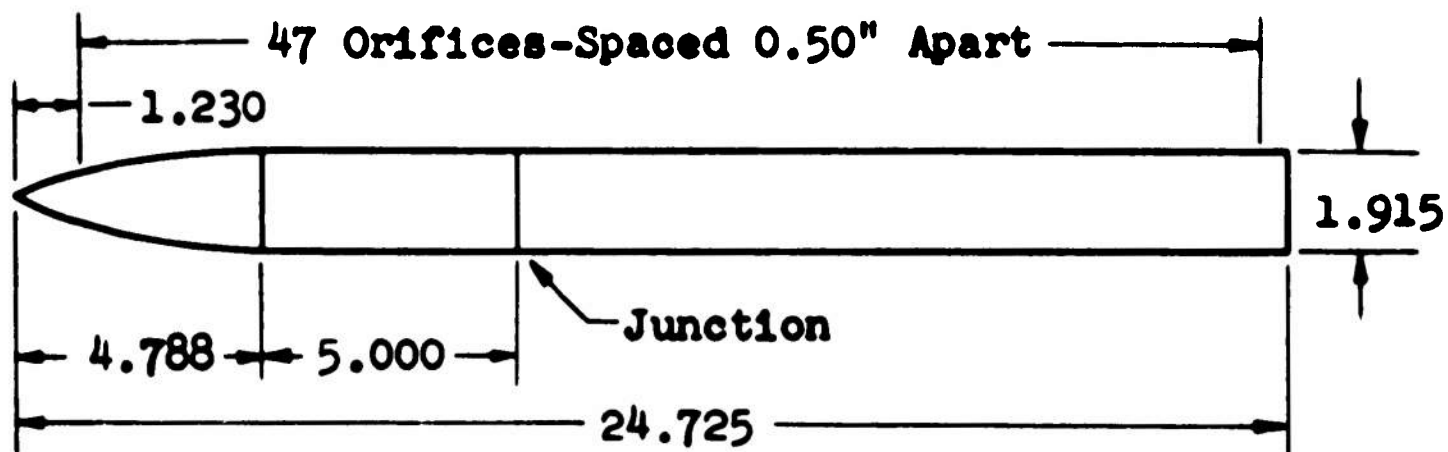
2% Blockage Parabolic Nose-Cylinder Model

Fig. 4 Basic Dimensions of Models Tested in 1-Foot Transonic Tunnel

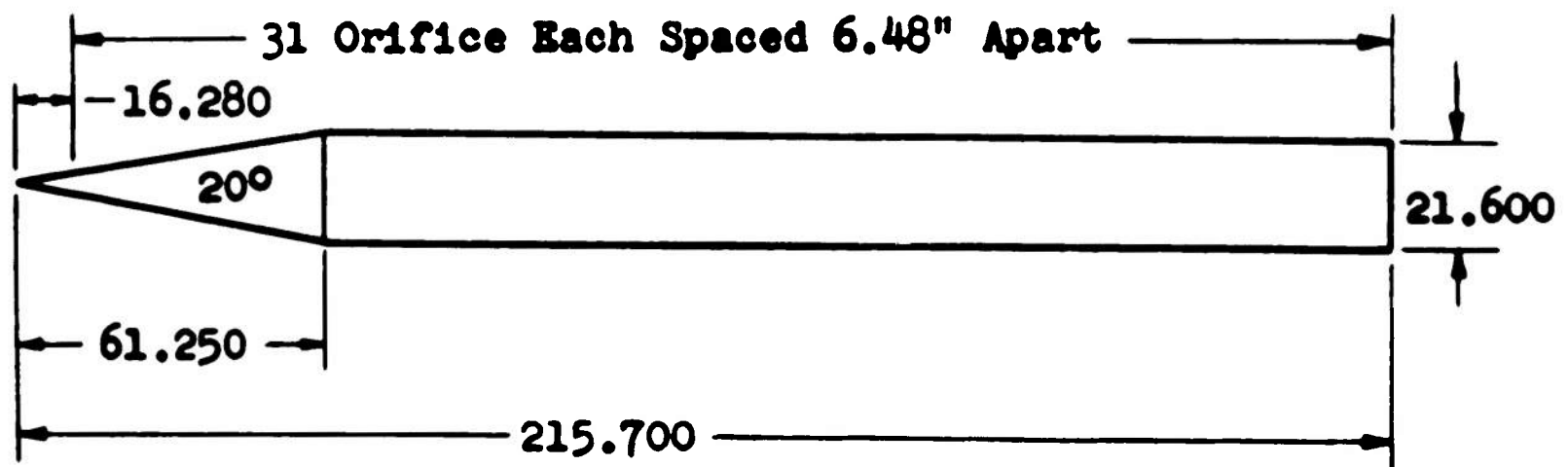
All Dimensions in Inches



0.008% Blockage Cone-Cylinder Model



0.008% Blockage Parabolic Nose-Cylinder Model



1.000% Blockage Cone-Cylinder Model

Fig. 5 Basic Dimensions of Models Tested in 16-Foot Transonic Circuit

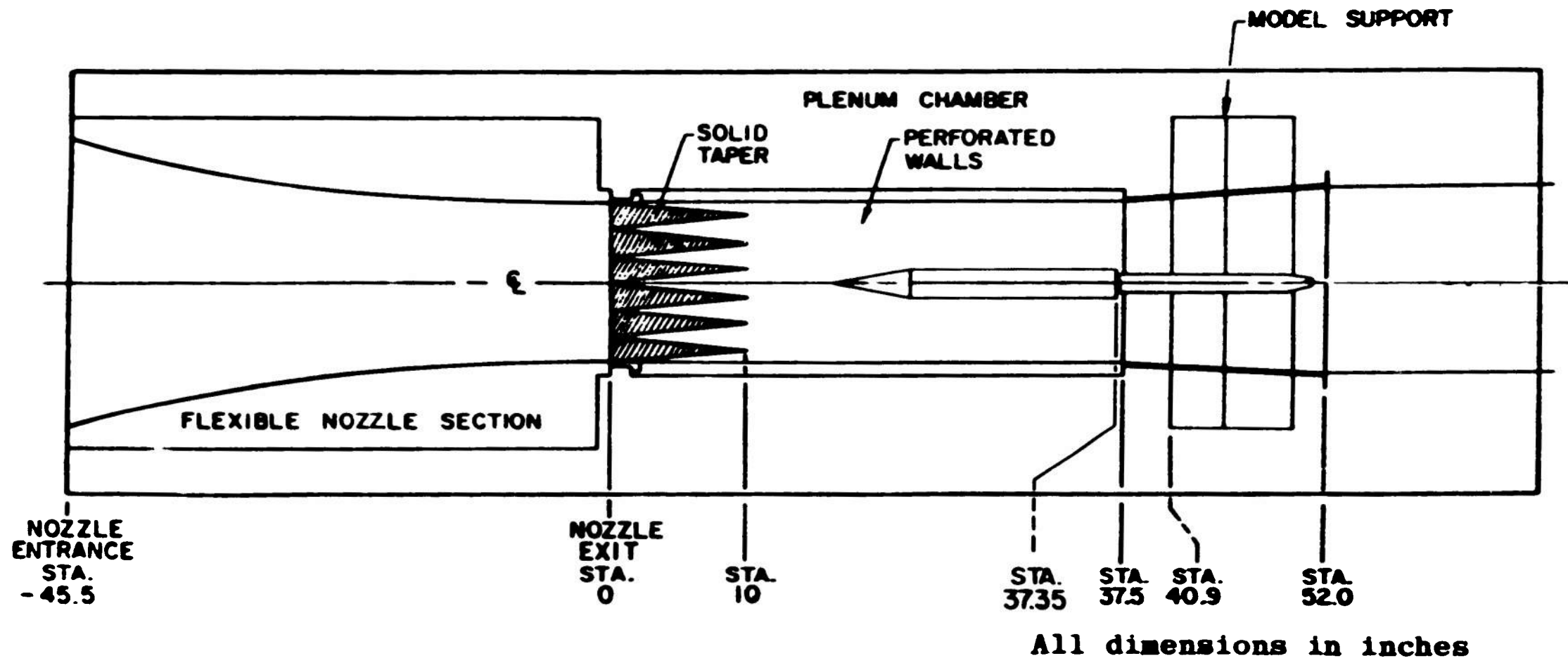


Fig. 6 Installation of Model and Support in 1-Foot Transonic Tunnel

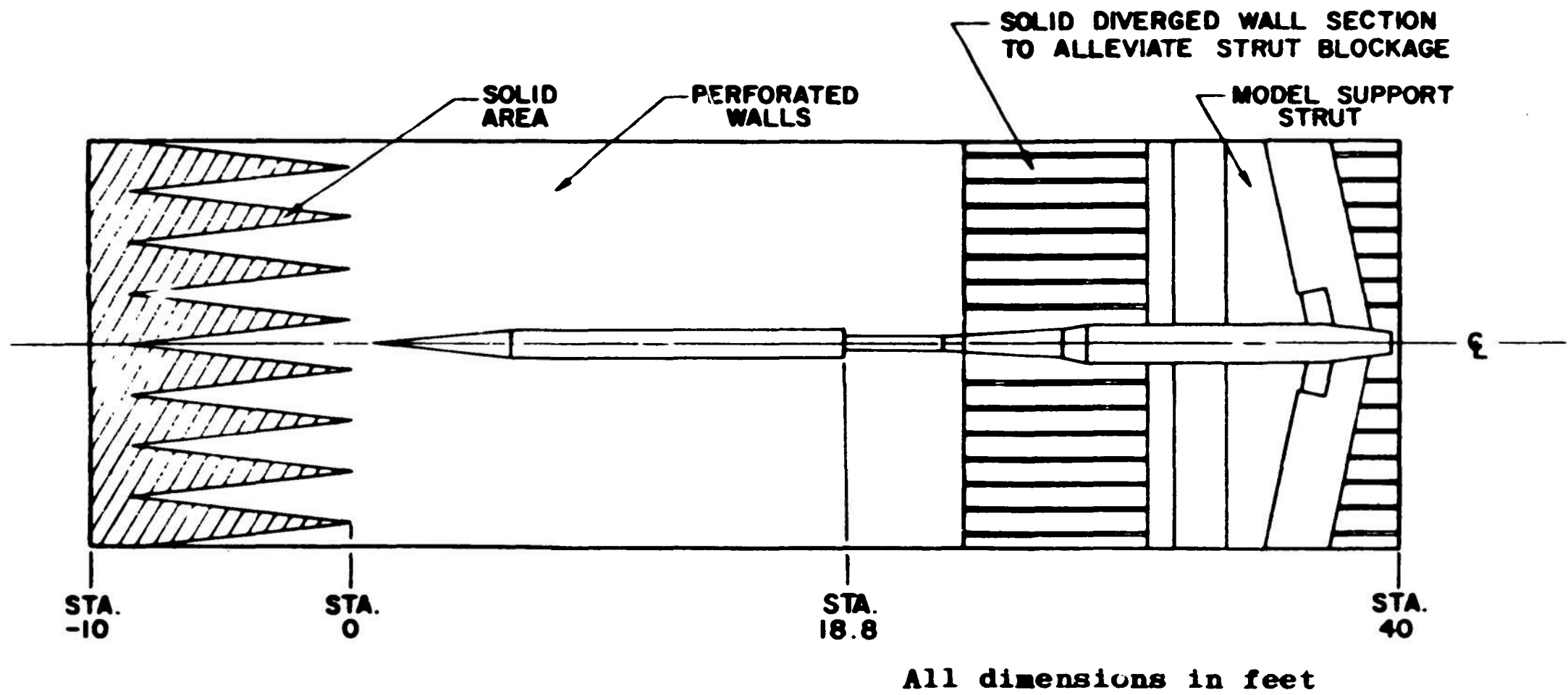
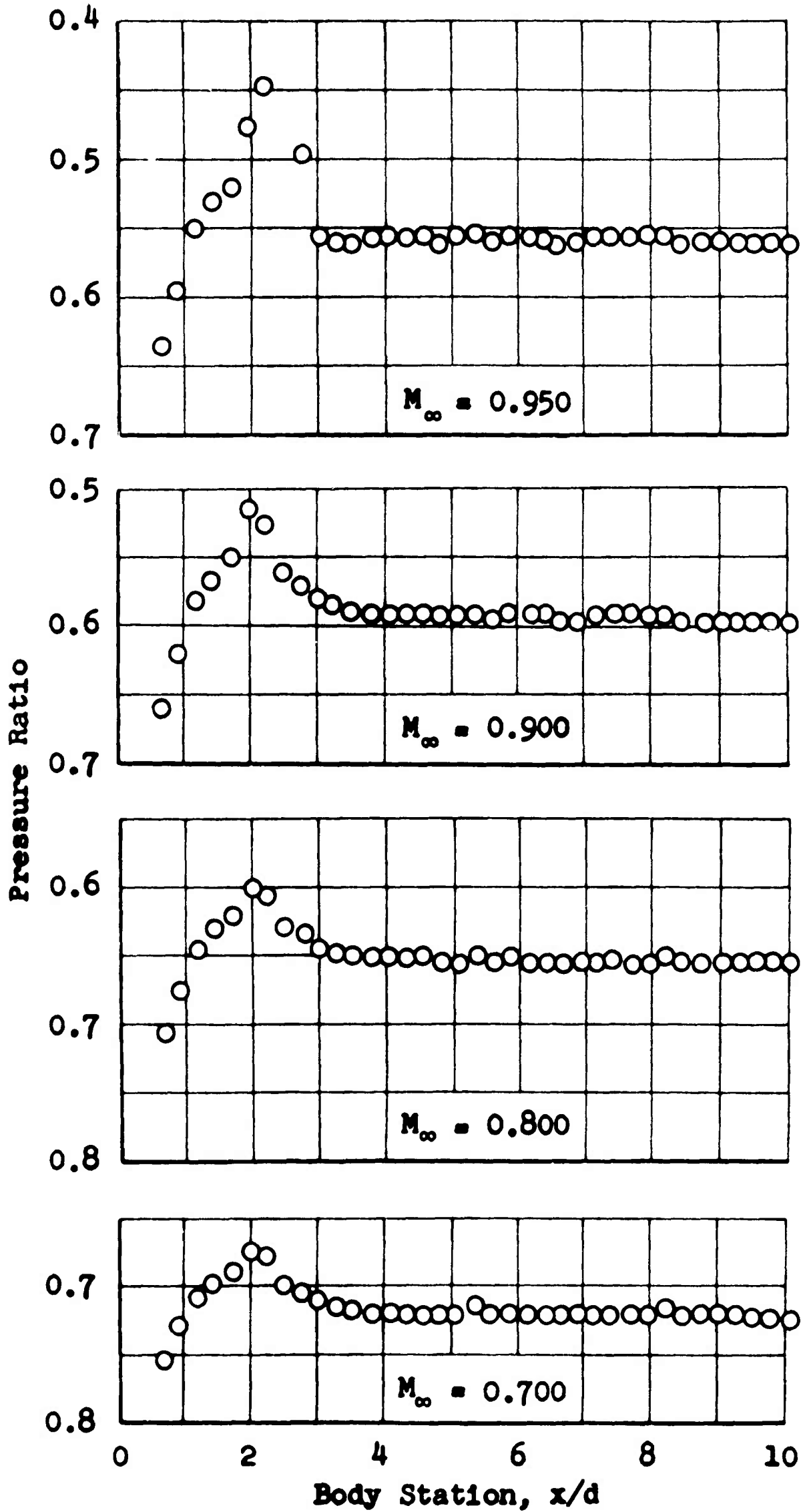
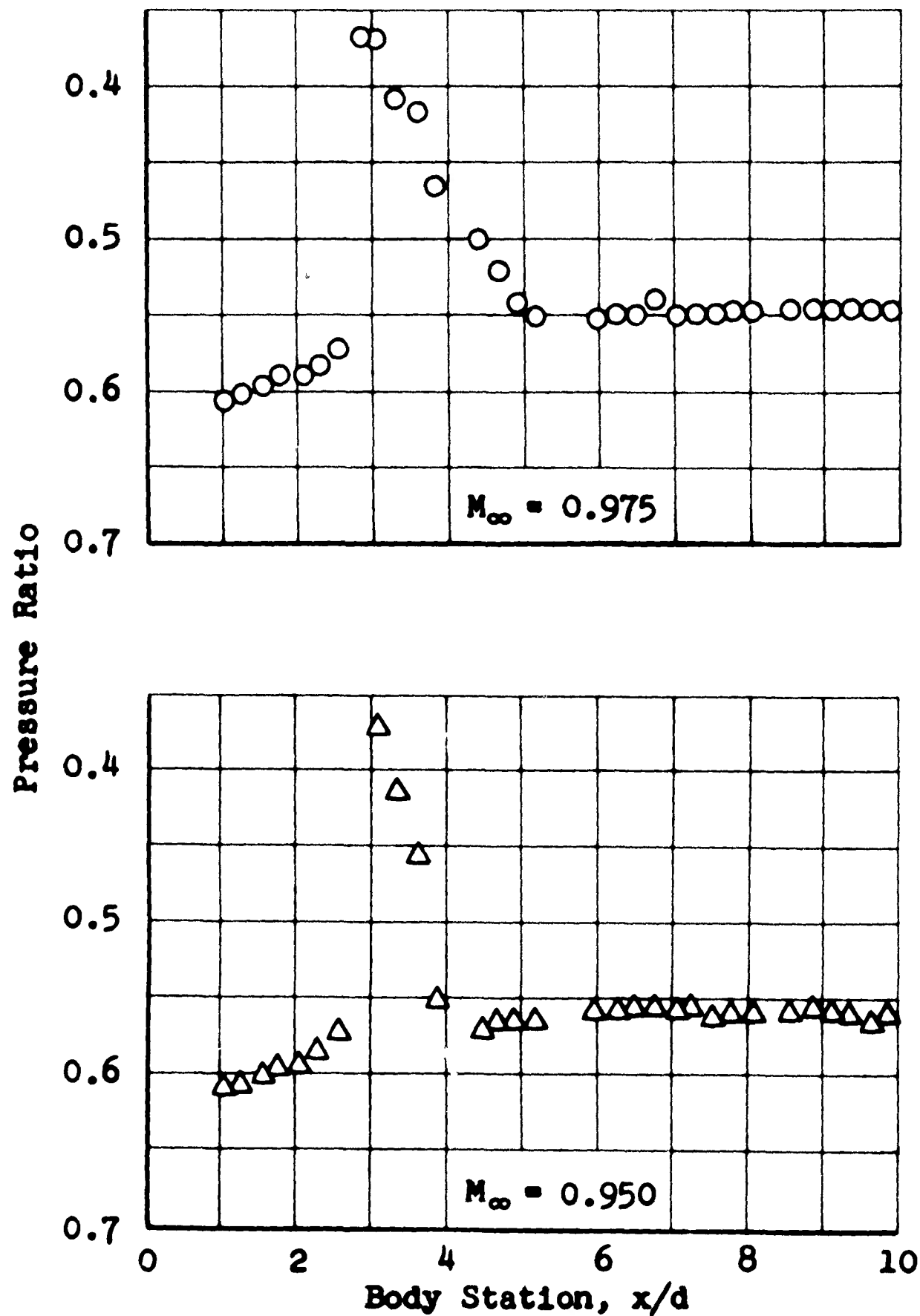


Fig. 7 Installation of Model and Support in 16-Foot Transonic Circuit



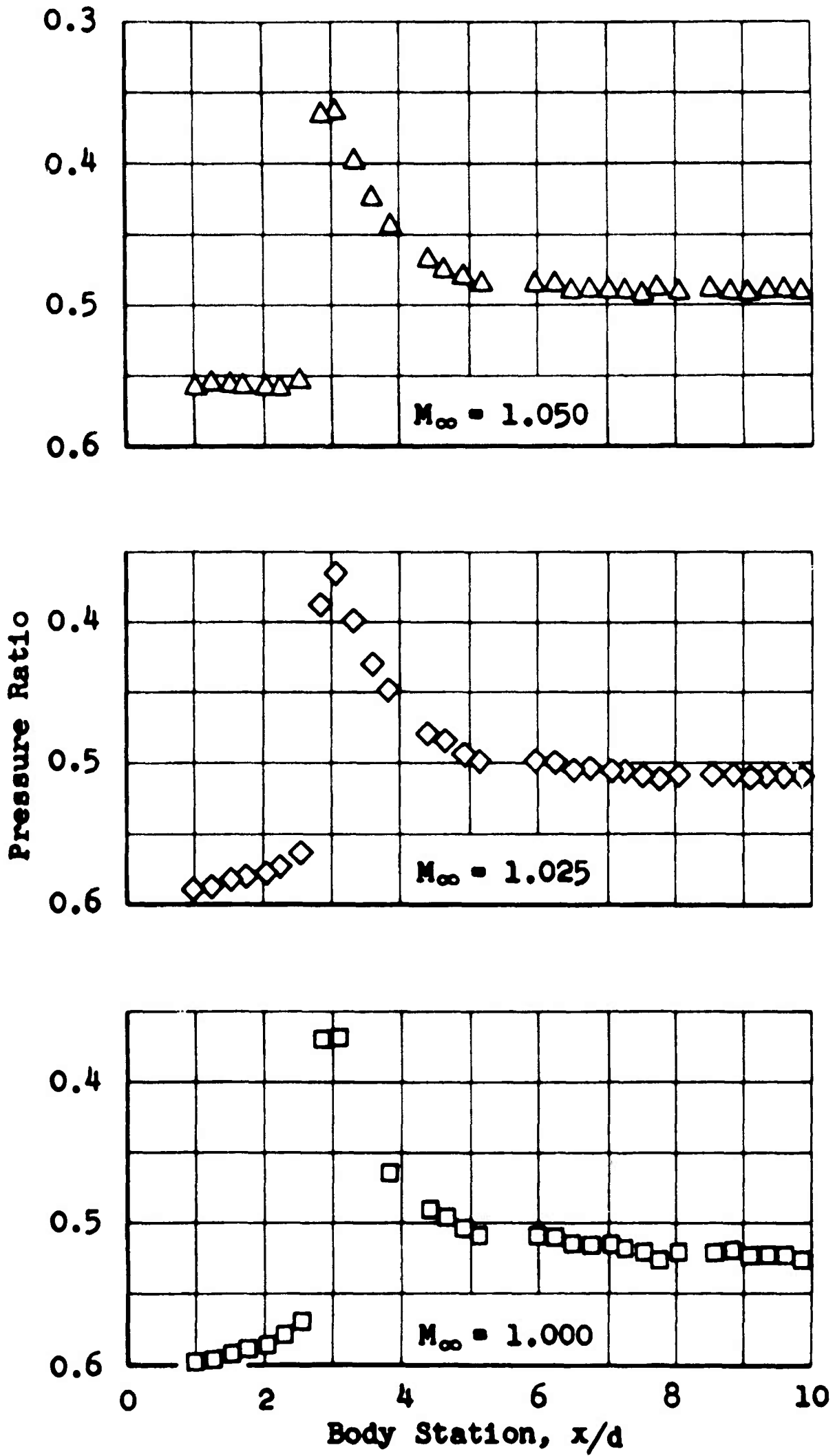
a. $M = 0.700, 0.800, \text{ and } 0.900$

Fig. 8 Body Pressure Distributions on the 0.008-Percent Blockage, 20° Cone-Cylinder Model in the 16T



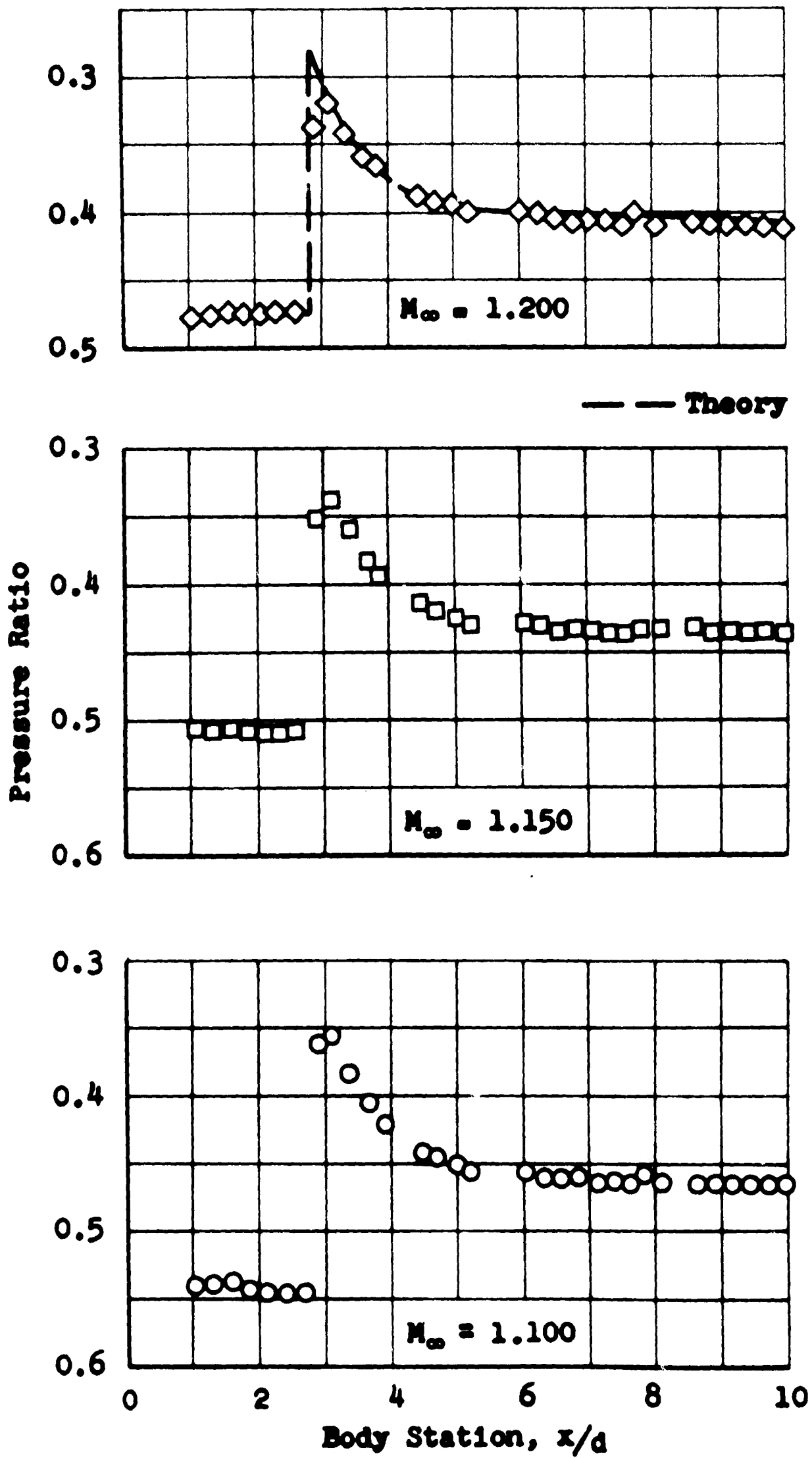
b. $M = 0.950$ and 0.975

Fig. 8 Continued



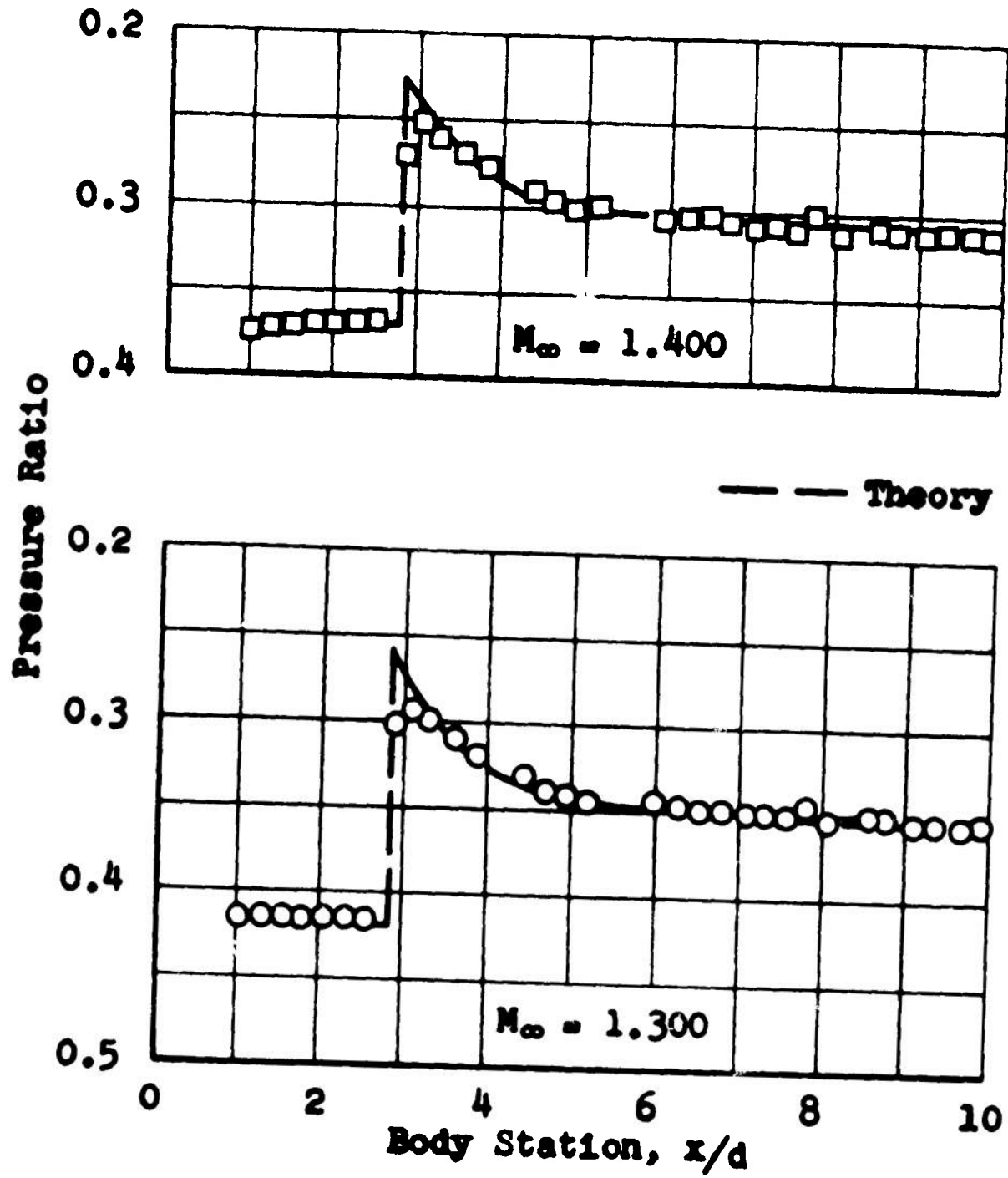
c. $M = 1.000, 1.025, \text{ and } 1.050$

Fig. 8 Continued



d. $M = 1.100, 1.150, \text{ and } 1.200$

Fig. 8 Continued



e. $M = 1.300$ and 1.400

Fig. 8 Concluded

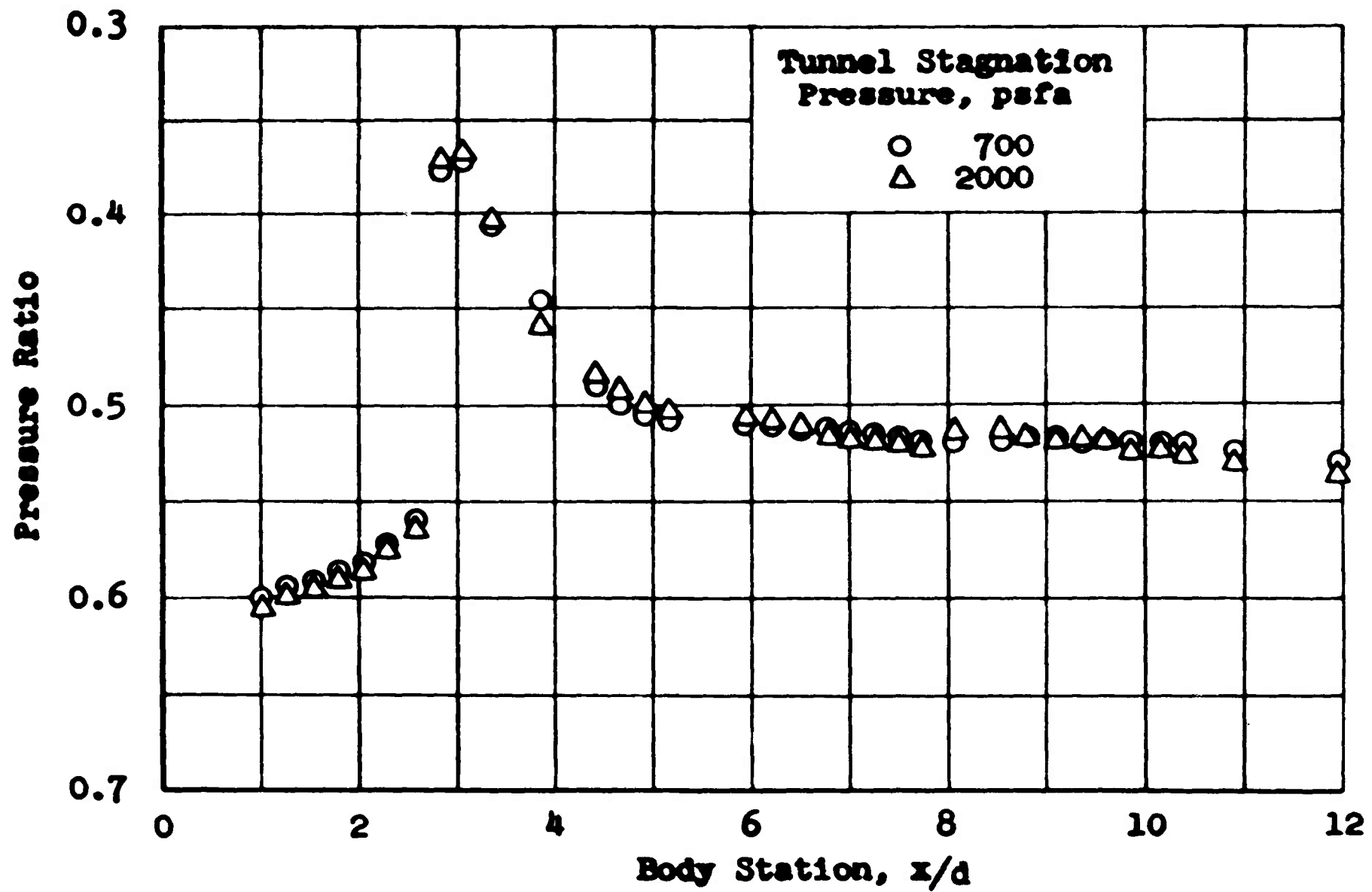


Fig. 9 Comparison of Body Pressure Distributions on the 0.008-Percent Blockage, 20° Cone-Cylinder Model at Tunnel Stagnation Pressures of 700 and 2000 psfa and Mach Number 1.00

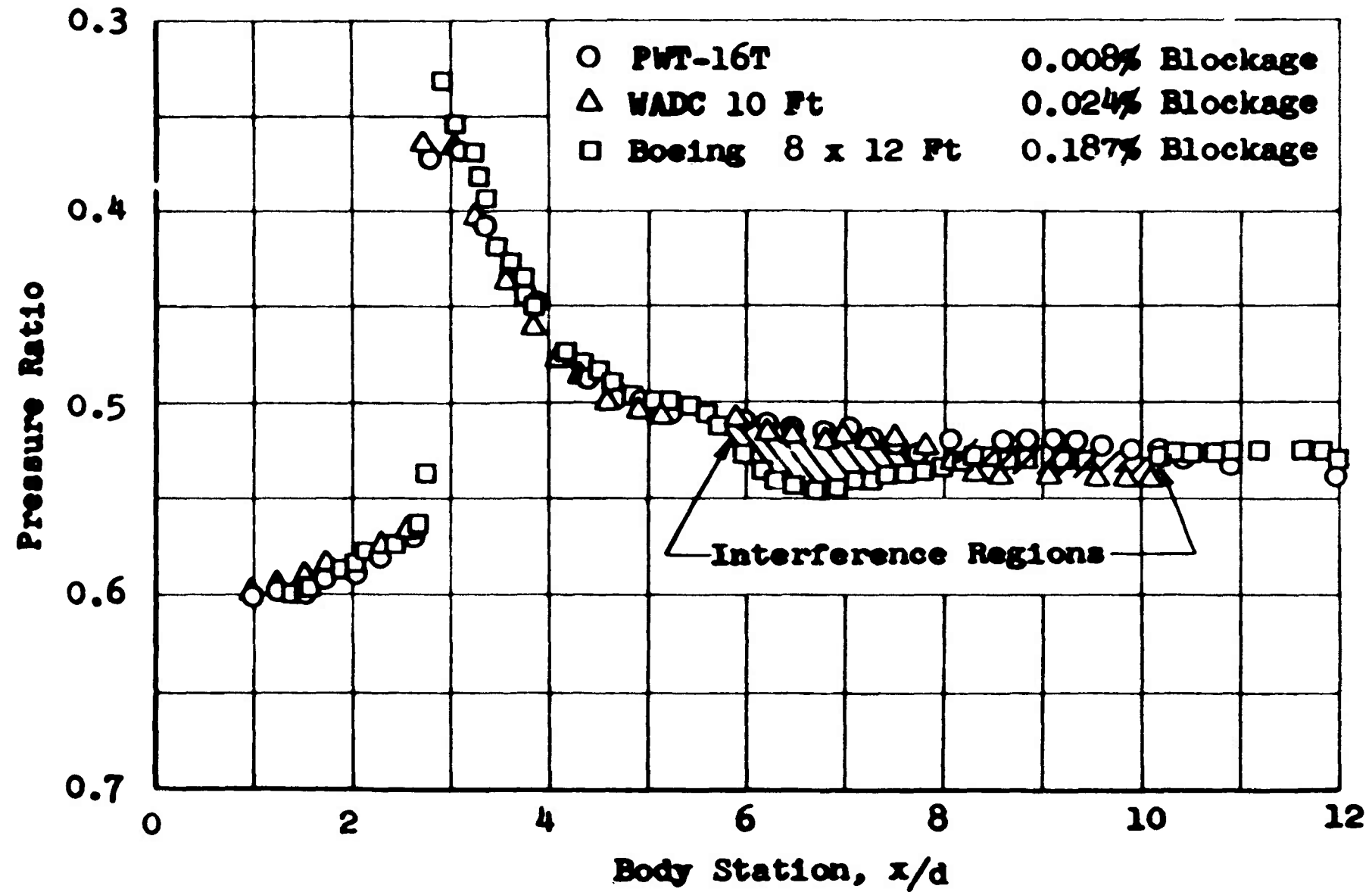


Fig. 10 Comparison of Body Pressure Distributions on Several Small Blockage, 20° Cone-Cylinder Model at Mach Number 1.00

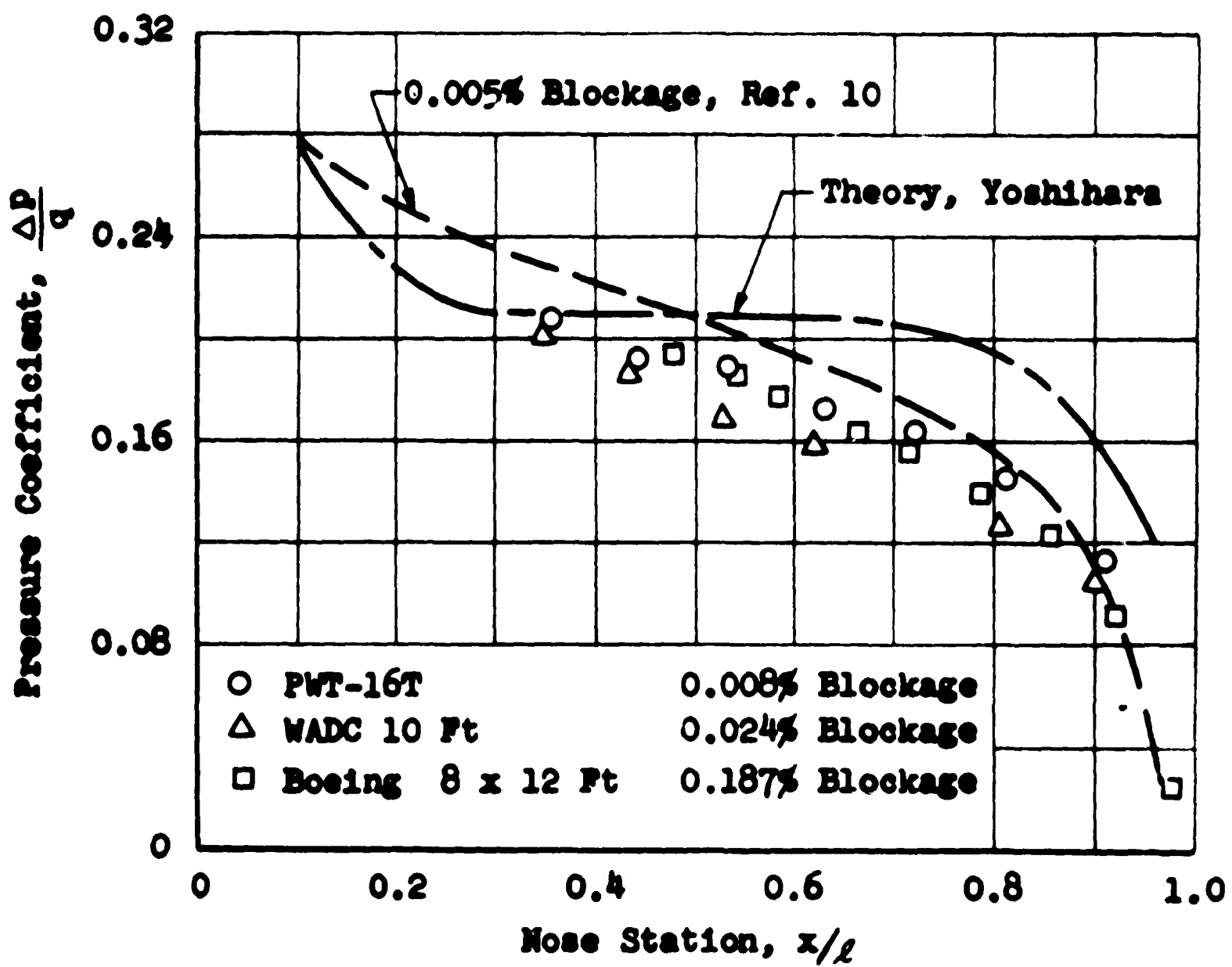
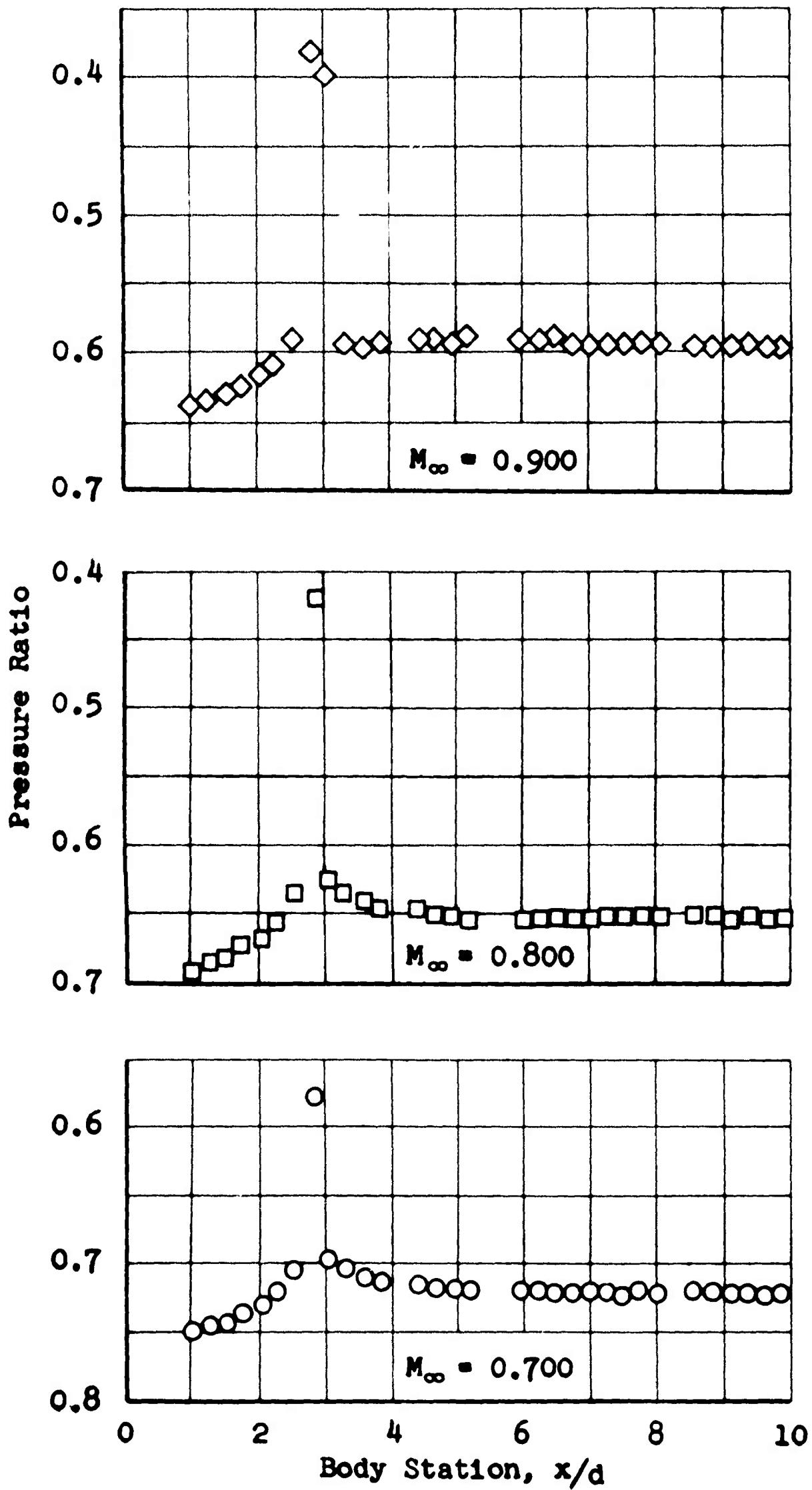
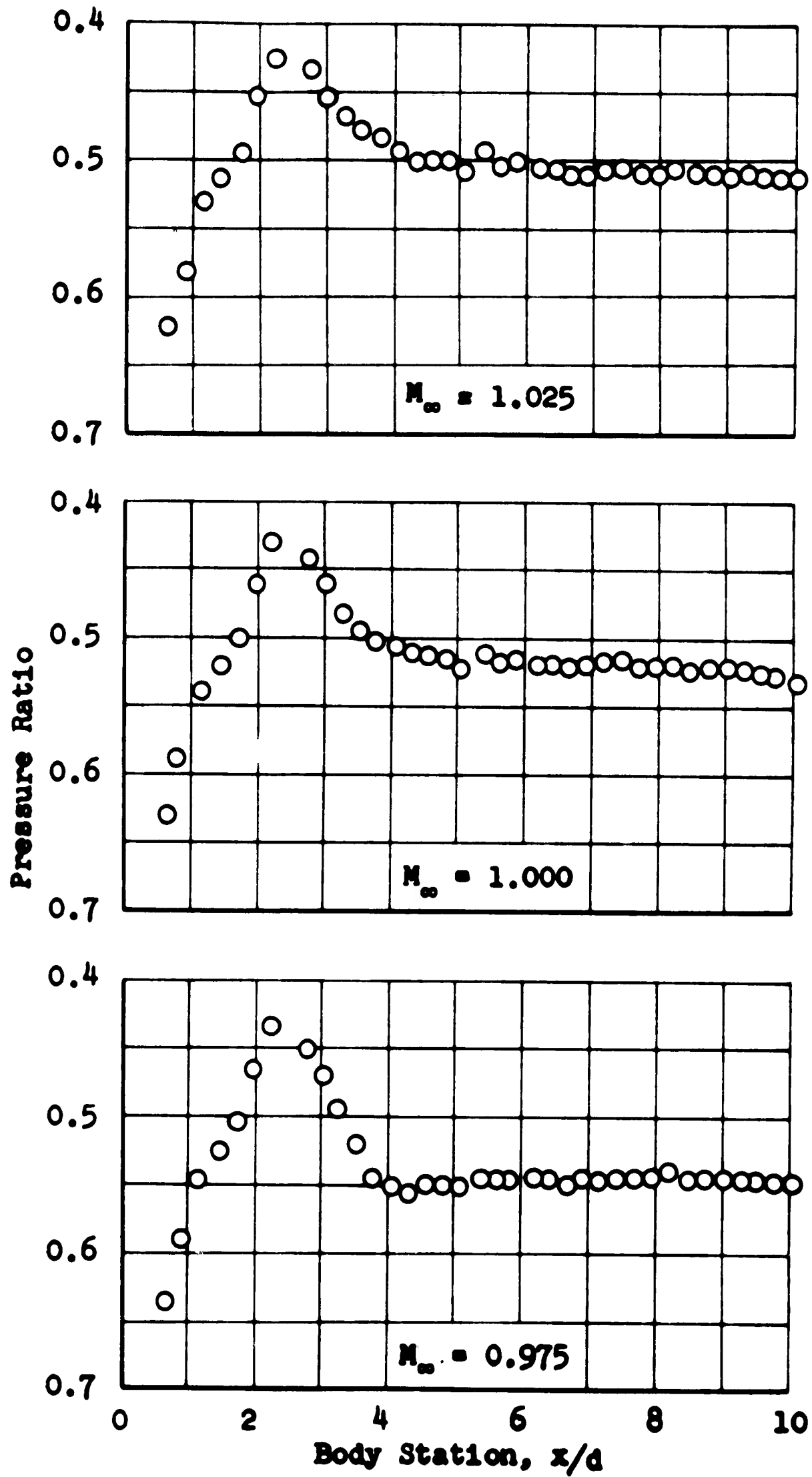


Fig. 11 Comparison of Experimental and Theoretical Pressure Distributions on 20° Conical Bodies at Mach Number 1.00



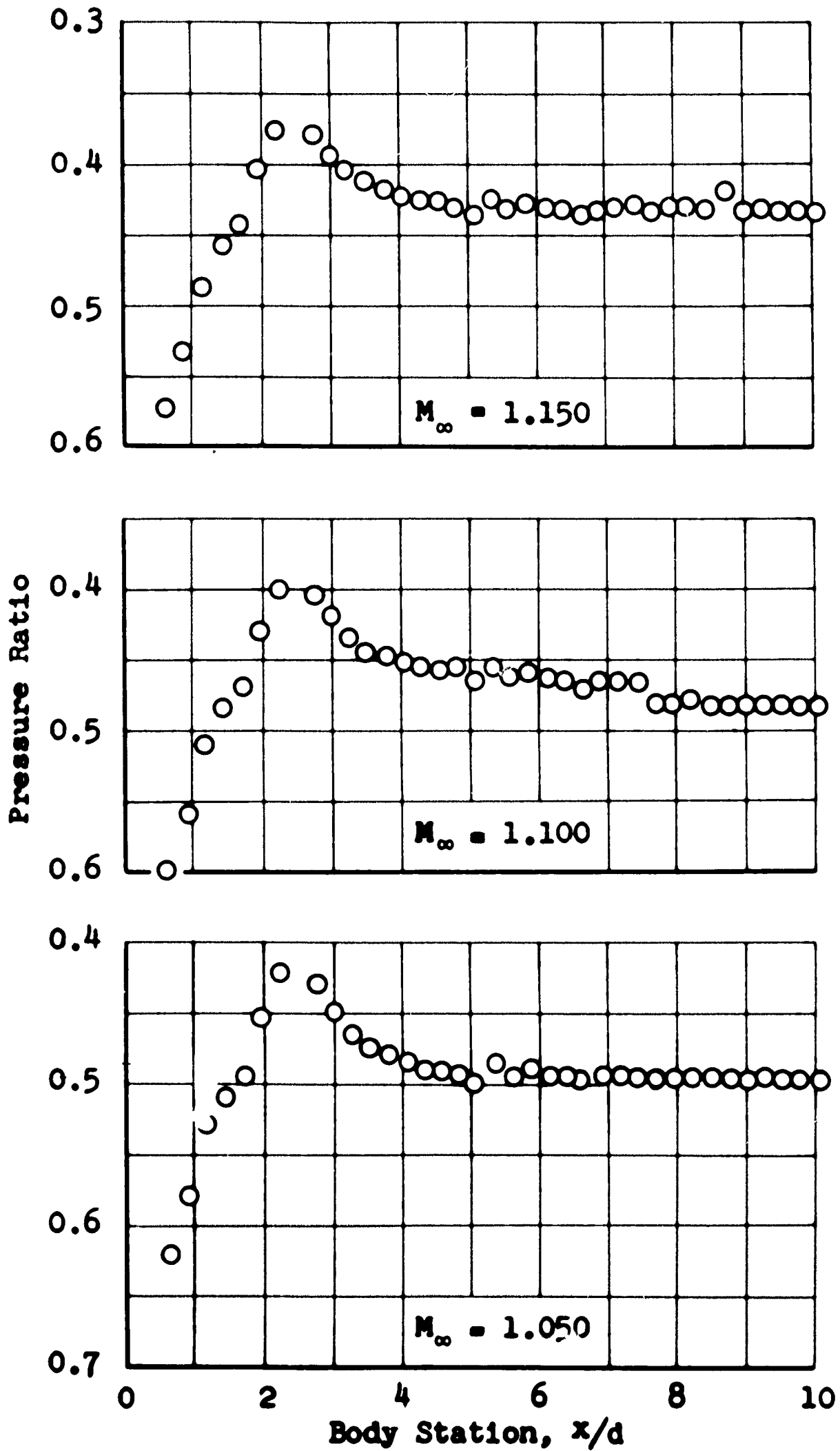
a. $M = 0.700, 0.800, 0.900, \text{ and } 0.950$

Fig. 12 Body Pressure Distributions on the 0.008-Percent Blockage, Parabolic Nose-Cylinder Model in the 16T



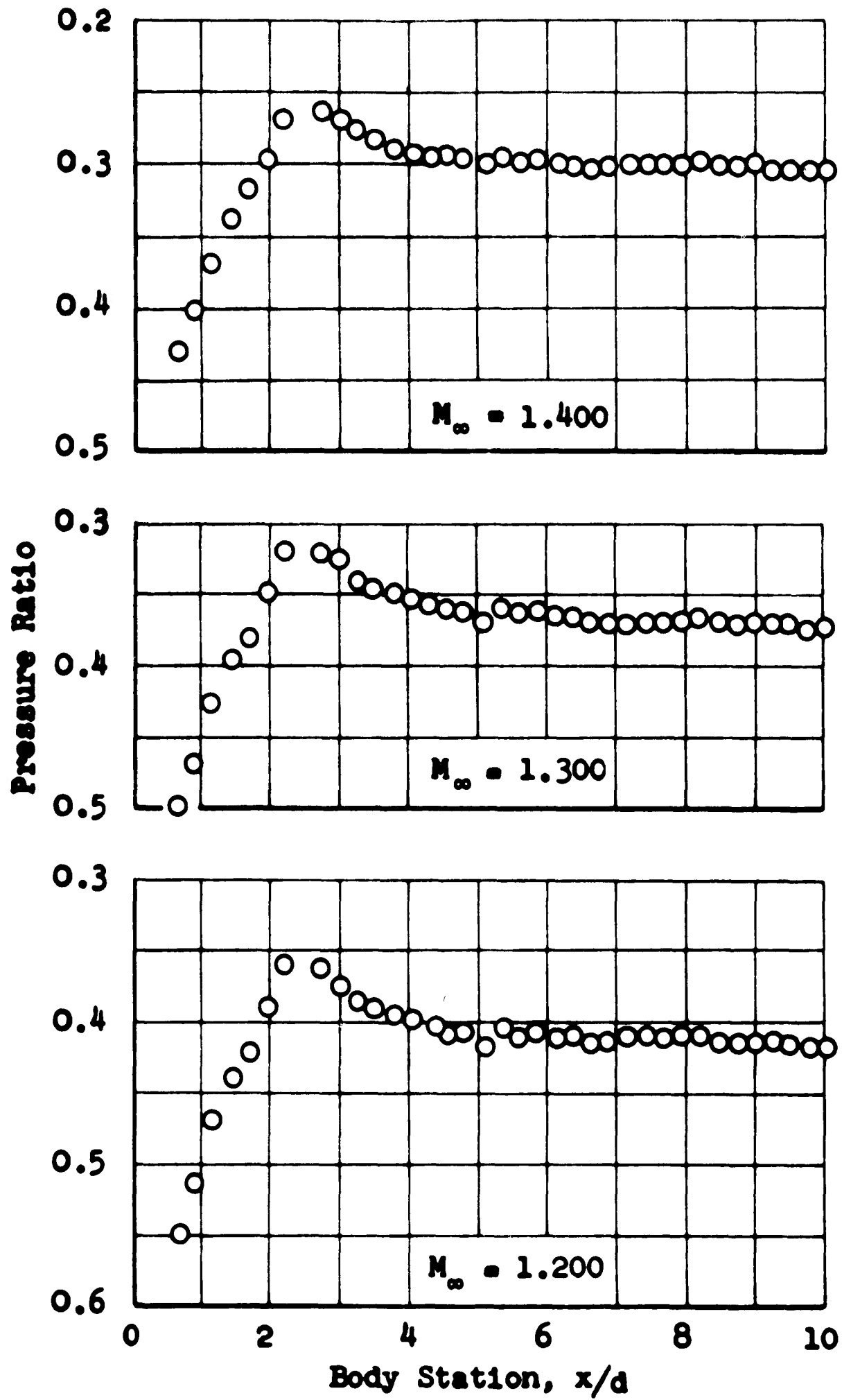
b. $M = 0.975, 1.000, \text{ and } 1.025$

Fig. 12 Continued



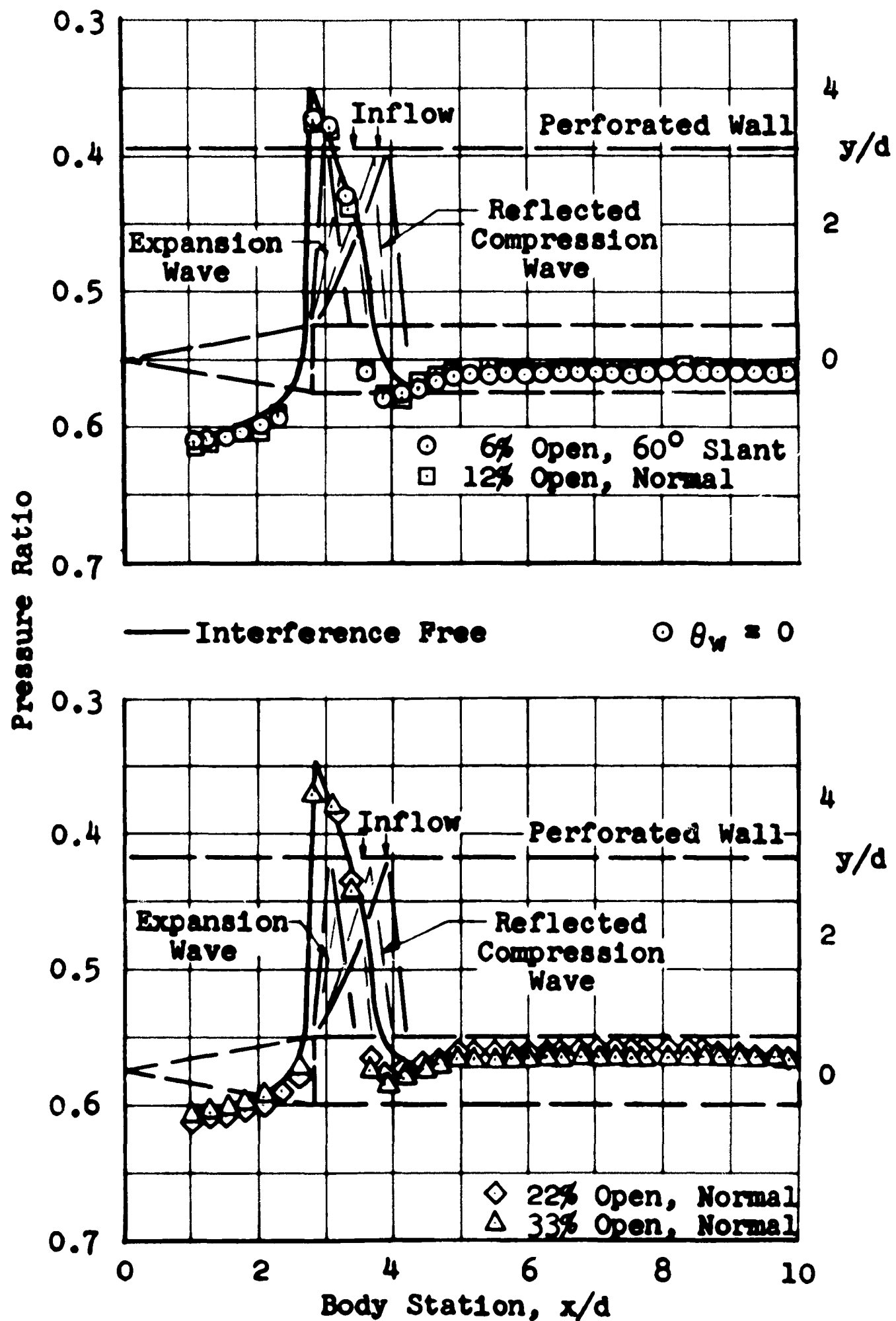
c. $M = 1.050, 1.100, \text{ and } 1.150$

Fig. 12 Continued



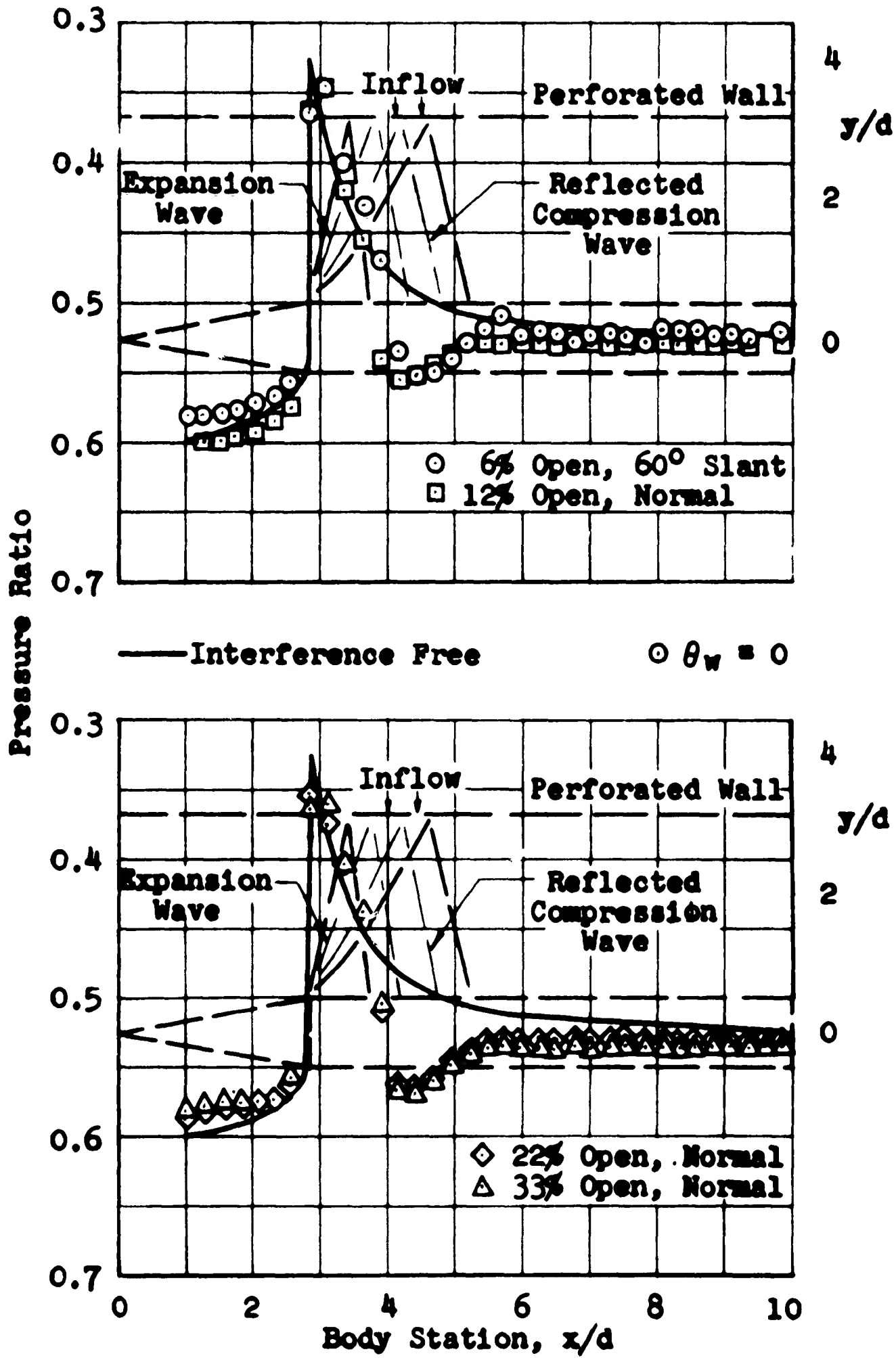
d. $M = 1.200, 1.300, \text{ and } 1.400$

Fig. 12 Concluded



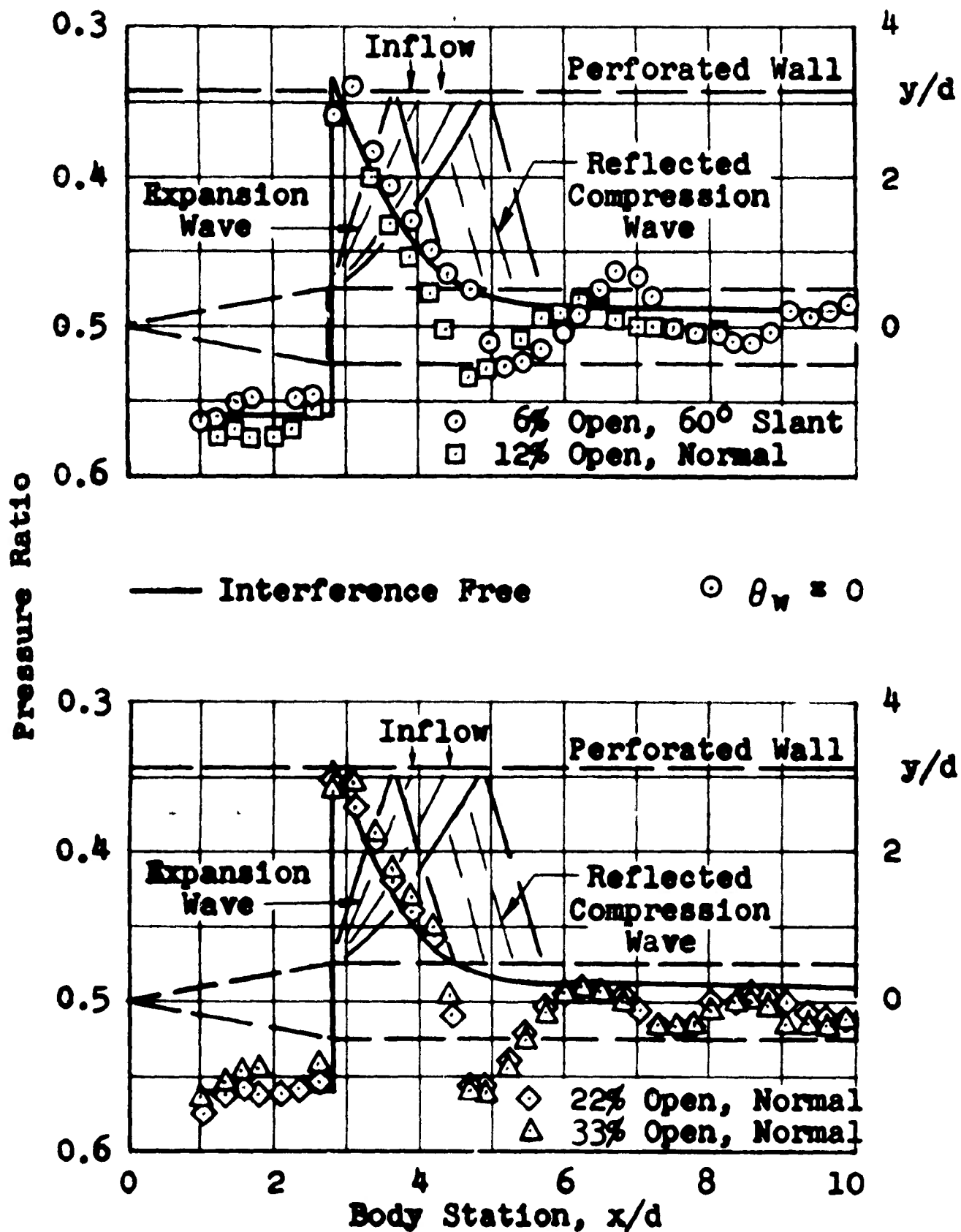
a. $M = 0.95$

Fig. 13 Body Pressure Distributions on the 2-Percent Blockage, 20° Cone-Cylinder Model in the 1T-Effect of Wall Geometry



b. M - 1.00

Fig. 13 Continued



c. $M = 1.05$

Fig. 13 Continued

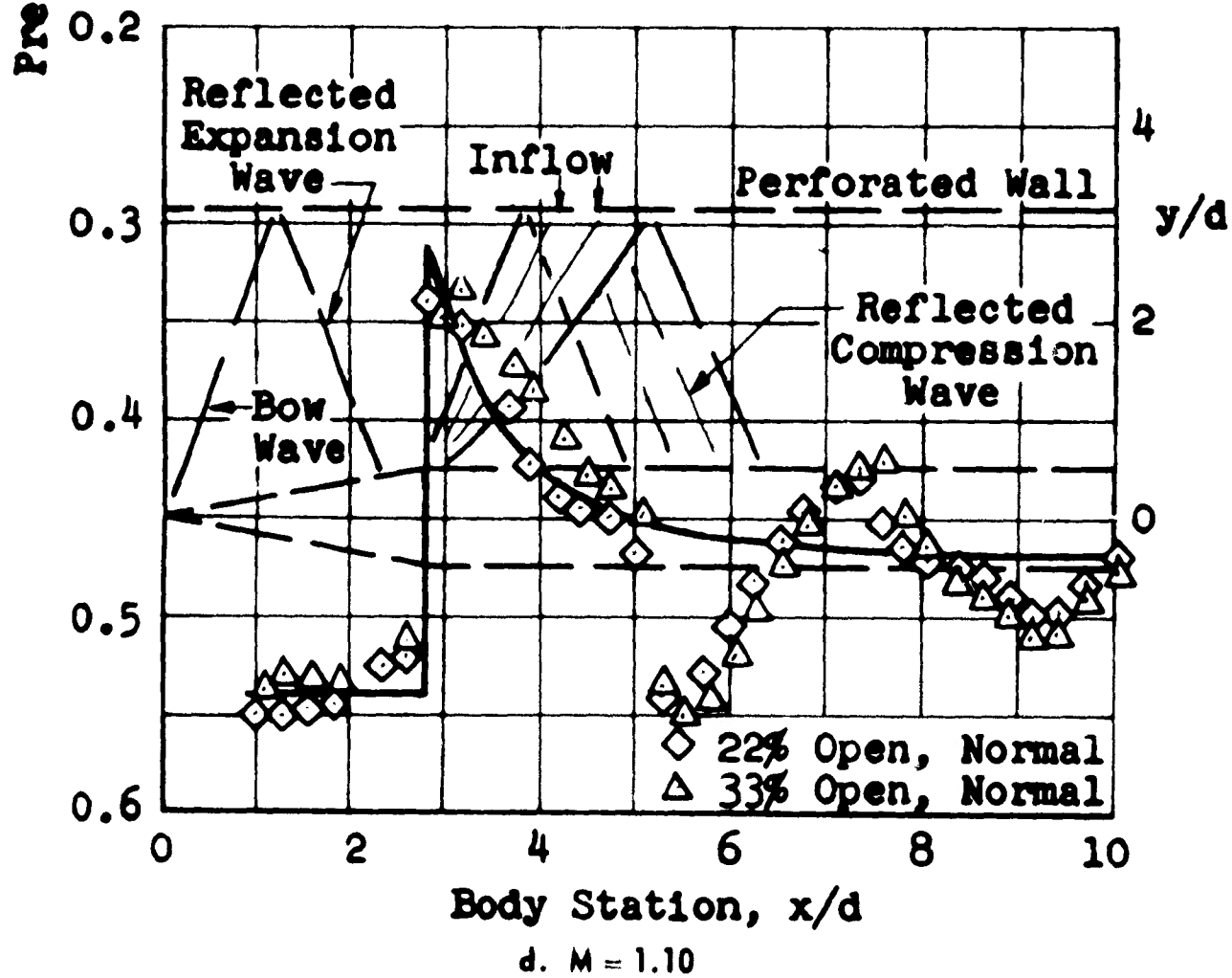
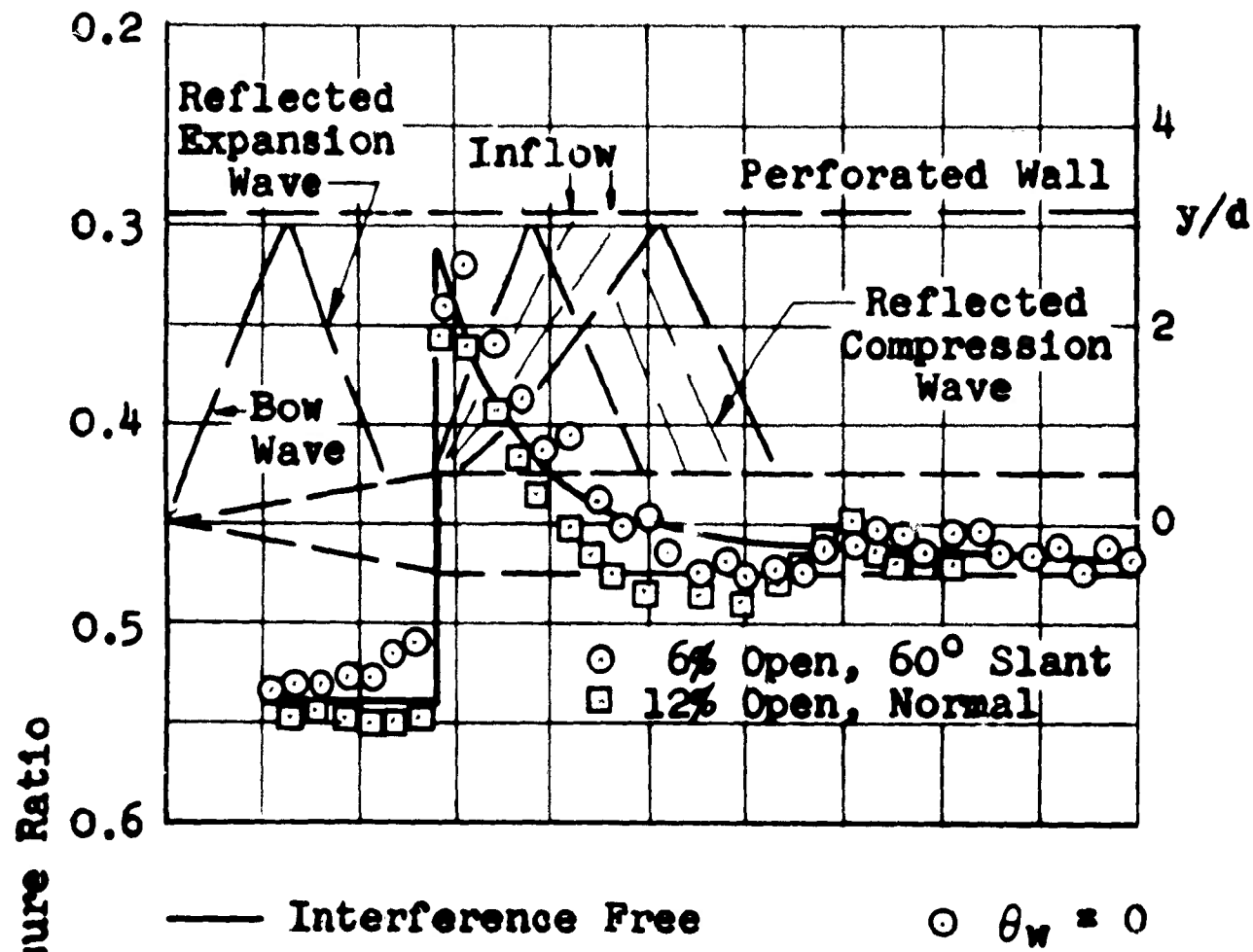
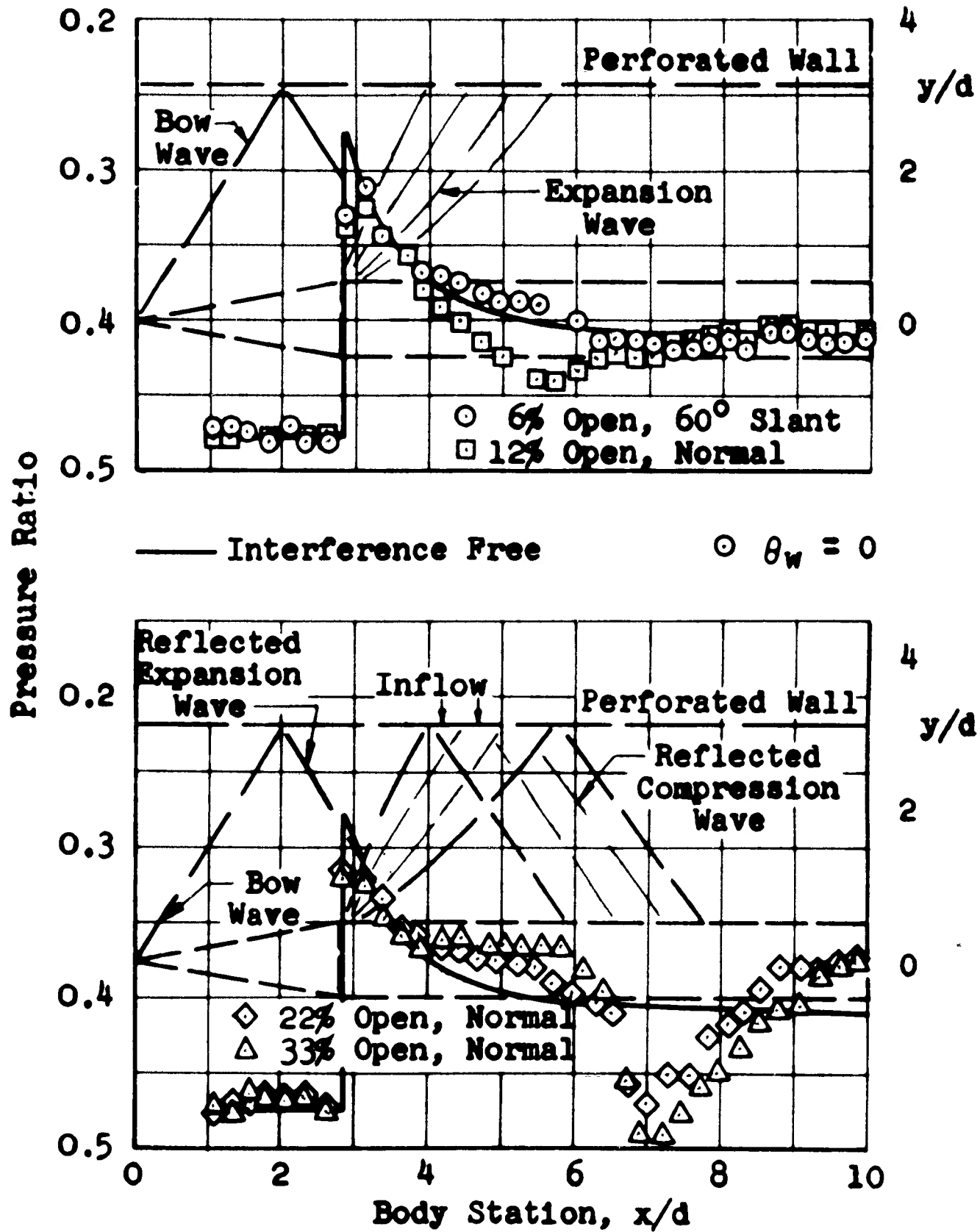
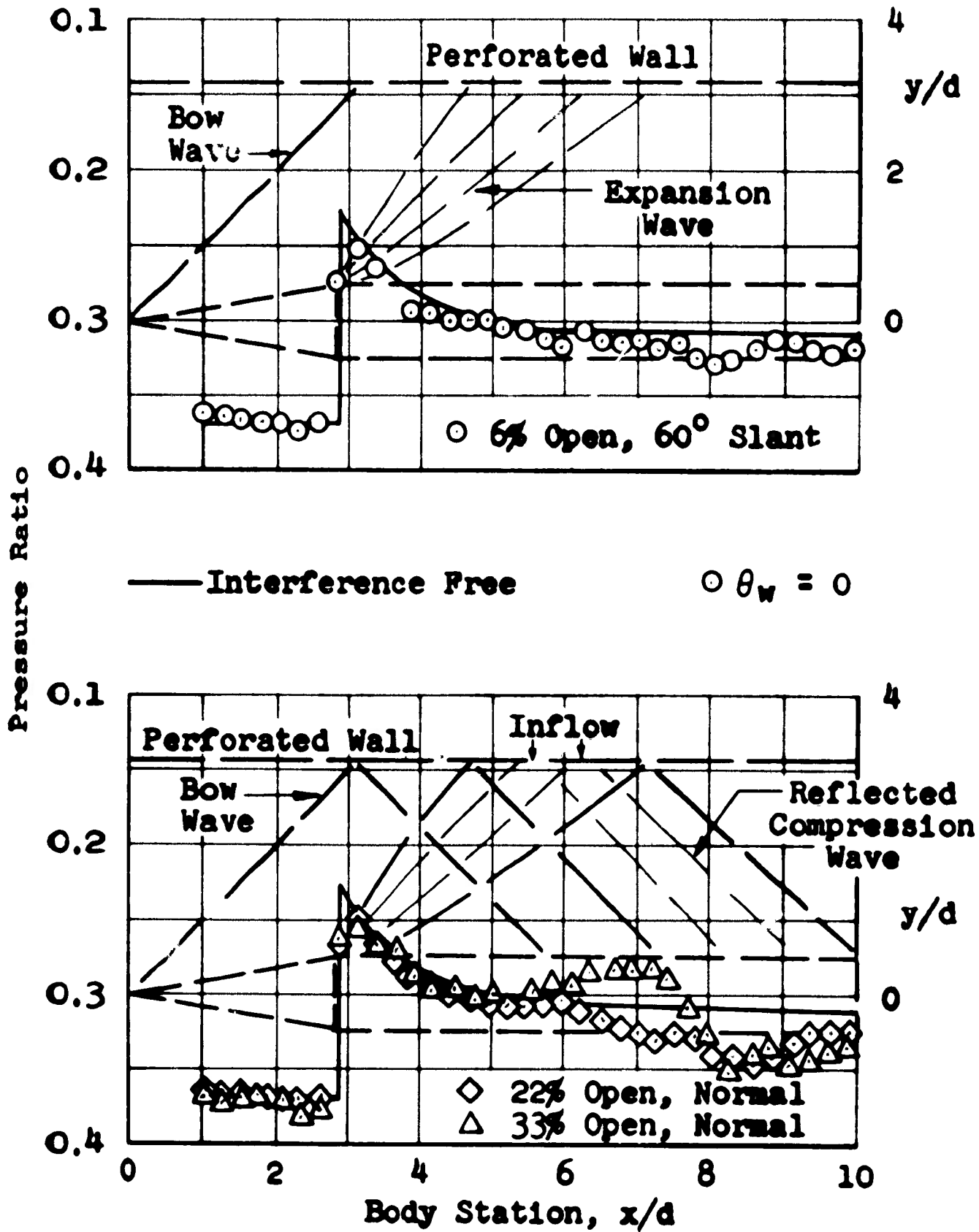


Fig. 13 Continued

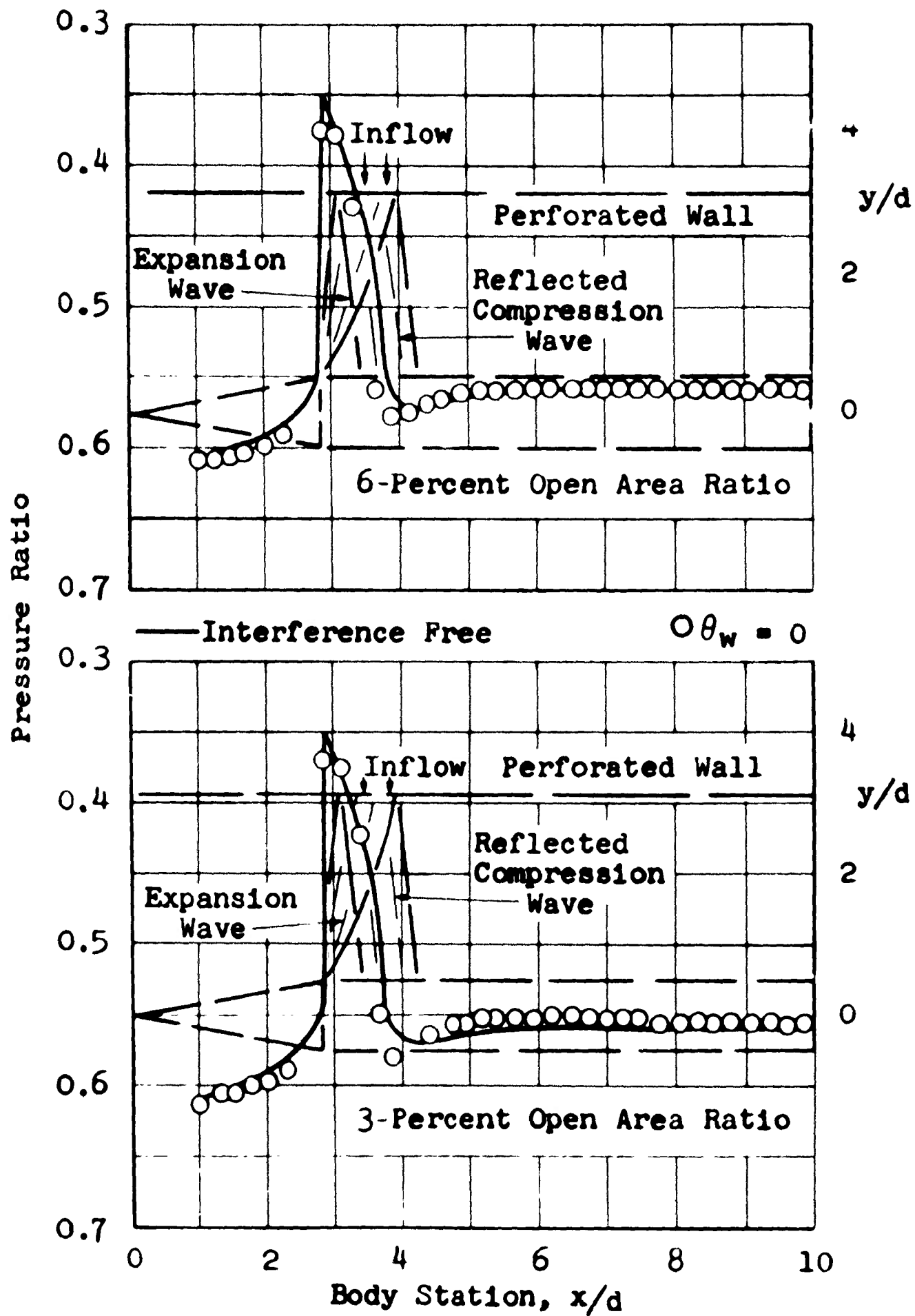


e. $M = 1.20$

Fig. 13 Continued

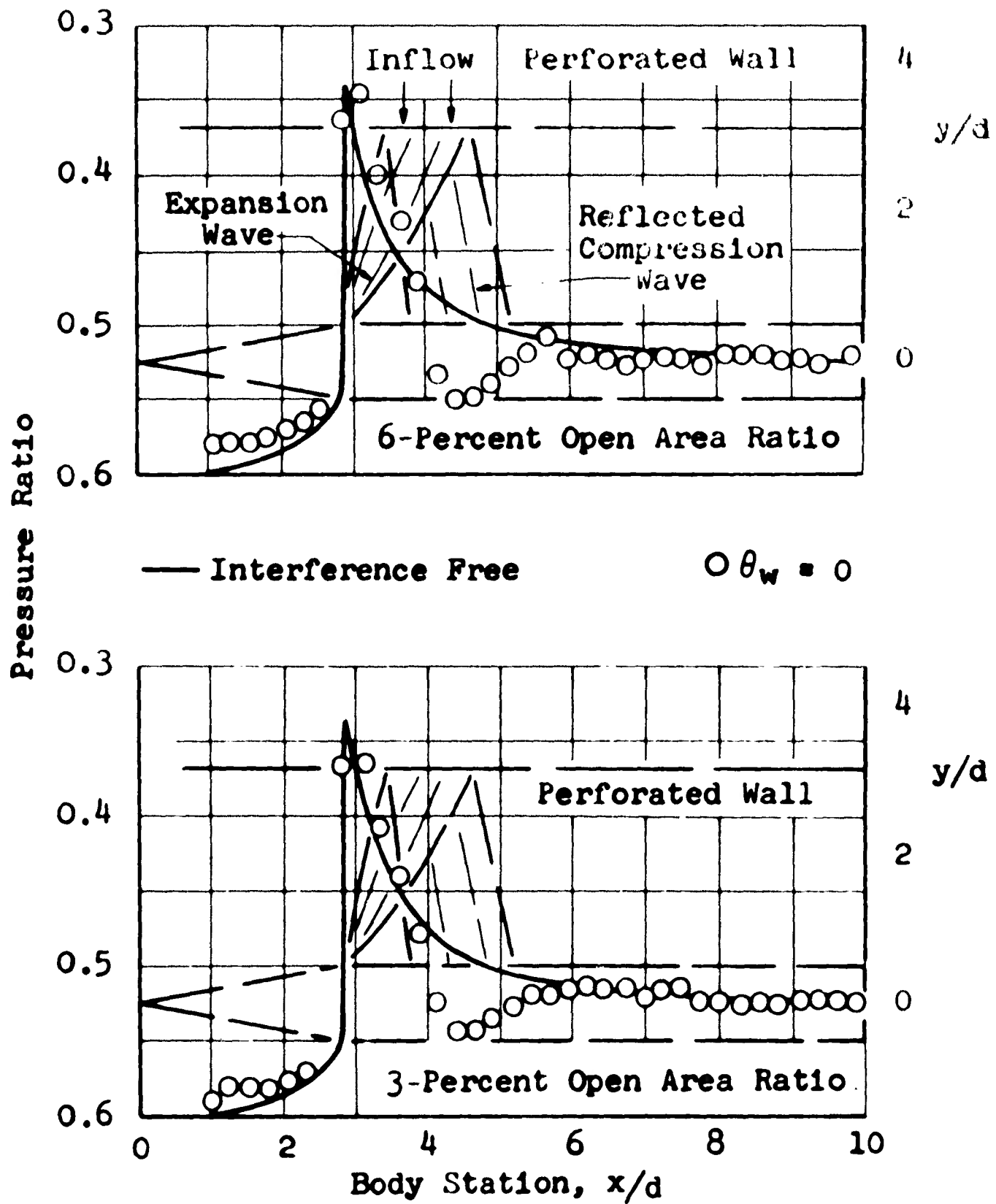


f. $M = 1.40$
 Fig. 13 Concluded



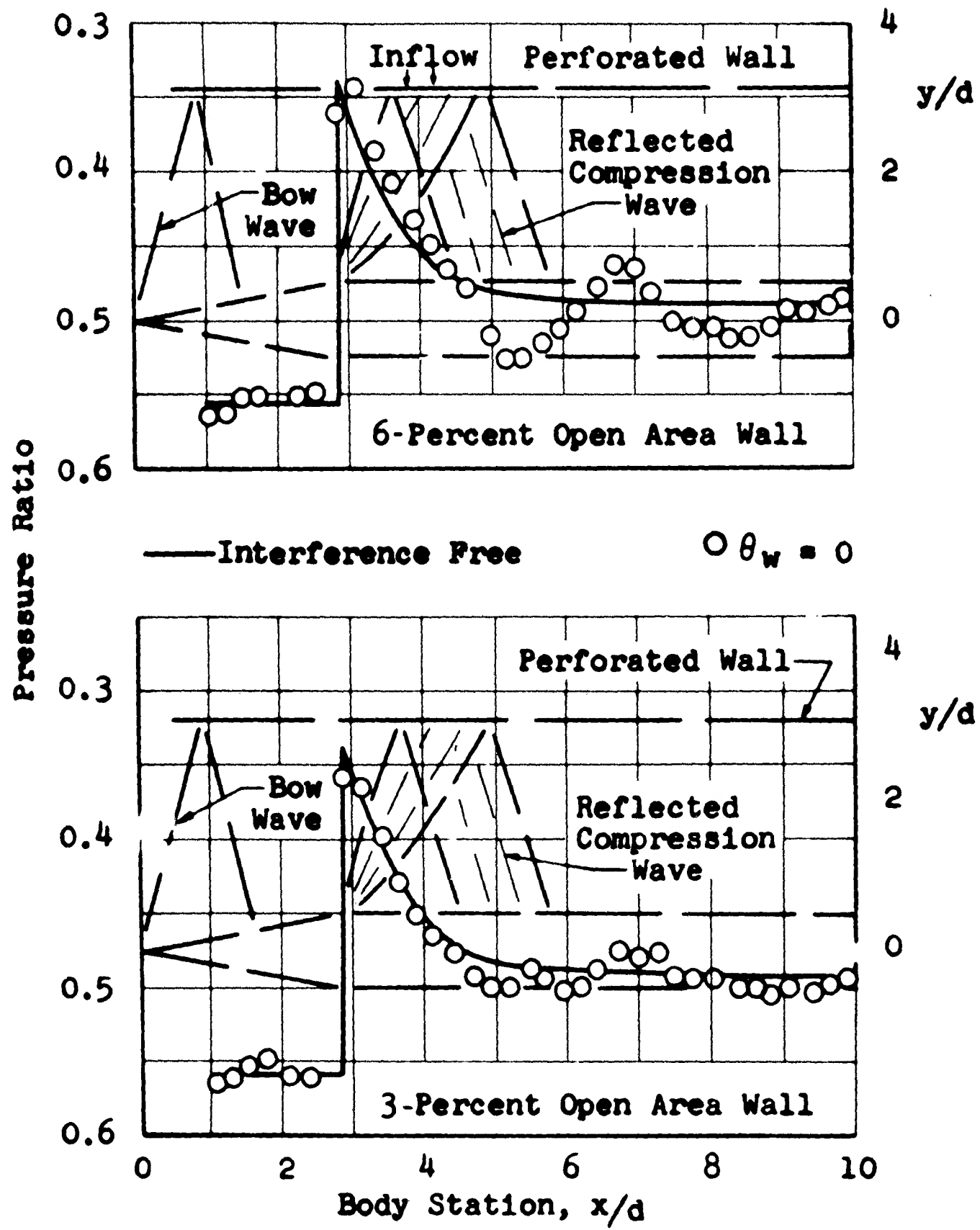
a. M - 0.95

Fig. 14 Body Pressure Distributions on the 2-Percent Blockage, 20° Cone-Cylinder Model in the 1T-Effect of Open-Area Ratio with 60° Inclined-Hole Walls



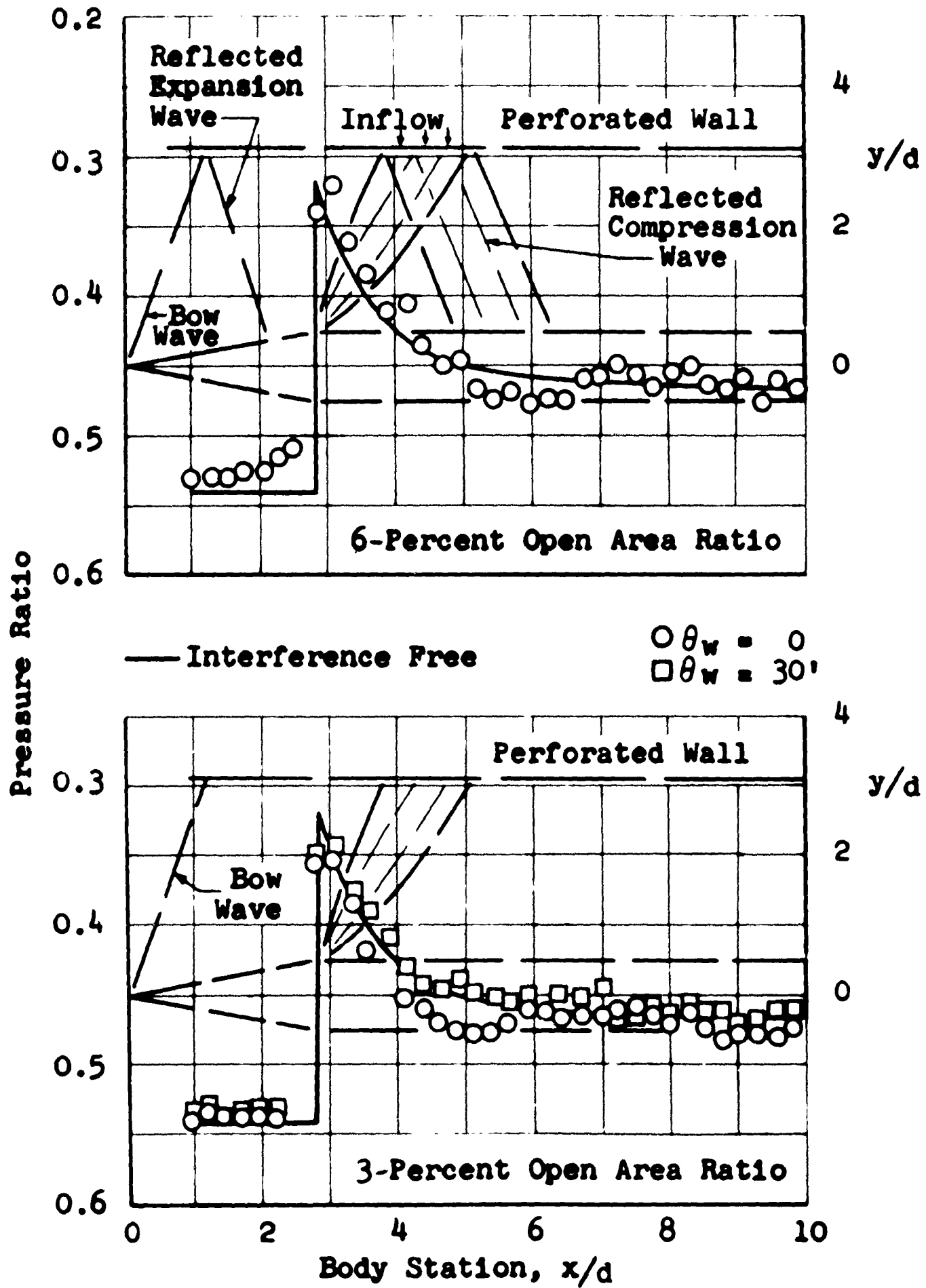
b. $M = 1.00$

Fig. 14 Continued



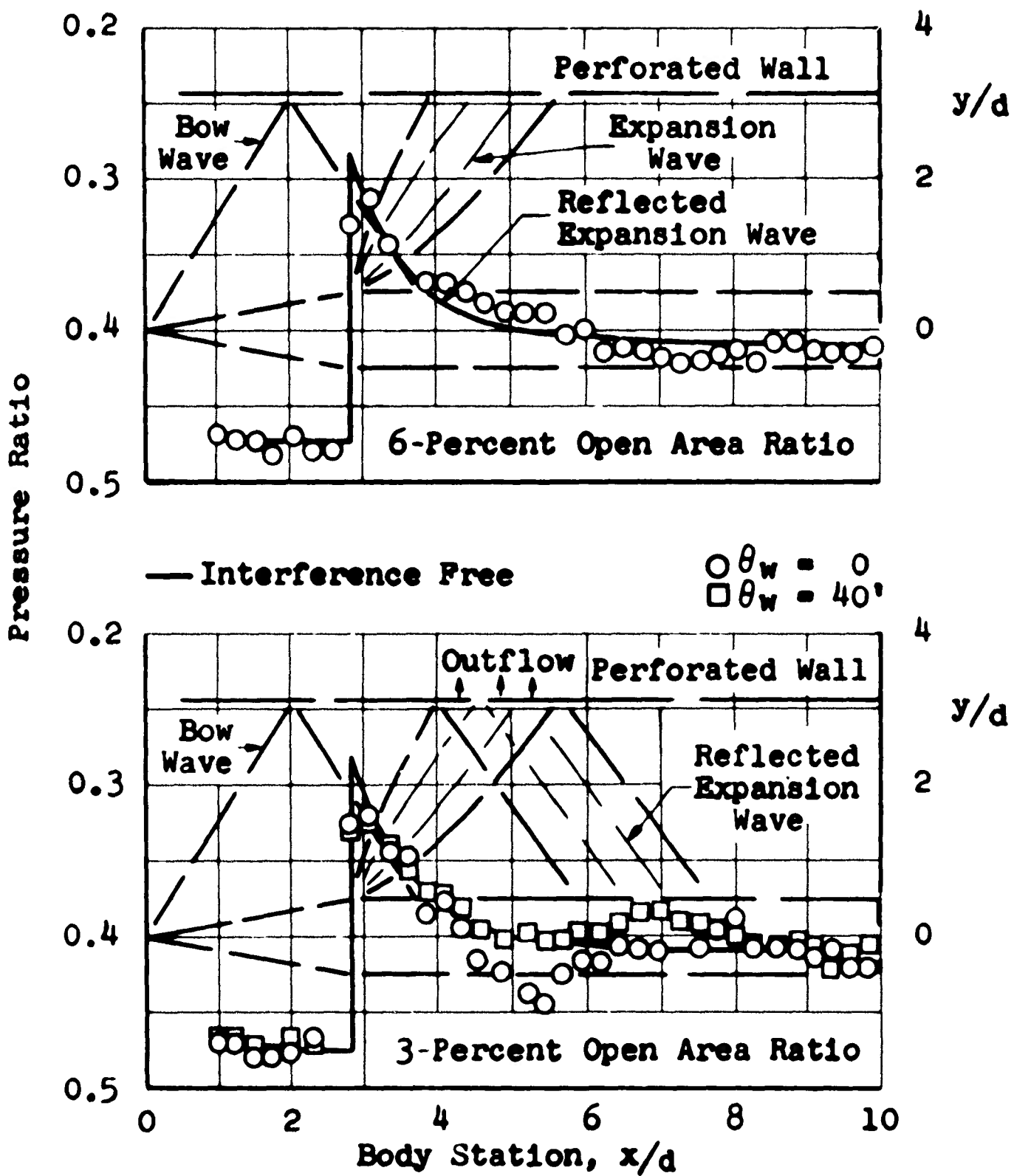
c. $M = 1.05$

Fig. 14 Continued



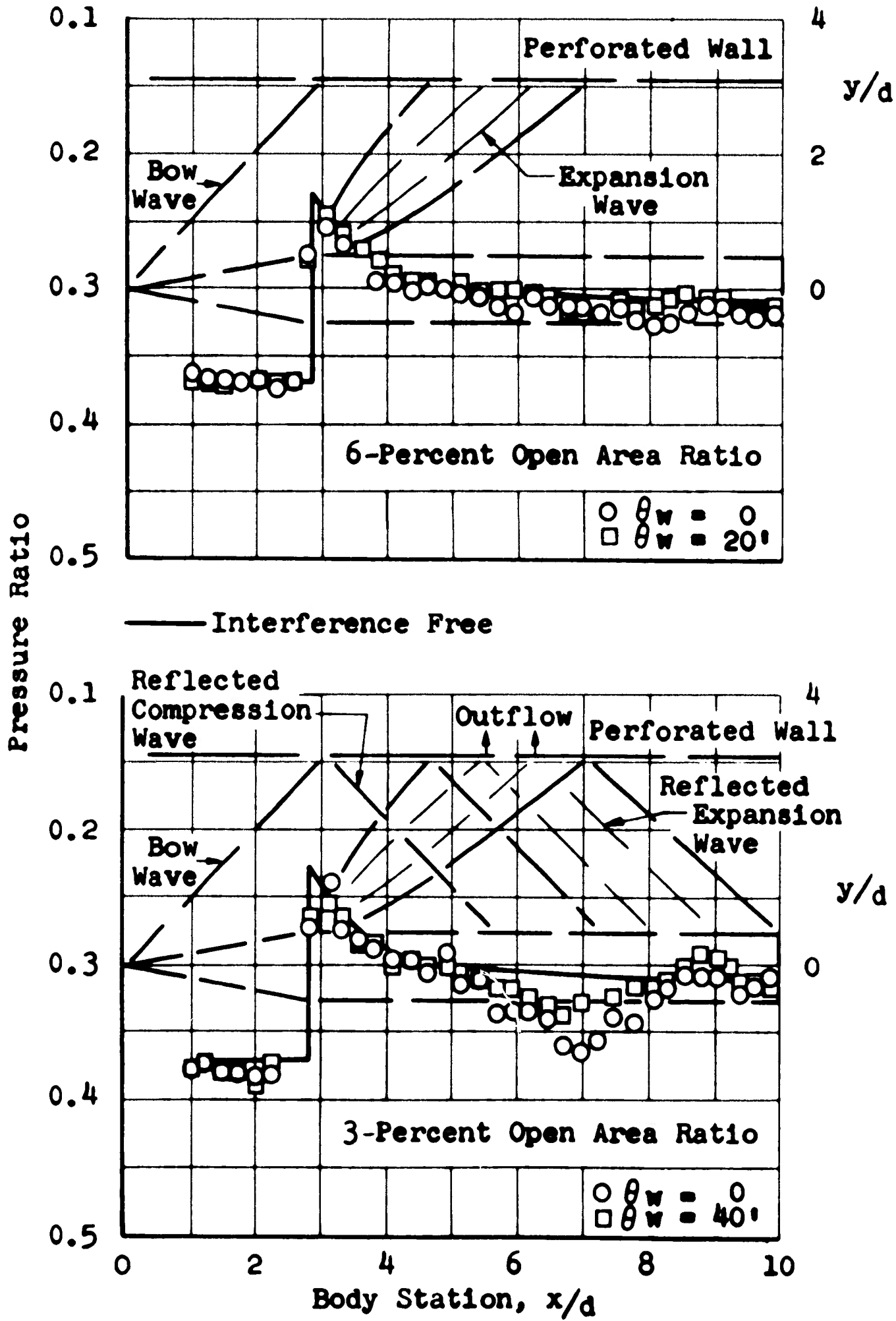
d. $M = 1.10$

Fig. 14 Continued



e. $M = 1.20$

Fig. 14 Continued



f. $M = 1.40$

Fig. 14 Concluded

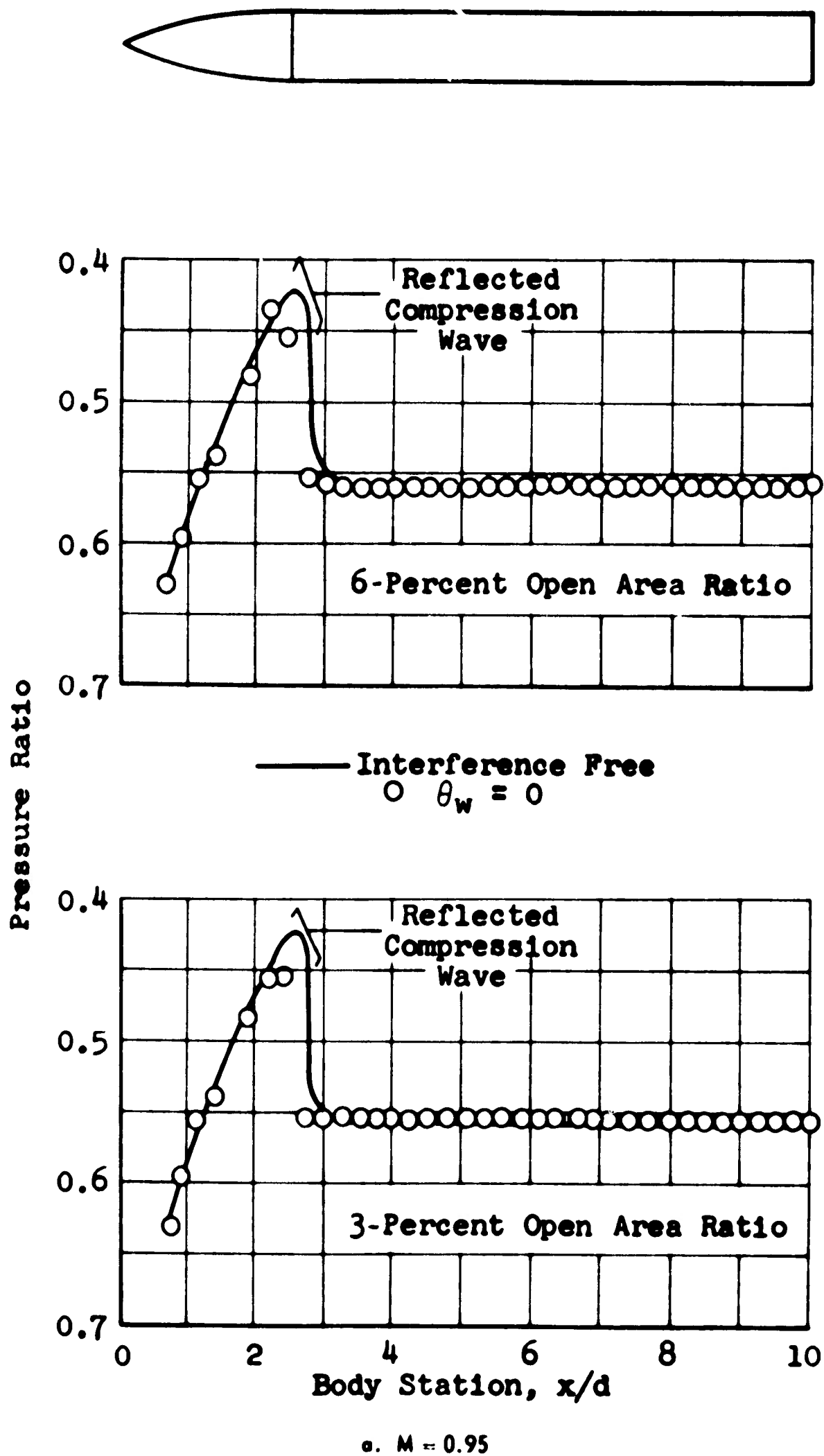
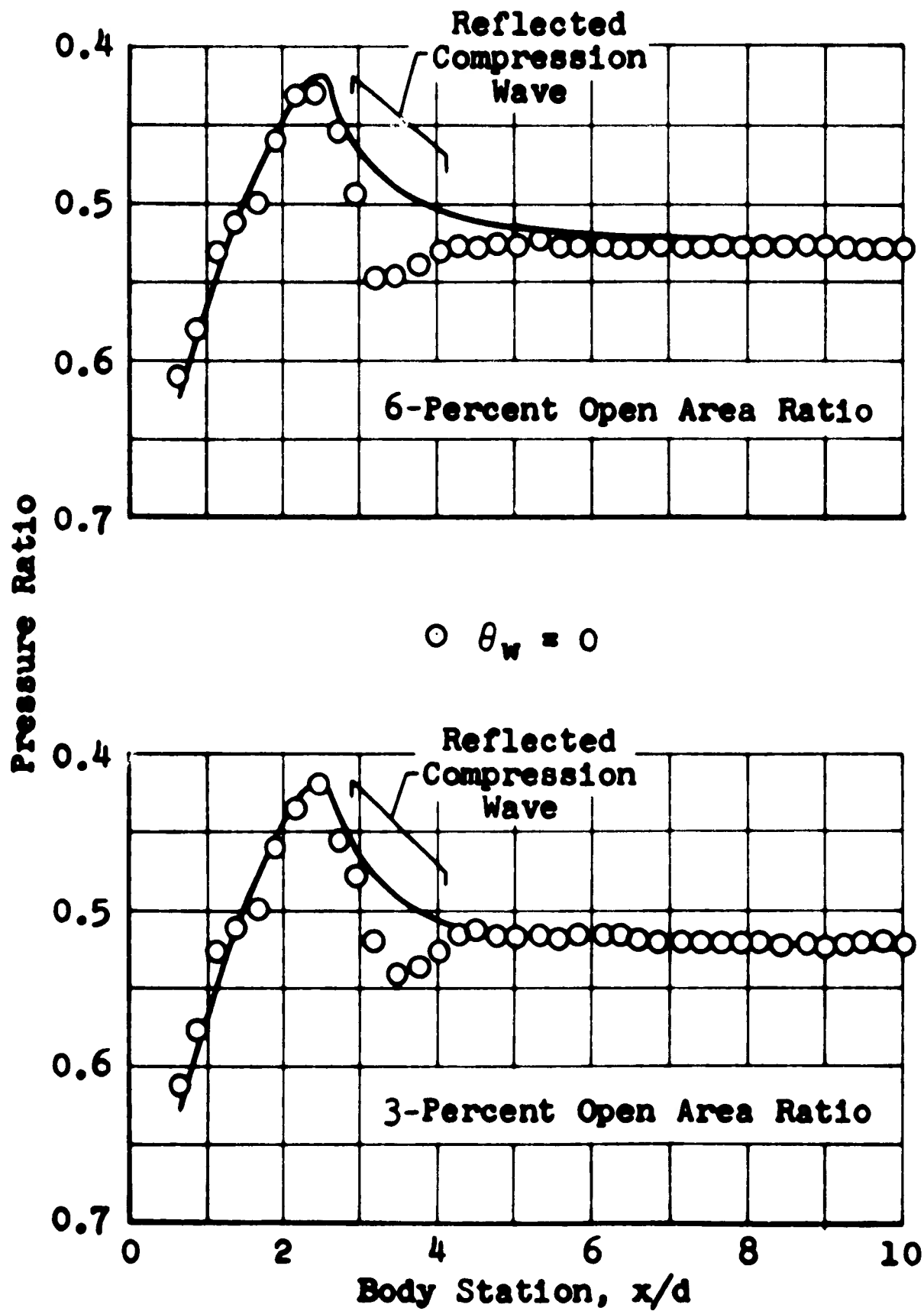
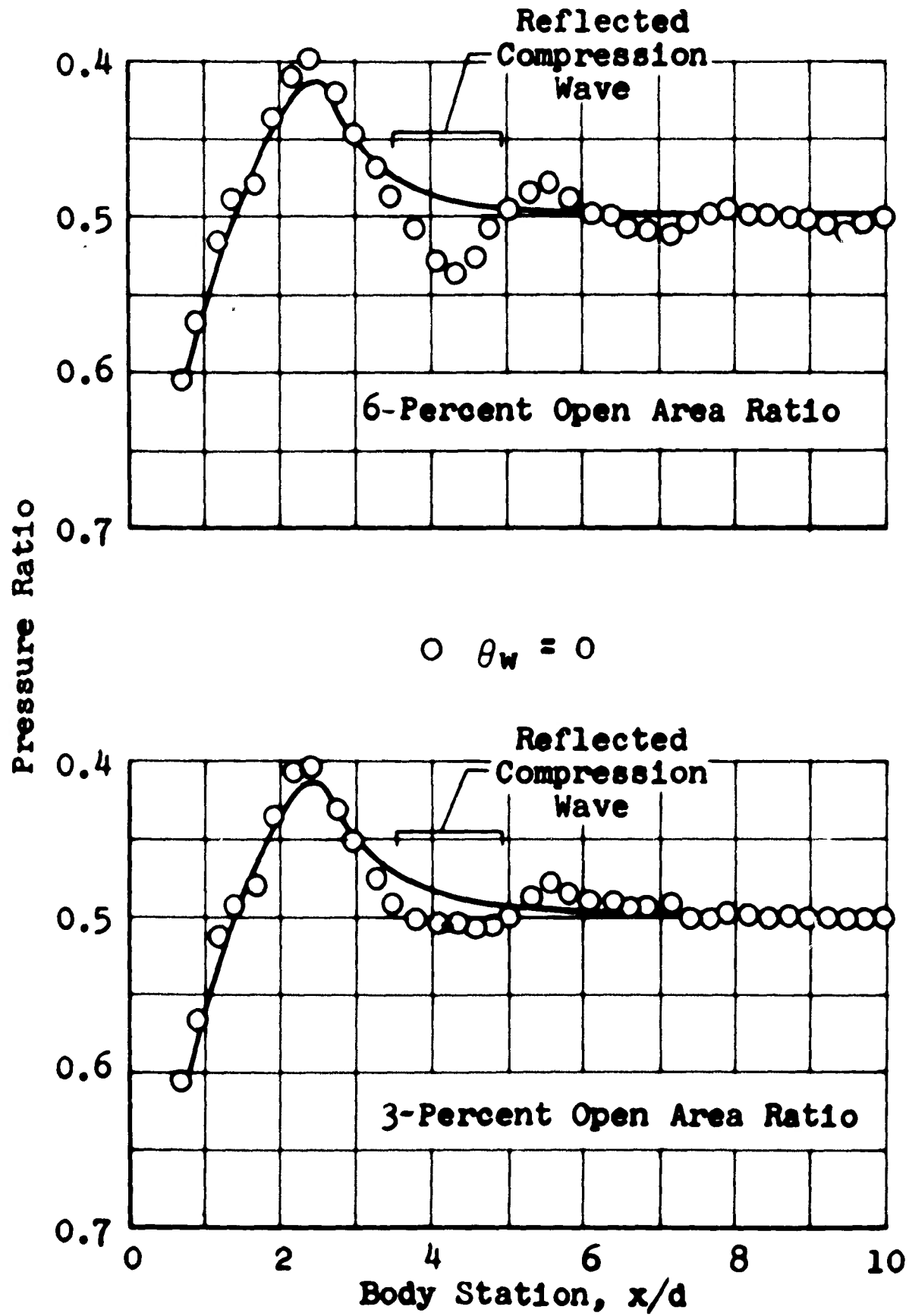


Fig. 15 Body Pressure Distributions on the 2-Percent Blockage, Parabolic Nose-Cylinder Model in the 1T-Effect of Open-Area Ratio with 60° Inclined-Hole Walls



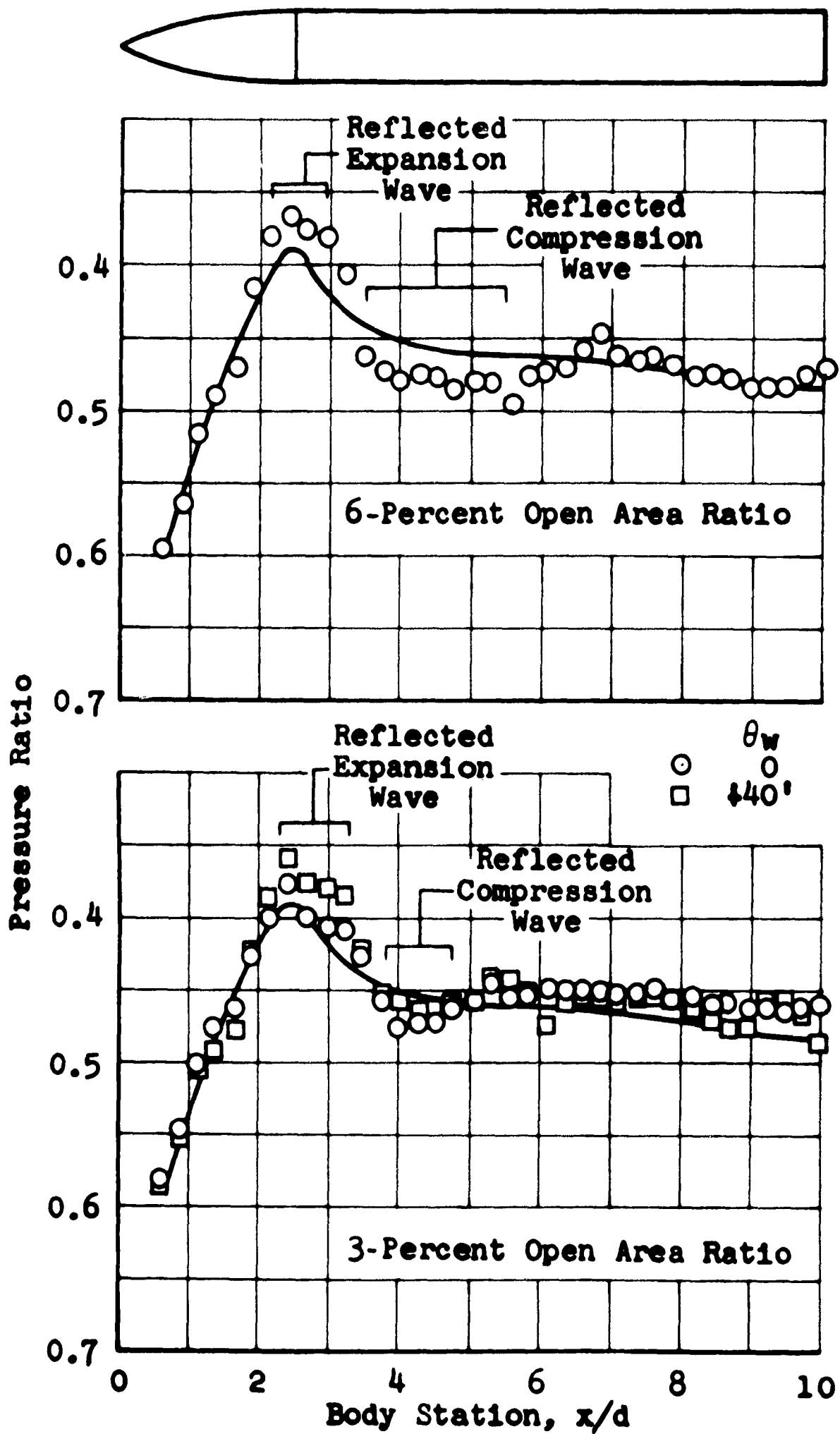
b. $M = 1.00$

Fig. 15 Continued



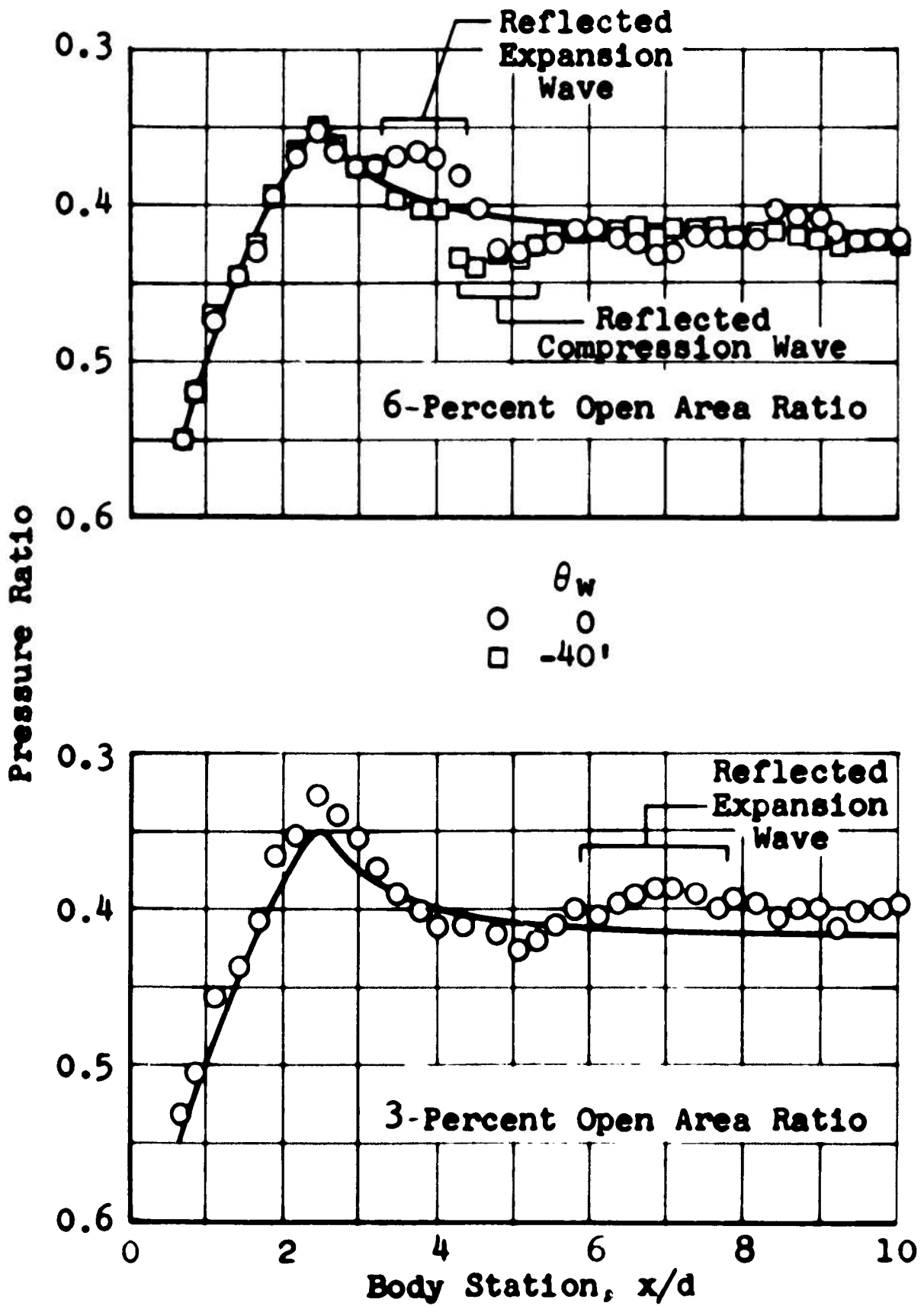
c. $M = 1.05$

Fig. 15 Continued



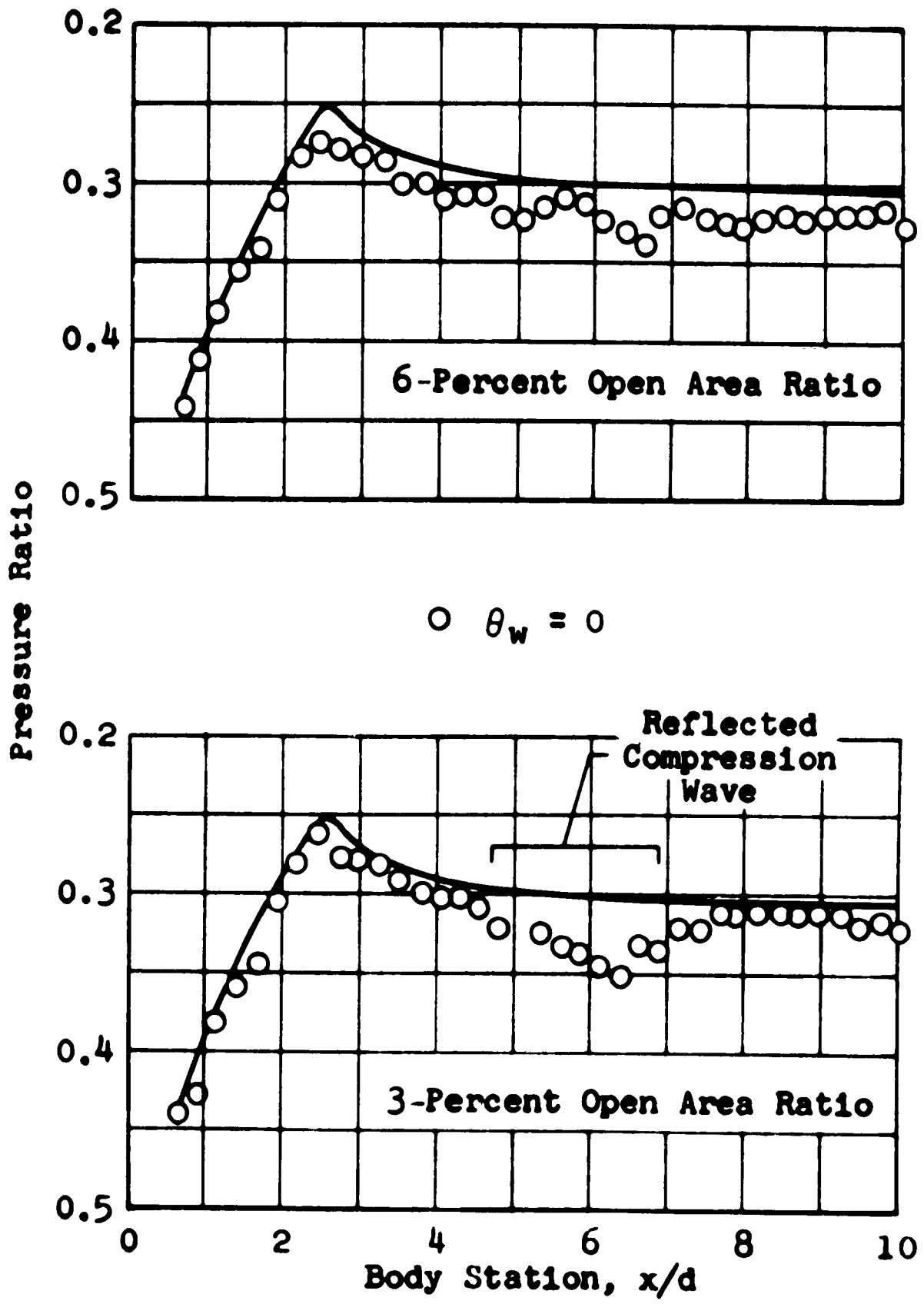
d. $M = 1.10$

Fig. 15 Continued



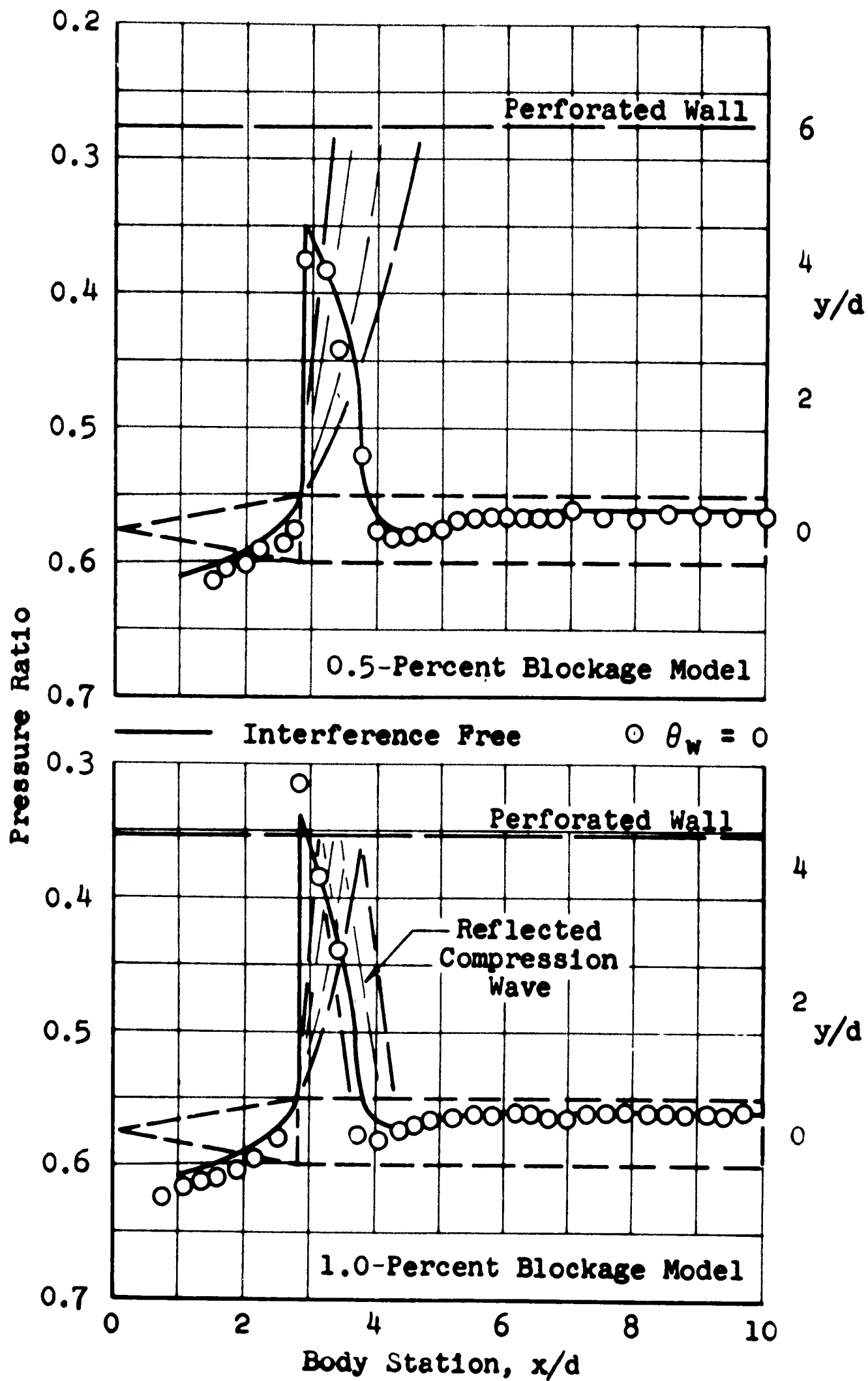
e. $M = 1.20$

Fig. 15 Continued



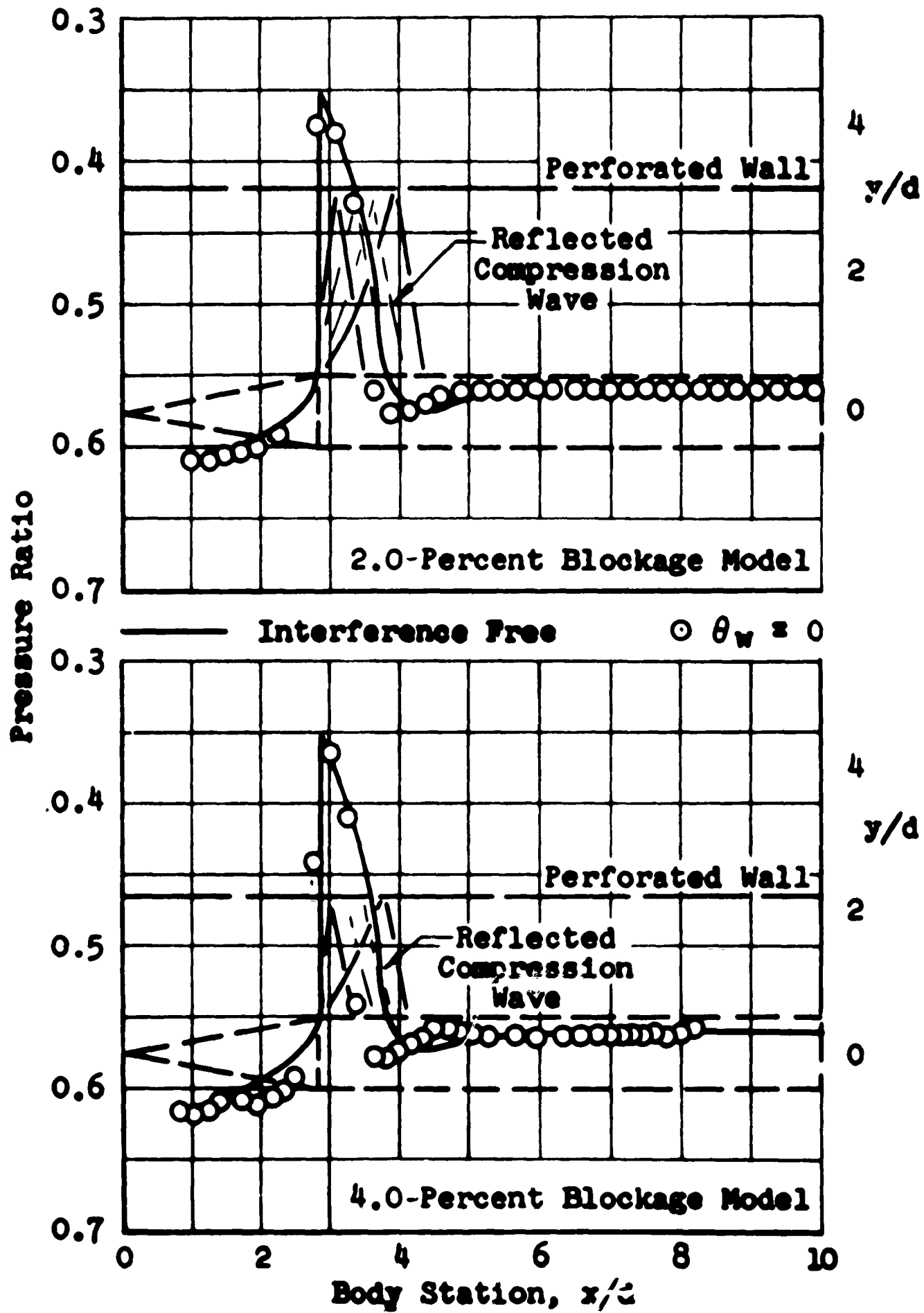
f. M - 1.40

Fig. 15 Concluded



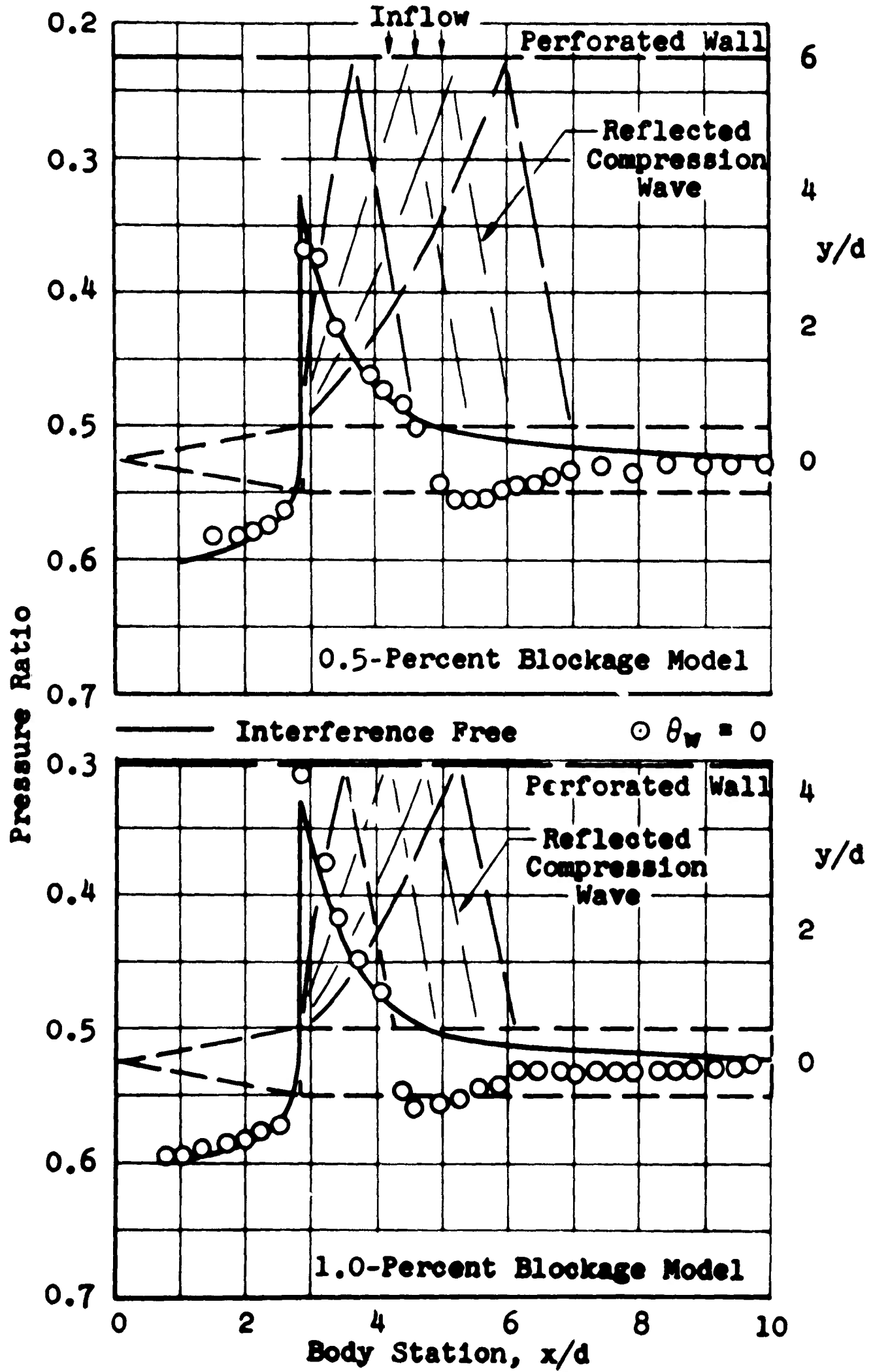
a. $M = 0.95$

Fig. 16 Body Pressure Distributions on 20° Cone-Cylinder Models in the 1T and 16T—Effect of Model Blockage Ratio with 60° Inclined-Hole, 6-Percent Open-Area Ratio Walls

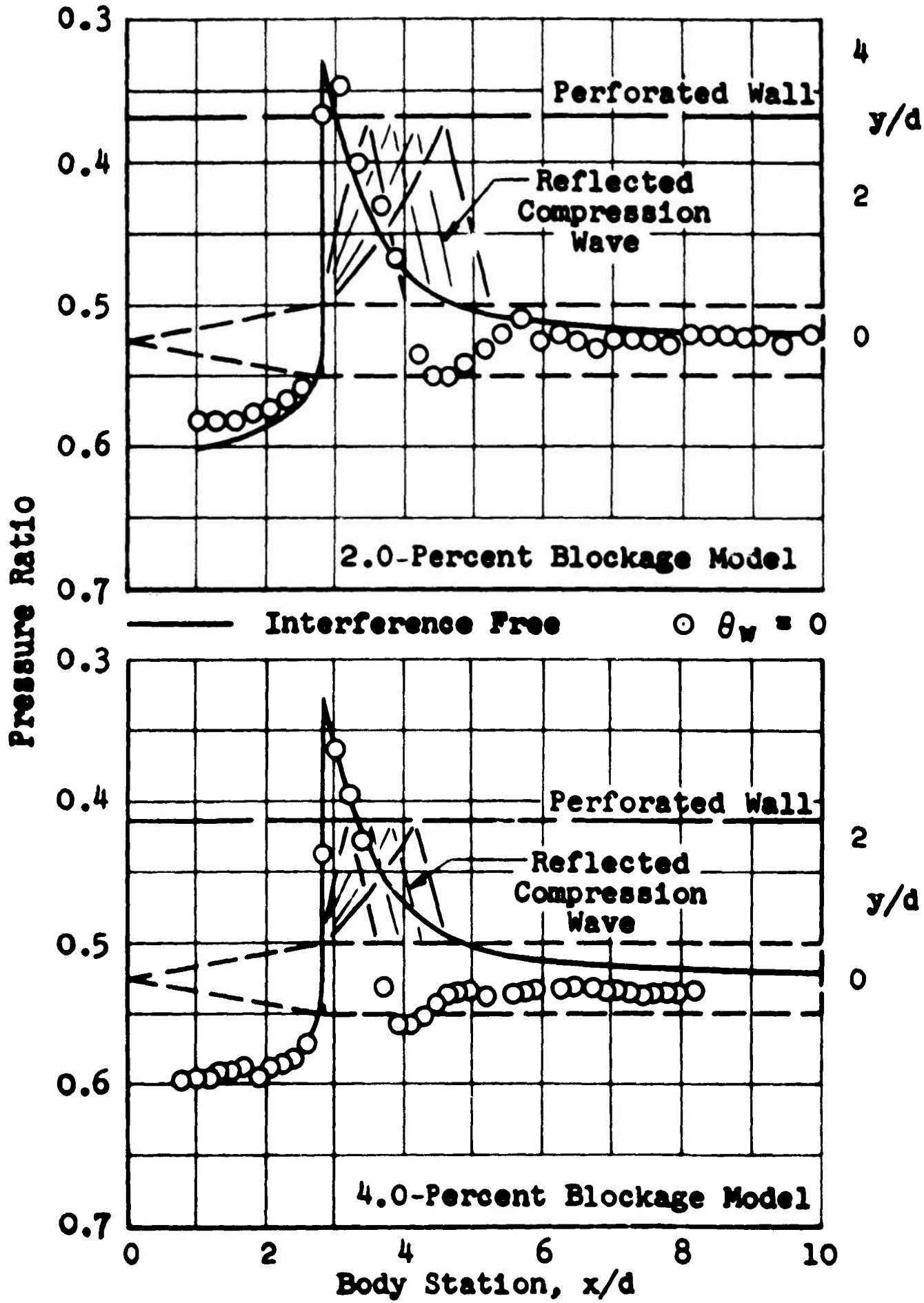


e. Concluded

Fig. 16 Continued

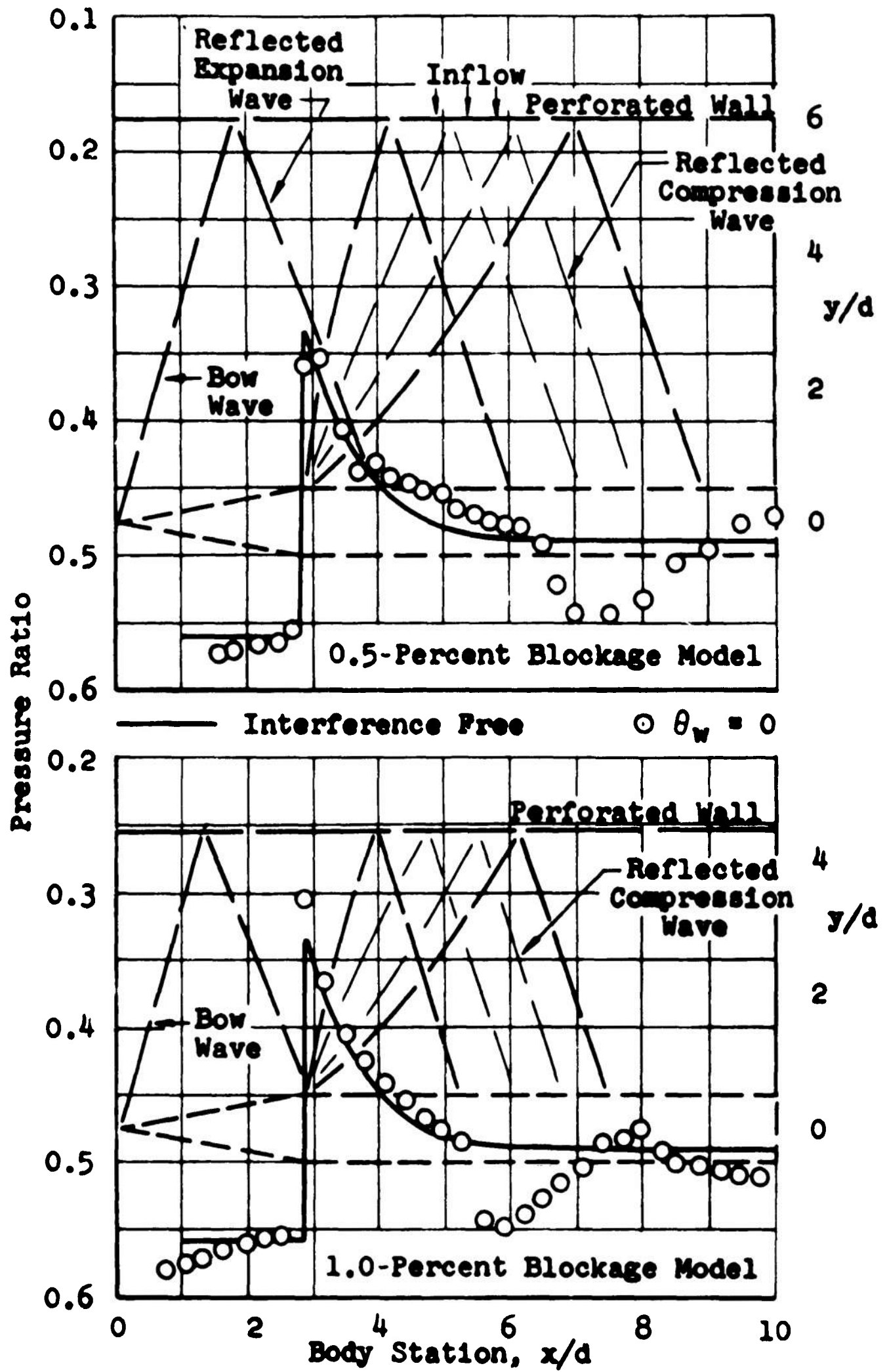


b. $M = 1.00$
 Fig. 16 Continued



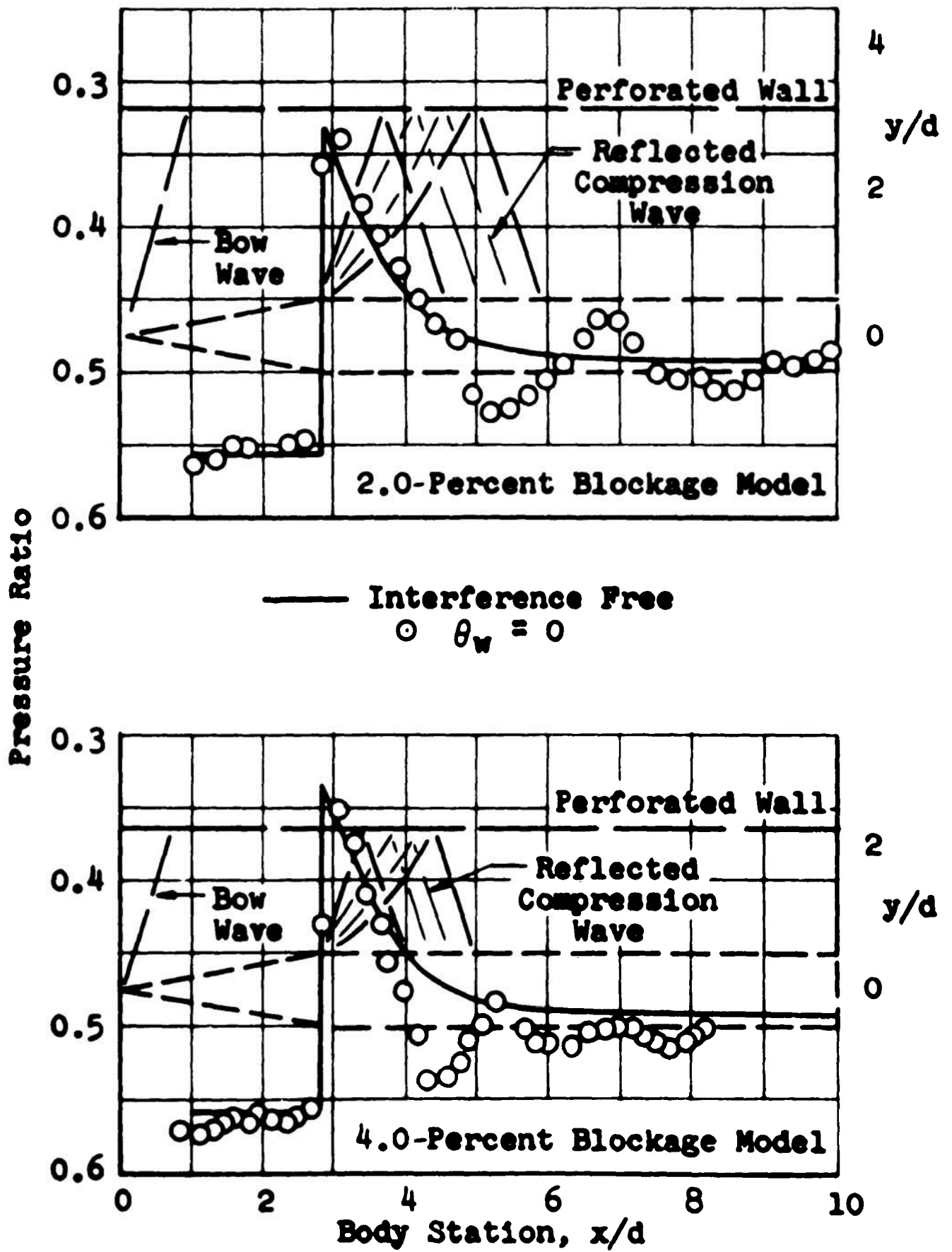
b. Concluded

Fig. 16 Continued



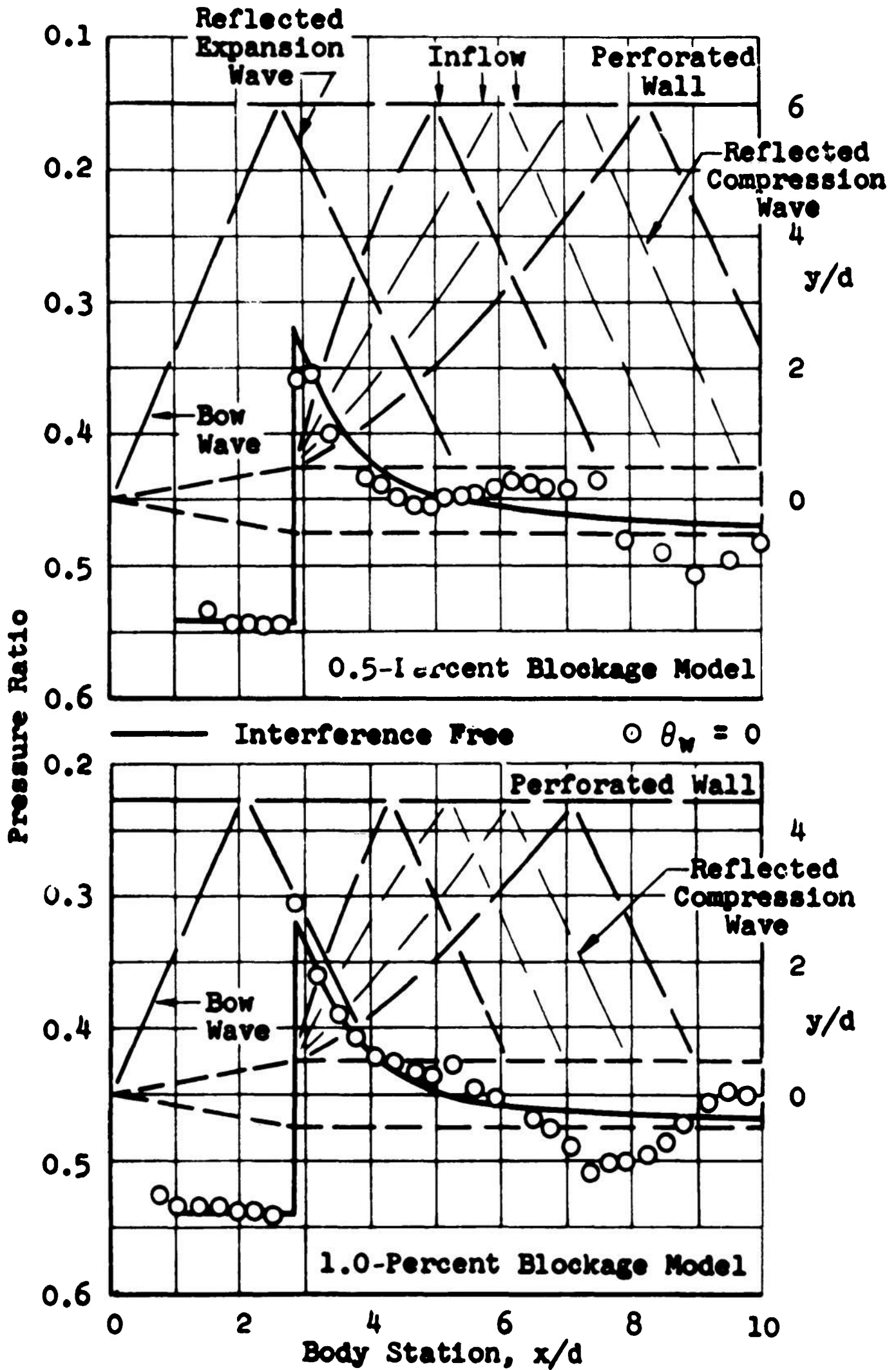
c. $M = 1.05$

Fig. 16 Continued



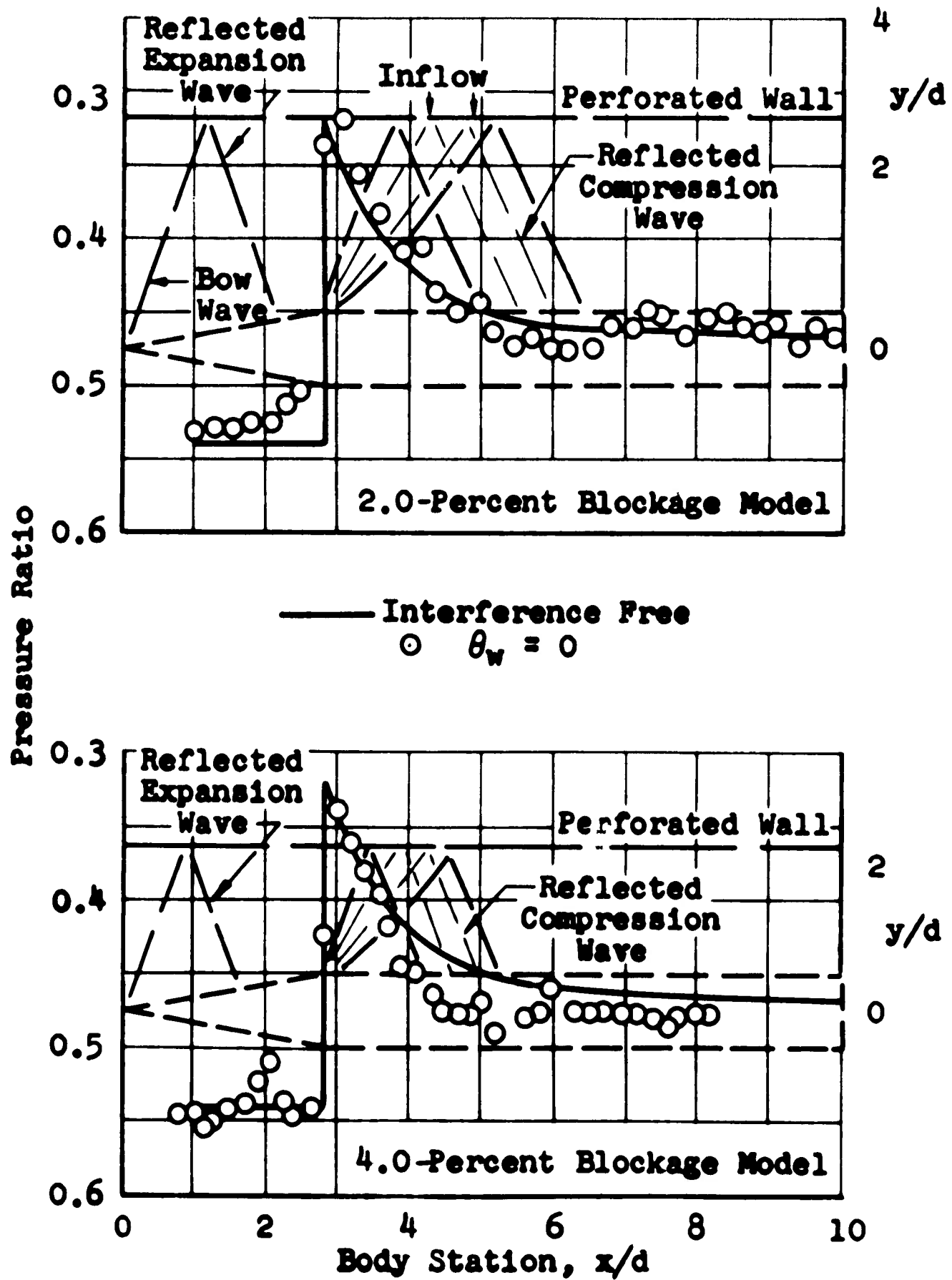
c. Concluded

Fig. 16 Continued



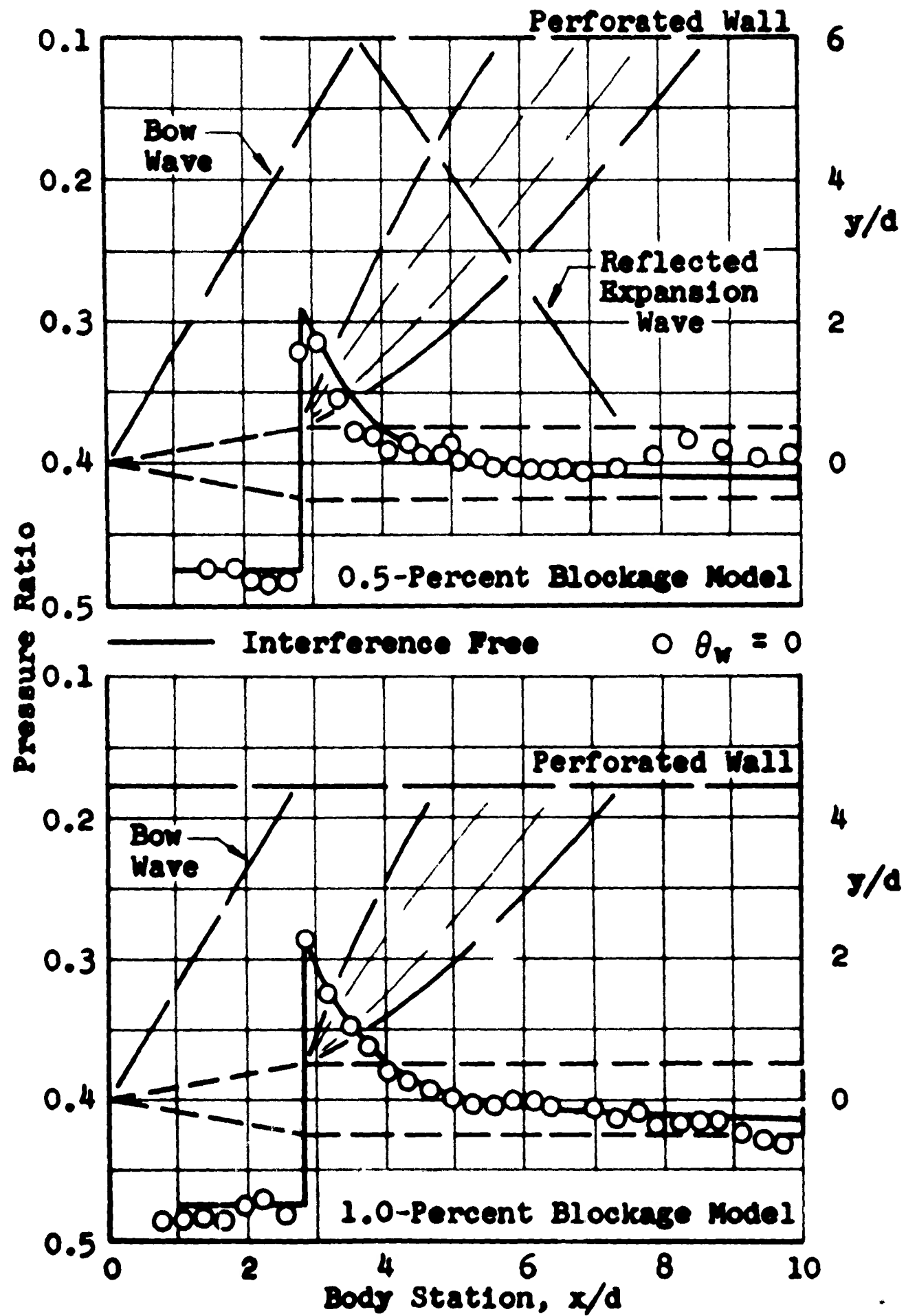
d. $M = 1.10$

Fig. 16 Continued



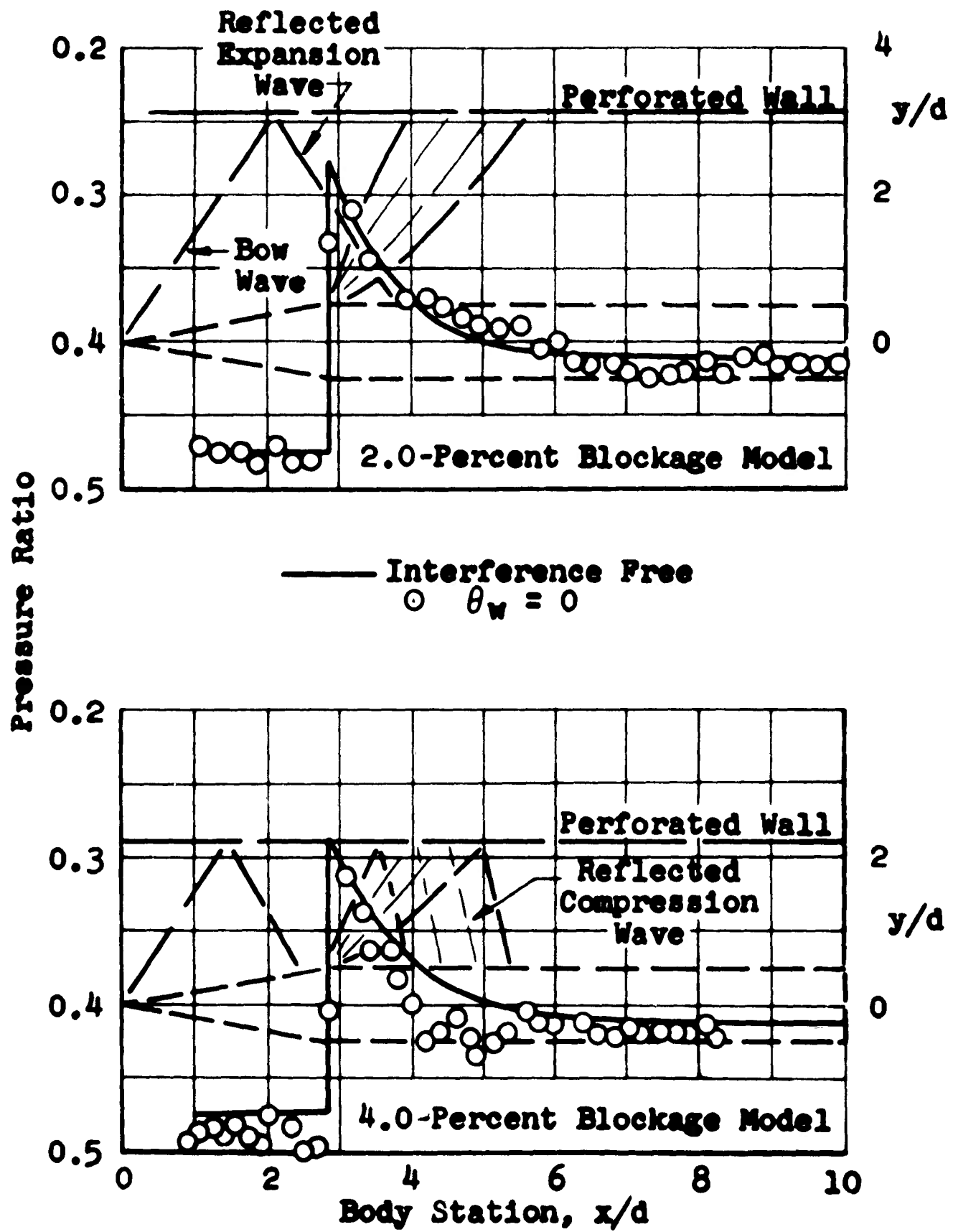
d. Concluded

Fig. 16 Continued



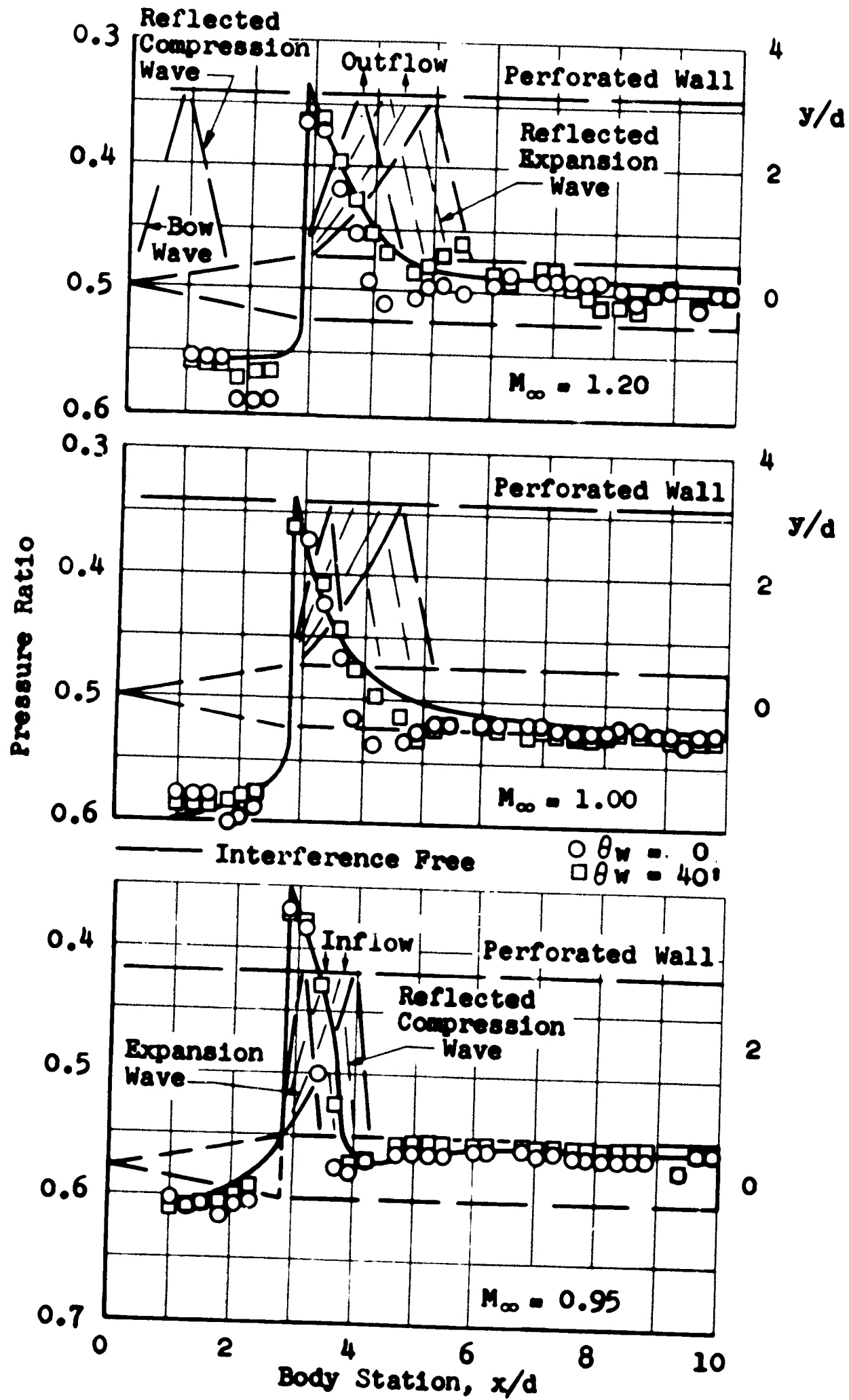
$\alpha = M = 1.20$

Fig. 16 Continued



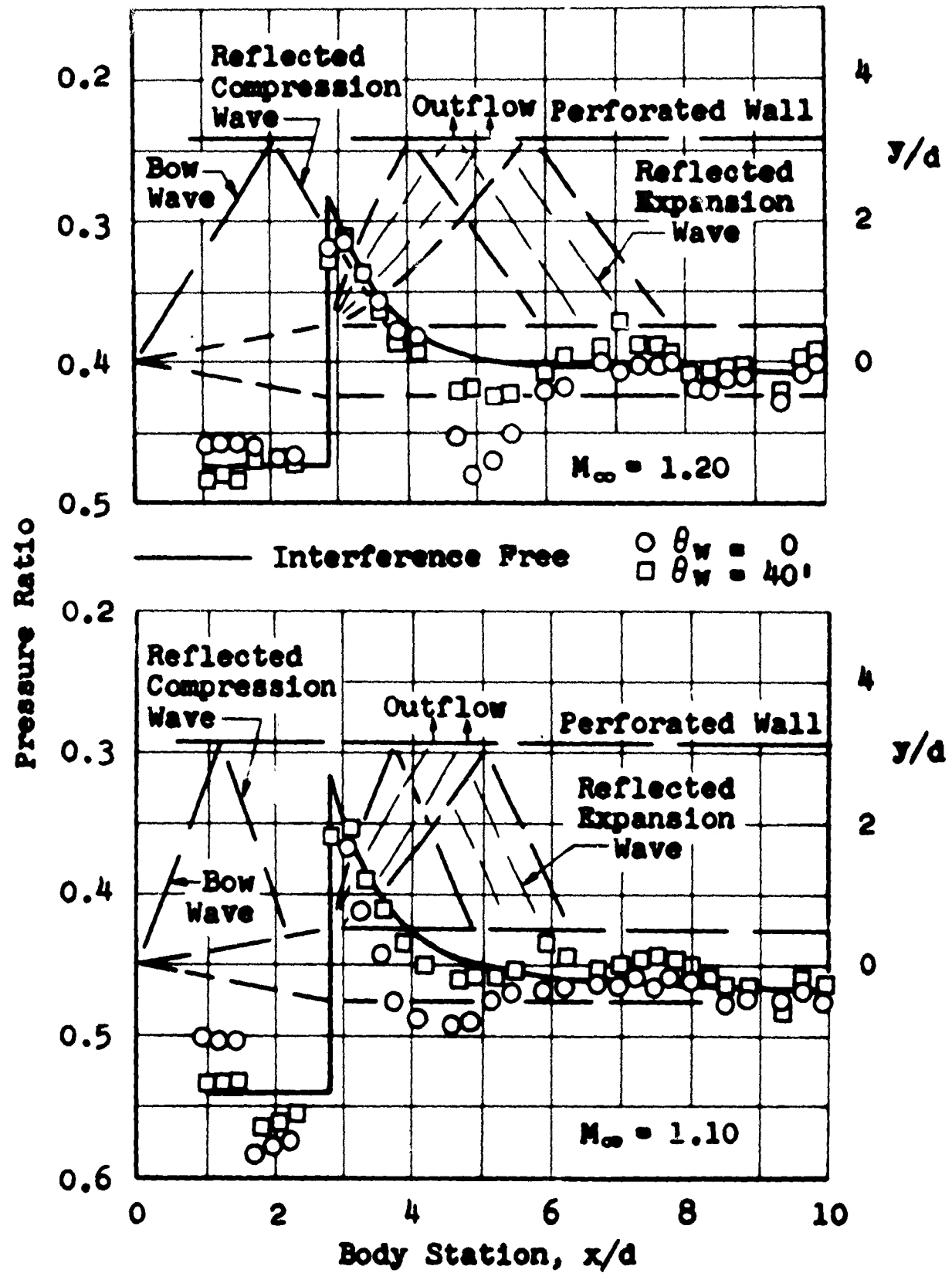
e. Concluded

Fig. 16 Concluded



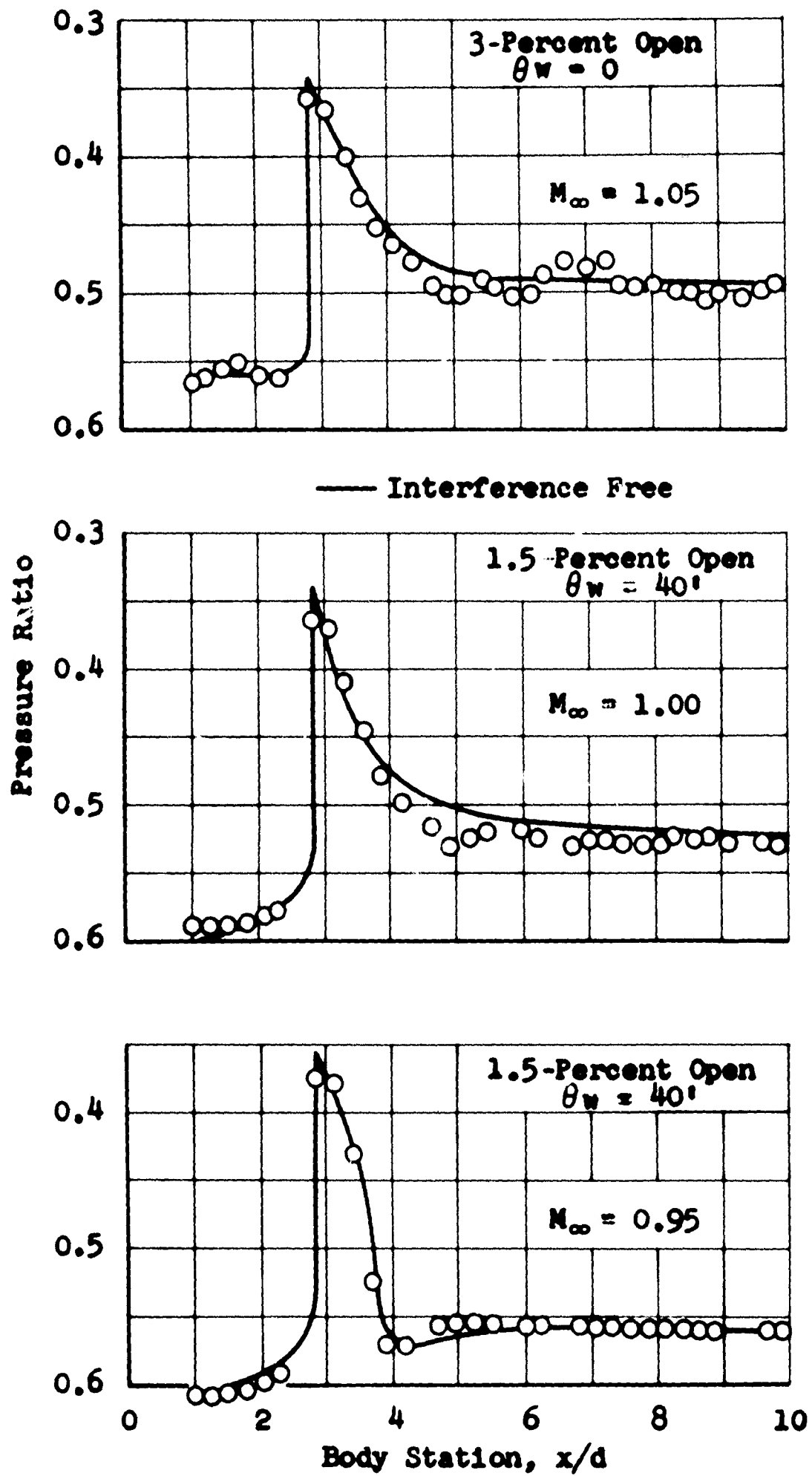
a. $M = 0.95, 1.00, \text{ and } 1.05$

Fig. 17 Body Pressure Distributions on the 2-Percent Blockage, 20° Cone-Cylinder Model in the IT-Effect of Reducing the Open-Area Ratio of the 60° Inclined-Hole Wall to 1.5 Percent



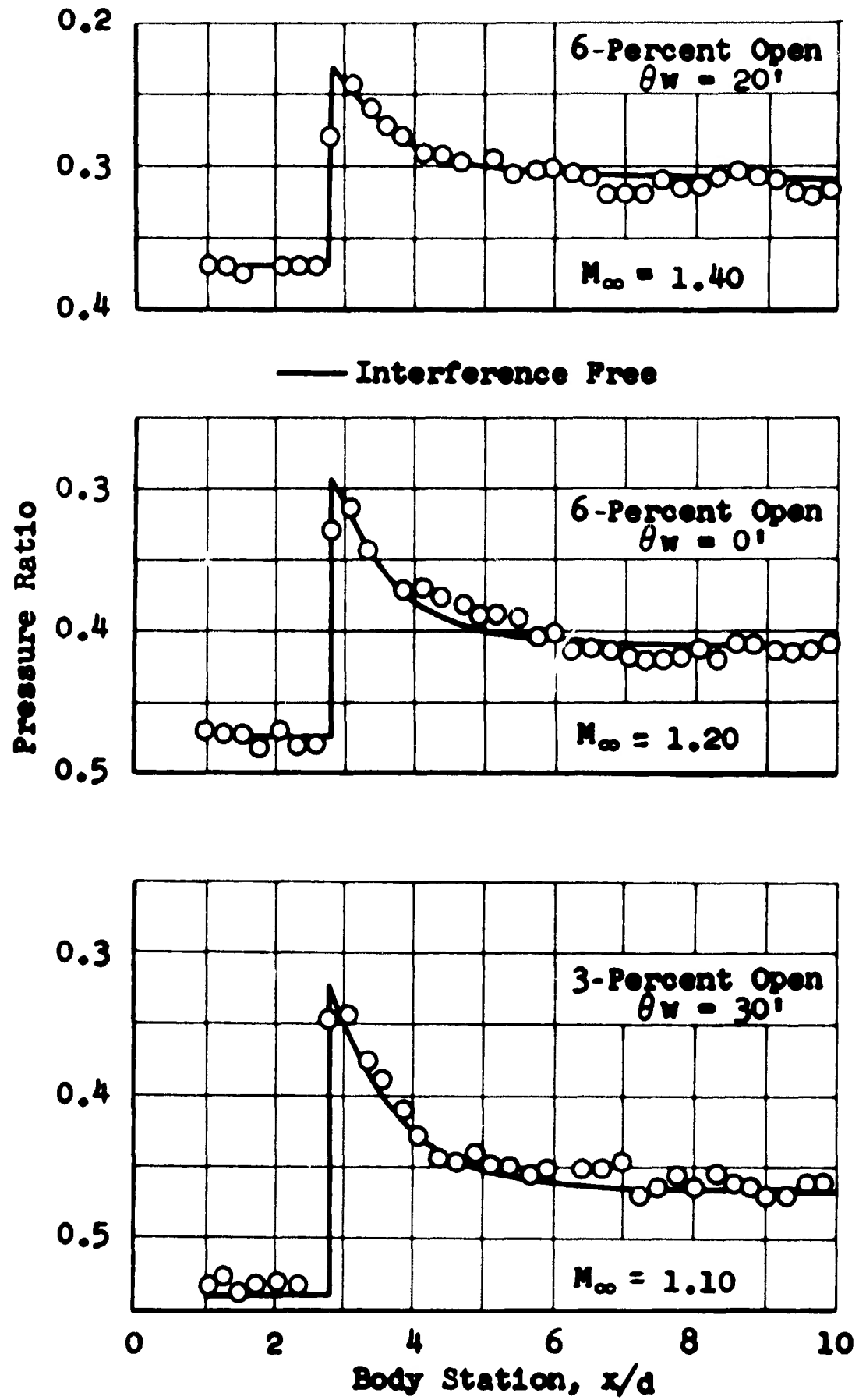
b. $M = 1.10$ and 1.20

Fig. 17 Concluded



a. $M = 0.95, 1.00, \text{ and } 1.05$

Fig. 18 Summary of the Most Favorable Body Pressure Distributions Obtained on the 2-Percent Blockage, 20° Cone-Cylinder Model in the 1T with 60° Inclined-Hole Walls



b. $M = 1.10, 1.20, \text{ and } 1.40$

Fig. 18 Concluded

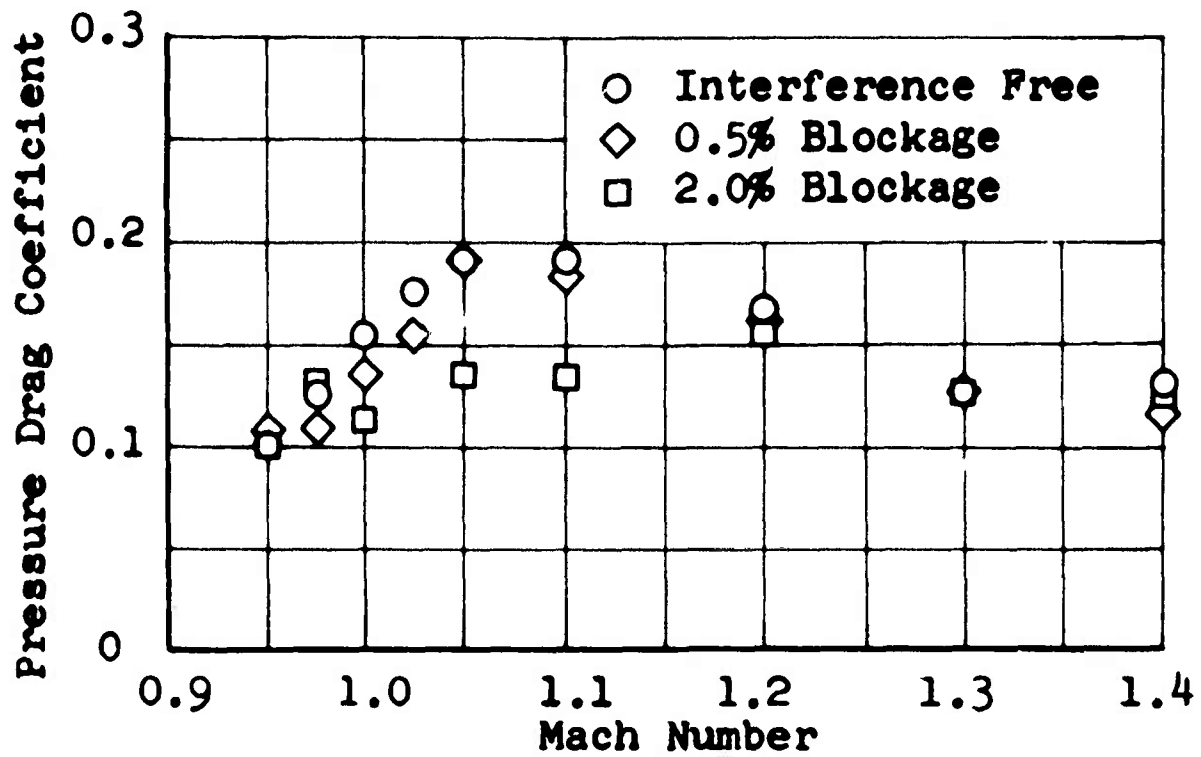


Fig. 19 Effect of Boundary Interference on the Forebody Pressure Drag of the 0.5- and 2-Percent Blockage, Cone-Cylinder Models Tested with the 60° Inclined-Hole, 6-Percent Open-Area Ratio Walls

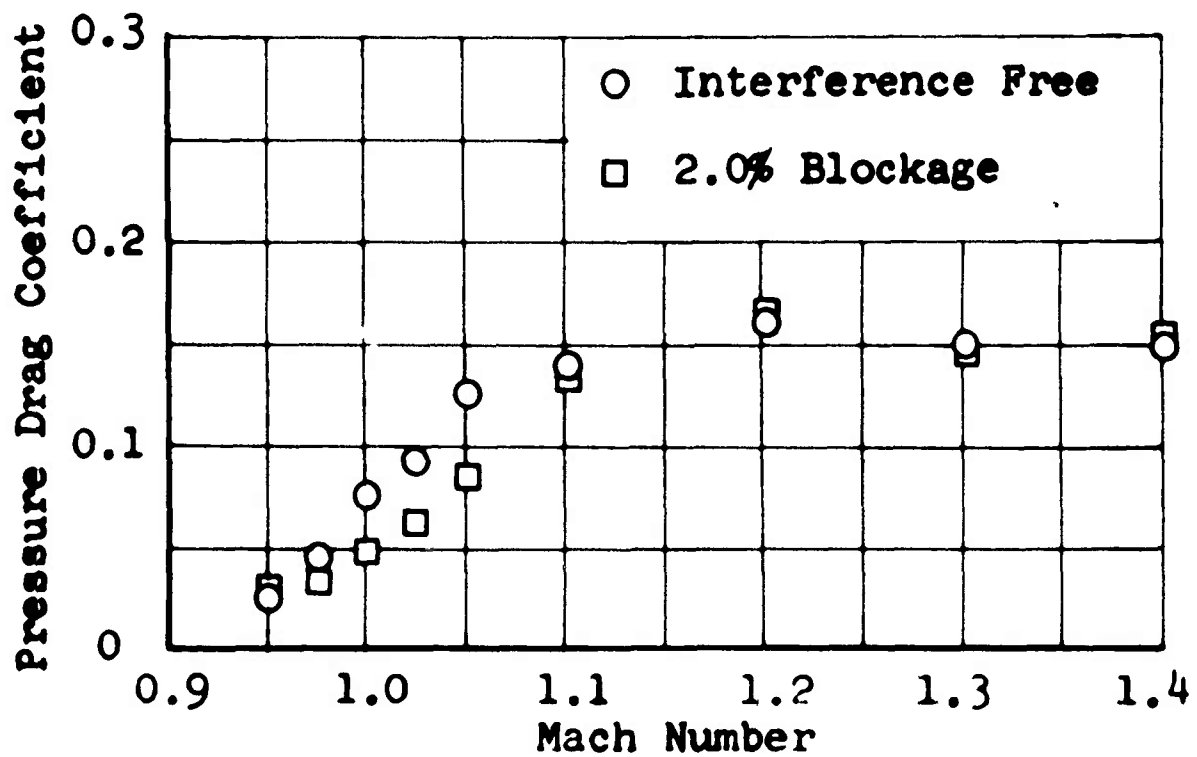


Fig. 20 Effect of Boundary Interference on the Forebody Pressure Drag of the 2-Percent Blockage, Parabolic Nose-Cylinder Model Tested with the 60° Inclined-Hole, 6-Percent Open-Area Ratio Walls